Transcriptional Heterogeneity and Plasticity in Cone Photoreceptors

A Dissertation
Presented in Partial Fulfillment of the Requirements for the
Degree of Doctor of Philosophy
with a
Major in Neuroscience
in the
College of Graduate Studies
University of Idaho
by
Ashley A. Farre

Approved by:
Major Professor: Deborah L. Stenkamp, Ph.D.
Committee Members: Allan Caplan, Ph.D.; Diana Mitchell, Ph.D.; Scott Grieshaber, Ph.D.
Department Administrator: Tanya Miura, Ph.D.

August 2023

Abstract

Photoreceptors are the light-sensing neurons in the vertebrate retina. While rod photoreceptors are responsible for low-light, low-acuity vision, cone photoreceptors mediate high-acuity color vision. The presence of multiple cone subtypes, each expressing a unique opsin protein and sensitive to particular wavelengths of light, serves as the basis of color vision. Humans possess three cone subtypes (red-, green-, and blue-sensing) which express long wavelength sensitive (LWS), middle wavelength sensitive (MWS), and short wavelength sensitive (SWS) opsins, respectively. Zebrafish possess eight cone types, including LWS1 and LWS2. While much is known about transcriptional regulation in cones, more remains to be uncovered, especially the mechanism by which opsin genes located in tandem arrays are regulated. Expanding our knowledge of how gene expression in cone subtypes is regulated represents an important step in improving treatments for retinal diseases.

This dissertation begins with an overview of retinal development, emphasizing factors involved in retinal cell type patterning. In Chapter 2, I present my accepted manuscript that explores the transcriptional heterogeneity between and within the LWS cone subtypes in zebrafish beyond opsin expression. The LWS cone subtypes express the opsin genes *lws1* and *lws2*, which are tandemly replicated opsin genes that are regulated by thyroid hormone. In Chapter 3, I introduce my unpublished manuscript in which we investigate the extent of transcriptional plasticity in zebrafish cones, determining whether gene expression remains plastic to thyroid hormone treatment in adult fish. Chapter 4 is an update on our progress in determining how thyroid hormone and retinoic acid regulate opsin expression in three-dimensional, human induced-pluripotent stem cell-derived retinal organoids. We also propose a multicomponent strategy for rigorous analysis of opsin expression in retinal organoids. Overall, the work presented here expands scientific knowledge of gene expression in cones and how it can be altered.

Acknowledgments

First and foremost, I would like to thank my major professor and mentor, Dr. Deborah L. Stenkamp, for keeping me steady with your relentlessly good attitude. You showed me how to make potentially confusing results into something cool. Thank you to Dr. Allan Caplan, Dr. Diana Mitchell, Dr. Scott Grieshaber, and Dr. Peter Fuerst for providing invaluable feedback on my work. Thank you to Gina Tingley and Kristi Accola for always making sure I stayed on track with administrative requirements.

Thank you to the best undergraduate/graduate student mentor Dr. Robert Mackin, Ruth Frey, for countless things including keeping the lab running. Thank you to my fellow Stenkamp Lab PhD students Lindsey Barrett and Emmanuel Owusu Poku. Audrey Duncan, Johnson Huang, Rachael Poulsen, and Preston Thomas for being amazing trainees and friends.

I would like to thank Dr. Shoji Kawamura for the *lws:PAC(H)* transgenic line, Linn Gieser and Matthew Brooks for technical assistance. The staff of the UI Laboratory Animal Research Facility for zebrafish care. Onesmo Balemba of the UI Imaging and Data Analysis Core, Melissa Oatley of the WSU FACS Core, the UI IIRC Genomics and Bioinformatics Resources Core, and the Baylor College of Medicine Single Cell Genomics Core.

Lastly, the work presented in this dissertation was made possible by NIH R01 EY012146 (DLS), NIH R01 EY012146-16S1 (DLS), NIH F31 EY031962 (AAF), NSF REU Site 146096 (AD), a UI Summer Undergraduate Research Fellowship (AD), and support of undergraduate (RP) and medical student (PT) research from Idaho INBRE (NIH P20 GM103408). NIH Grant S10 OD0108044 (DLS) funded the purchase of the Nikon/Andor spinning disk confocal microscope and camera.

Dedication

For those who have loved and supported me during these incredible years. Especially for my family, who didn't let me give up on myself.

Thank you to Brad, for keeping me mostly stable and for believing in me more than I did. To Indy, for refusing to leave my side throughout the writing process. Thank you to Mellisa, for being my PhD requirement buddy and my motivation a lot of the time. My labmates, Lindsey, Emma, and Rob for your amazing friendship and for being in this with me.

I dedicate this dissertation to you, because you all knew I could do this even when I didn't.

Table of Contents

List of Tables

List of Figures

Statement of Contribution

I declare that I am first author on all chapters included in this dissertation, and that the research presented is my own. The specific contributions by others are included below.

Complete list of authors for Chapter 2: (*co-first author) Ashley A. Farre*, Chi Sun*, Margaret R. Starostik, Samuel S. Hunter, Milton A. English, Audrey Duncan, Abirami Santhanam, Eyad Shihabeddin, John O'Brien, Anand Swaroop, and Deborah L. Stenkamp

Author Contributions for Chapter 2: Data acquisition: AAF, CS, ME, and AD. All authors analyzed the data, conceived the project, and wrote the manuscript.

Complete list of authors for Chapter 3: Ashley A. Farre, Preston Thomas, Johnson Huang, Rachael Poulsen, Emmanuel Owusu Poku, and Deborah L. Stenkamp

Author Contributions for Chapter 3: Data acquisition: AAF, PT, JH, RP, EOP. Data analysis: AAF, PT, JH. All authors assisted with data interpretation. AAF generated figures. AAF and DLS conceived the project and wrote the manuscript.

Complete list of authors for Chapter 4: Ashley A. Farre, Emmanuel Owusu Poku, Blake Baker, Valeria Canto-Soler, Deborah L. Stenkamp

Author Contributions for Chapter 4: Data acquisition: AAF, EOP, BB. AAF, EOP, VCS and DLS interpreted data. VCS, DLS, and AAF conceived the project. AAF generated figures and wrote the manuscript.

Chapter 1: Introduction to Retinal Development

The nervous system is one of the most complex and important systems in an organism. The nervous system allows us to perceive, think, feel, and do, connecting us to the world and to each other. Tightly controlled cell type patterning underlies nervous system function, enabling groups of cells to communicate with other cells in specific networks. The senses are some of the primary functions of the nervous system, and vision serves as one of the most important senses for humans. Vision begins when light enters the eye and interacts with the retina, the light-sensitive tissue of the eye. The retina is responsible for encoding visual information into electrical signals that can be decoded in the brain. The neural retina is composed of five main classes of neurons: photoreceptor, bipolar, horizontal, amacrine, and ganglion cells. These cells are arranged in five layers, with photoreceptor cell bodies in the outer nuclear layer (ONL), photoreceptor-bipolar synapses (modulated by synapses with horizontal cells) in the outer plexiform layer (OPL), bipolar, amacrine, and horizontal cell bodies in the inner nuclear layer (INL), bipolar-ganglion cell synapses (modulated by synapses with amacrine cells) in the inner nuclear layer (INL), and ganglion cell nuclei in the ganglion cell layer [1]. Non-neuronal glial cells are also present, including Müller glia and microglia. Müller glia are arranged radially and span the retinal layers, providing support to the retinal neurons while microglia serve as the resident immune cells of the retina [2].

Phototransduction is the process by which photons of light are converted into a neurological signal. Photoreceptors are the primary light-sensing cells in the retina and express light-sensitive visual pigments. Opsin proteins, coupled with a chromophore (11-cis retinal, A1; or 11-cis dehydroretinal, A2), form the visual pigments. When the chromophore absorbs a photon, it isomerizes to all-trans retinal and activates the opsin protein, which is a heterotrimeric G protein coupled receptor. The activated opsin releases the G-protein, which splits into its alpha subunit and beta/gamma subunits and subsequently leads to a signaling cascade that causes the photoreceptor to hyperpolarize and stop releasing glutamate. The signal from the photoreceptor transmits light information to bipolar cells, which communicate with retinal ganglion cells (RGCs) [3].

Ganglion cell axons form the optic nerve and project to the dorsal lateral geniculate nucleus of the thalamus in mammals (LGN). Axons of the LGN neurons terminate at the

primary visual cortex, where the retinal signals are decoded. This pathway is known as the primary visual pathway and is responsible for the image forming aspect of vision. Ganglion cell axons project to additional targets as well, and these pathways mediate non-image forming aspects of vision. Ganglion cells project to the pretectum, then pretectal neurons project to the Edinger-Westfall nucleus in the midbrain to form the pathway that controls the pupillary light reflex. The retinohypothalamic pathway is formed by ganglion cells projecting to the suprachiasmatic nucleus of the hypothalamus and is important in circadian function. Finally, ganglion cell projections to the superior colliculus help with coordinating head movements [4].

The process of retinal development is largely conserved in vertebrates [5-7]. The retina is developed from lateral bulges of the neural ectoderm, specified by the transcription factors *six3a* and *pax6* in zebrafish [8, 9]. In the zebrafish embryo, the optic primordia form by 12 hpf (hours post-fertilization) [5]. Around 15 hpf, the optic primordia invaginate into a double layer, in which the outer/more lateral layer eventually becomes the retina and the inner/more medial layer will become the retinal pigmented epithelium, a non-neuronal tissue that is essential for maintaining the retina [5]. The RPE is specified by the action if *mitf* [10]. Retinal progenitors begin differentiating into neurons at 28 hpf in a ventronasal to dorstemporal wave in zebrafish, resulting in a ventral patch that is further developed than the rest of the retina [6]. Ganglion cells are among the first neurons to develop, specified by *atonal5* in mice and zebrafish [11, 12]. Next are amacrine cells, specified by *ptf1a*; followed by horizonal and bipolar interneurons, which are generated due to the expression *ptf1a/neurod4* and *vsx1/2*, respectively [13-15]. Most of the zebrafish retina is laminated by 48 hpf with most cells of the INL postmitotic by this point as well (bipolar and horizontal cells) [6]. Cones begin to develop shortly after ganglion cells, around 34-46 hpf, and are specified by the expression of *otx2*, *crx*, and *prdm1* [16-18]. Müller Glia and rods are some of the last cell types to be generated, becoming detectable around 50 hpf [19]. Rods are specified by the expression of the transcription factor *nrl* [19, 20]. Rhodopsin and red cone opsin can be detected around 50 hpf, followed by UV and green opsins [21]. Visual system function begins by 72 hpf, as evidenced by behavioral response to light and presence of photoreceptor outer segments (layers of membrane that contain opsin proteins) and synaptic ribbons [21].

The retina contains two main types of photoreceptors: rods and cones. Rod photoreceptors are responsible for low light, low acuity vision while cone photoreceptors mediate high acuity color vision. Cones allow for the perception of color due to the expression of different opsins (which possess different peak spectral sensitivities) in separate subpopulations [22, 23]. There are five major classes of vertebrate opsin genes: rhodopsin, UV-sensitive *sws1*, blue-sensitive *sws2*, green-sensitive *rh2*, and red-sensitive *lws*. Zebrafish possess each of these types of opsins, with one *sws1* gene, one *sws2* gene, four *rh2* genes and two *lws* genes [24]. Humans have only three types of cone photoreceptors: blue-sensing *SWS*, green-sensing *MWS*, and red-sensing *LWS* [25]. The human *LWS* and *MWS* genes are arranged in tandem on the X chromosome in a head-to-tail configuration [26]. As such they are known as tandemly replicated opsins. The human *LWS* and *MWS* genes are located downstream of a locus control region which has shown to interact with the promoters of *LWS* and *MWS* [27]. Both the *LWS* and *MWS* opsins in humans are *LWS*-type opsins, and human *LWS* and *MWS* and zebrafish *lws1* and *lws2* evolved from an ancestral *LWS* opsin gene [28].

Extensive research has been dedicated to determining the factors that control cone subtype patterning in humans and other species. *Tbx2a* and *tbx2b* are required for UV cone development in zebrafish while *foxq2* is important in specifying S cones [29, 30]. *Gdf6a* is required for sws2 expression [31]. *Nrl* is a key regulator of rod fate in multiple species, and *nr2e3*, a target of *nrl*, is also required for rod development [29, 32]. Interestingly, however, *nrl* is not necessary for rod specification in adult zebrafish [33]. Thyroid hormone receptor *thrb2* is required for green cone development in mice and L cone development in zebrafish [34, 35]. Further, a gradient of thyroid hormone signaling is responsible for the M:S cone gradient in the mouse retina, promoting the expression of green-sensitive opsin [36]. Retinoid x receptor gamma (*rxrg*) is also required for S cone patterning in mice [37]. While the literature is extensive on cone subtype patterning, the mechanisms by which tandemly replicated cone opsin genes are regulated remain largely unknown. Previous work in our lab has shown that *lws1* and *lws2* are endogenously regulated by thyroid hormone (TH) and retinoic acid (RA), and that exogenous TH treatment alters the expression of these opsins in larvae and juveniles [38, 39]. Further, TH appears to have a conserved role in redshifting cone opsin expression, as it also regulates the tandemly replicated *rh2* array, and suppresses *sws* opsins in zebrafish, salmonids (Rob 18,41) and mammals (Rob 15,39) [36, 38, 40-42].

New studies show that TH and *thrb2* are important in regulating multiple genes that exhibit gradient expression in the mouse retina, implicating TH in determining spatial patterning of many non-opsin photoreceptor transcripts [43]. Retinoic acid receptors are also essential in photoreceptor patterning in the chick and in other species [39, 44].

TH serves as an important endocrine signal in humans and in other species. The thyroid gland synthesizes the thyroid hormones, thyroxine (T4) and triiodothyronine (T3). T3 is the more active form of thyroid hormone, binding to nuclear receptors at a higher rate than T4 [45]; however, T4 can be converted to T3 in target tissues by the enzyme deiodinase 2 (*dio2*) [46]. Additionally, T3 can be deactivated by *dio3* [46]. T4 is the primary product of the thyroid, and is more abundant than the other thyroid hormones in the blood [47]. T4 is transported through blood to target tissues by thyroid hormone transport proteins [48, 49], and enters cells through the TH transporter MCT8 [50]. After T4 is converted to T3 by *dio2* in the cytoplasm, it diffuses into the nucleus and binds nuclear hormone receptors called thyroid hormone receptors, which function as transcription factors (THRs) [51]. There are two main classes of thyroid hormone receptors, alpha thyroid hormone receptors (*thra*) and beta thyroid hormone receptors (*thrb*) [52]. The alpha THRs are expressed throughout the body, while the beta THRs are mainly found in nervous system structures, including the retina [49]. Thyroid hormone receptors alter transcription by binding to thyroid hormone response elements (TREs) on DNA (usually AGGTCA or similar sequences) [53-55]. The canonical model for nuclear hormone receptor function is that unliganded TRs recruit corepressors to block gene expression and liganded TRs recruit coactivators [45]. Interestingly, some beta TRs function noncanonically. Indeed, it has been shown that both liganded and unliganded forms of *thrb2* can associate with coactivators and promote transcription of positively regulated genes [56], though the activity level of liganded receptor is higher. Further, *thrb1*, a splice variant of *thrb2* has been shown to control gene expression by altering ratios of coactivators and corepressors, rather than recruiting either coactivators or corepressors [57]. Thyroid hormone receptors have the ability to homodimerize or heterodimerize, and they have been shown to heterodimerize with retinoid x receptors (RXRs) [54, 58].

Retinoic acid (RA) serves as another key developmental signal in retinal development and cone subtype patterning. RA is considered a paracrine signal, meaning it is produced by cells that are nearby the target cell [59]. RA is synthesized by aldehyde dehydrogenase and degraded by cytochrome P450, encoded by the gene *cyp26*. Retinoic acid binds to nuclear retinoic acid receptors (RARs), and RARs can heterodimerize with retinoid X receptors (RXRs) to modulate transcription by binding to retinoic acid response elements (RAREs) [59]. RA is essential for patterning the high acuity area (HAA) in the chick retina; specifically, lower retinoic acid signaling promotes the formation of the HAA [60] chick. Further, the expression of *cyp26a1*, an RA-degrading enzyme, was found to be expressed in the presumptive fovea in the human embryonic retina [60], and RA also regulates the zebrafish *lws* array [39]. In zebrafish, there is evidence that retinoic acid receptors do not function through an "all or nothing" mechanism in which they act as transcriptional repressors in the absence of ligand and activators when ligand is available; but rather, that their function is time and context-dependent [61].

Thyroid hormone signaling is essential for metamorphoses in fish and amphibians, triggering a vast array of postembryonic changes in an organism, including body structure, pigmentation, and visual system function, which are accompanied by a change in habitat and/or ecological niche [62-65]. In teleosts (ray-finned fish), downregulation of thyrotropin by T4 allows for an increase in whole-body T4 levels and subsequently more thyroid hormone signaling [64]. In flatfish, the symmetric larva develops into an asymmetric juvenile (one eye migrating to the other side of the head) and shifts habitat from the open water to the benthic zone [66]. In zebrafish, jaw morphology and feeding strategy change [65]. Across several fish species, skin pigmentation is altered, and the adult pattern begins to develop [64]. In salmonids, TH is an important regulator of smolification, a post-embryonic life stage transition that occurs as juveniles change from freshwater-dwelling to saltwater-dwelling [67]. During smoltification, skin pigmentation lightens and cone photoreceptor subtypes switch, redshifting retinal spectral sensitivity [40, 68]. Indeed, TH is important in metamorphosis-associated changes in cone photoreceptor subtype patterning in several fish species. In coho salmon and rainbow trout, TH signaling induces a shift in opsin expression from UV-sensing *sws1* to blue-sensing *sws2* [40, 69]. TH signaling also underlies a change in opsin expression during metamorphosis in flounder as they move to a dimmer environment

[70, 71]. Additionally, salmonids are known to experience a seasonal shift in opsin chromophore from vitamin A1 to A2, which redshifts opsin spectral sensitivity [72], and TH has been shown to induce the expression of *cyp27c1*, an enzyme that converts vitamin A1 to A2, providing an additional mechanism through which TH redshifts retinal sensitivity naturally in fish [38, 73].

Photoreceptor degeneration is associated with blinding disorders, such as retinitis pigmentosa and age-related macular degeneration [74, 75]. Photoreceptors in mammals cannot regenerate, so cell replacement strategies represent a promising option for helping patients with advanced retinal degeneration. Retinal organoids represent potential sources of cells for retinal transplant, and a recent study has shown that retinal organoid-derived human photoreceptors incorporate into the degenerating mouse retina and establish functional synaptic connections, lasting for up to 6 months in the recipient retina [76]. Retinal organoids are three-dimensional, laminated retinal structures that contain functioning photoreceptors and other retinal cell types in layers similar to the structure in a normal human retina [77]. Retinal organoids are also helpful in investigating the development of cell types in the human retina. Recently, work in retinal organoids has shown that thyroid hormone receptor beta 2 (*thrb2*) is important in promoting L/M cone fate as opposed to S cone fate in the human retina [78].

In this dissertation, we sought to further scientific understanding of cone subtypes and the role of TH in cone subtype patterning. In our first study, we explore the transcriptional heterogeneity between and within the LWS cone subtypes in zebrafish beyond opsin expression. Chapter 2 shows our findings that LWS1 and LWS2 cones differ beyond opsin expression. Using bulk RNA-Seq, we found 95 LWS1-enriched transcripts and 186 LWS2-enriched transcripts (FC>2, FDR<0.05). Multiplex *in situ* hybridization revealed underlying heterogeneity within *lws1* and *lws2*-expressing populations. For example, gamma transducin *gngt2b* transcript was shown to be enriched in LWS2 cones; though many LWS2 cones expressed *gngt2b*, some did not. Experiments in which zebrafish larvae were treated with exogenous TH showed that the expression of some but not all of the differentially expressed transcripts in LWS1 and LWS2 cones are plastic to exogenous TH treatment, indicating that

transcriptional differences between LWS1 and LWS2 cones are likely controlled by multiple signals including TH.

Chapter 3 describes our investigation of the extent to which photoreceptor gene expression remains plastic to TH in zebrafish. Using a transgenic *lws* reporter line, multiplex fluorescence hybridization chain reaction (HCR) *in situ* hybridization, and qPCR, we determined that opsin gene expression (and the expression of other photoreceptor genes) does remain plastic to TH treatment in adult zebrafish. This plasticity was observed within 7 hours. Further, we found that exogenous TH treatment alters skin pigmentation patterns in adult zebrafish in as little as 5 days, building upon previous studies showing that ablating the thyroid of adult zebrafish can alter pigmentation patterns after 6 months. In total, our results revealed a remarkable level of TH-mediated plasticity in the adult zebrafish.

Chapter 4 updates our work in determining the role of TH and RA in regulating opsin expression in human embryonic stem cell (ESC) or induced pluripotent stem cell (IPSC)-derived retinal organoids (retina cups, RCs), and proposes a multifaceted strategy for examining opsin expression in retinal organoids. Building upon previous work in our lab that shows how TH and RA alter opsin expression dynamics in 90-180 day old RCs, our more recent experiments show how combinatorial TH/RA treatments affect opsin expression, and explores variations in treatment timing and concentration. We also show that multiplex HCR *in situ* hybridization is a powerful tool for imaging RCs and determining whether and where opsins are being expressed, and we introduce droplet digital PCR (ddPCR) as an additional, powerful method for quantifying opsin transcript abundance from RCs.

Understanding the regulation of gene expression in retinal cell types is essential for improving treatments for retinal diseases. The CDC estimates that 80 million Americans have potentially blinding eye diseases, notes that vision loss is among the top ten causes of disability, and predicts that the cost of vision loss exceeds $35 billion [79, 80] It is the ultimate hope of science that advancing our knowledge of the retina, retinal development, and retinal diseases can help people experiencing vision loss and retinal disease. This body of work is intended to provide another small step toward that ultimate goal.

References

1. Masland, R.H., *The neuronal organization of the retina.* Neuron, 2012. **76**(2): p. 266-80.
2. Kolb, H., *Glial Cells of the Retina*, in *Webvision*. 2001, Moran Eye Center.
3. Fu, Y. *Phototransduction in Rods and Cones*. Webvision 2018 July 30, 2018 6/29/23].
4. *Central Projections of Retinal Ganglion Cells*, in *Neuroscience*, A.G. Purves D, Fitzpatrick D, et al., editors, Editor. 2001, Sinauer Associates: Sunderland, MA.
5. Schmitt, E.A. and J.E. Dowling, *Early-eye morphogenesis in the zebrafish Brachydanio rerio.* J Comp Neurol, 1994. **344**: p. 532-542.
6. Schmitt, E.A. and J.E. Dowling, *Early Retinal Development in the Zebrafish, Danio rerio: Light and Electron Microscopic Analyses.* J Comp Neurol, 1999. **404**: p. 515-536.
7. YR, B., *Embryology of the eye and its adnexae.* Dev Ophthalmol, 1992. **21**: p. 1-142.
8. Loosli, F., R.W. Koster, M. Carl, A. Krone, and J. Wittbrodt, *Six3, a medaka homologue of the Drosophila homeobox gene sine oculis is expressed in the anterior embryonic shield and the developing eye.* Mechanisms of Development, 1998. **74**: p. 159-164.
9. Nornes, S., M. Clarkson, I. Mikkola, M. Pedersen, A. Bardsley, J.P. Martinez, S. Krauss, and T. Johansen, *Zebrafish contains two Pax6 genes involved in eye development.* Mechanisms of Development, 1998. **77**: p. 185-196.
10. Lister, J.A., J. Close, and D.W. Raible, *Duplicate mitf genes in zebrafish: complementary expression and conservation of melanogenic potential.* Dev Biol, 2001. **237**(2): p. 333-44.
11. Brown, N.L., S. Kanekar, M.L. Vetter, P.K. Tucker, D.L. Gemza, and T. Glaser, *Math5 encodes a murine basic helix-loop-helix transcription factor expressed during early stages of retinal neurogenesis.* Development, 1998. **125**: p. 4821-4833.
12. Kay, J.N., T. Roeser, K.C. Finger-Baier, W. Staub, and H. Baier, *Retinal Ganglion Cell Genesis Requires lakritz, a Zebrafish atonal Homolog.* Neuron, 2001. **30**: p. 725-736.
13. Fujitani, Y., S. Fujitani, H. Luo, F. Qiu, J. Burlison, Q. Long, Y. Kawaguchi, H. Edlund, R.J. MacDonald, T. Furukawa, T. Fujikado, M.A. Magnuson, M. Xiang, and C.V. Wright, *Ptf1a determines horizontal and amacrine cell fates during mouse retinal development.* Development, 2006. **133**(22): p. 4439-50.
14. Chow, R.L., B. Volgyi, R.K. Szilard, D. Ng, C. McKerlie, S.A. Bloomfield, D.G. Birch, and R.R. McInnes, *Control of late off-center cone bipolar cell differentiation and visual signaling by the homeobox gene Vsx1.* Proc Natl Acad Sci U S A, 2004. **101**(6): p. 1754-1759.
15. Bassett, E.A. and V.A. Wallace, *Cell fate determination in the vertebrate retina.* Trends Neurosci, 2012. **35**(9): p. 565-73.
16. Fossat, N., C. Le Greneur, F. Beby, S. Vincent, P. Godement, G. Chatelain, and T. Lamonerie, *A new GFP-tagged line reveals unexpected Otx2 protein localization in retinal photoreceptors.* BMC Dev Biol, 2007. **7**: p. 122.
17. Katoh, K., Y. Omori, A. Onishi, S. Sato, M. Kondo, and T. Furukawa, *Blimp1 suppresses Chx10 expression in differentiating retinal photoreceptor precursors to ensure proper photoreceptor development.* J Neurosci, 2010. **30**(19): p. 6515-26.
18. Chen, S., Q.-L. Wang, Z. Nie, H. Sun, G. Lennon, N.G. Copeland, D.J. Gilbert, N.A. Jenkins, and D.J. Zack, *Crx, a Novel Otx-like Paired-Homeodomain Protein, Binds to and Transactivates Photoreceptor Cell-Specific Genes.* Neuron, 1997. **19**: p. 1017–1030.
19. Mears, A.J., M. Kondo, P.K. Swain, Y. Takada, R.A. Bush, T.L. Saunders, P.A. Sieving, and A. Swaroop, *Nrl is required for rod photoreceptor development.* Nat Genet, 2001. **29**(4): p. 447-52.
20. Yoshida, S., A.J. Mears, J.S. Friedman, T. Carter, S. He, E. Oh, Y. Jing, R. Farjo, G. Fleury, C. Barlow, A.O. Hero, and A. Swaroop, *Expression profiling of the developing and mature Nrl-/- mouse retina: identification of retinal disease candidates and transcriptional regulatory targets of Nrl.* Hum Mol Genet, 2004. **13**(14): p. 1487-503.

21. Fadool, J.M. and J.E. Dowling, *Zebrafish: a model system for the study of eye genetics.* Prog Retin Eye Res, 2008. **27**(1): p. 89-110.
22. Baden, T. and D. Osorio, *The Retinal Basis of Vertebrate Color Vision.* Annu Rev Vis Sci, 2019. **5**: p. 177-200.
23. Bartel, P., T. Yoshimatsu, F.K. Janiak, and T. Baden, *Spectral inference reveals principal cone-integration rules of the zebrafish inner retina.* Curr Biol, 2021. **31**(23): p. 5214-5226 e4.
24. Chinen, A., T. Hamaoka, Y. Yamada, and S. Kawamura, *Gene Duplication and Spectral Diversification of Cone Visual Pigments of Zebrafish.* Genetics, 2003. **163**: p. 663–675.
25. Jeremy Nathans, D.T., David S. Hogness, *Molecular Genetics of Human Color Vision: The Genes Encoding Blue, Green, and Red Pigments.* Science, 1986. **232**.
26. Vollrath, D., J. Nathans, and R.W. Davis, *Tandem Array of Human Visual Pigment Genes at Xq28.* Science, 1988. **240**: p. 1669-1672.
27. Peng, G.H. and S. Chen, *Active opsin loci adopt intrachromosomal loops that depend on the photoreceptor transcription factor network.* Proc Natl Acad Sci U S A, 2011. **108**(43): p. 17821-6.
28. Hofmann, C.M. and K.L. Carleton, *Gene duplication and differential gene expression play an important role in the diversification of visual pigments in fish.* Integr Comp Biol, 2009. **49**(6): p. 630-43.
29. Angueyra, J.M., V.P. Kunze, L.K. Patak, H. Kim, K. Kindt, and W. Li, *Transcription factors underlying photoreceptor diversity.* Elife, 2023. **12**.
30. Ogawa, Y., T. Shiraki, Y. Fukada, and D. Kojima, *Foxq2 determines blue cone identity in zebrafish.* Sci Adv, 2021. **7**.
31. DuVal, M.G. and W.T. Allison, *Photoreceptor Progenitors Depend Upon Coordination of gdf6a, thrbeta, and tbx2b to Generate Precise Populations of Cone Photoreceptor Subtypes.* Invest Ophthalmol Vis Sci, 2018. **59**(15): p. 6089-6101.
32. Xie, S., S. Han, Z. Qu, F. Liu, J. Li, S. Yu, J. Reilly, J. Tu, X. Liu, Z. Lu, X. Hu, T.A. Yimer, Y. Qin, Y. Huang, Y. Lv, T. Jiang, X. Shu, Z. Tang, H. Jia, F. Wong, and M. Liu, *Knockout of Nr2e3 prevents rod photoreceptor differentiation and leads to selective L-/M-cone photoreceptor degeneration in zebrafish.* Biochim Biophys Acta Mol Basis Dis, 2019. **1865**(6): p. 1273-1283.
33. Oel, A.P., G.J. Neil, E.M. Dong, S.D. Balay, K. Collett, and W.T. Allison, *Nrl Is Dispensable for Specification of Rod Photoreceptors in Adult Zebrafish Despite Its Deeply Conserved Requirement Earlier in Ontogeny.* iScience, 2020. **23**(12): p. 101805.
34. Ng, L., J.B. Hurley, B. Dierks, M. Srinivas, C. Saltó, B. Vennström, T.A. Reh, and D. Forrest, *A thyroid hormone receptor that is required for the development of green cone photoreceptors.* Nature Genetics, 2001. **27**: p. 94-98.
35. Suzuki, S.C., A. Bleckert, P.R. Williams, M. Takechi, S. Kawamura, and R.O. Wong, *Cone photoreceptor types in zebrafish are generated by symmetric terminal divisions of dedicated precursors.* Proc Natl Acad Sci U S A, 2013. **110**(37): p. 15109-14.
36. Roberts, M.R., M. Srinivas, D. Forrest, G.M.d. Escoba, and T.A. Reh, *Making the gradient: Thyroid hormone regulates cone opsin expression in the developing mouse retina.* Proc Natl Acad Sci U S A, 2006. **103**(16): p. 6218–6223.
37. Roberts, M.R., A. Hendrickson, C.R. McGuire, and T.A. Reh, *Retinoid X receptor (gamma) is necessary to establish the S-opsin gradient in cone photoreceptors of the developing mouse retina.* Invest Ophthalmol Vis Sci, 2005. **46**(8): p. 2897-904.
38. Mackin, R.D., R.A. Frey, C. Gutierrez, A.A. Farre, S. Kawamura, D.M. Mitchell, and D.L. Stenkamp, *Endocrine regulation of multichromatic color vision.* Proc Natl Acad Sci U S A, 2019. **116**(34): p. 16882-16891.
39. Mitchell, D.M., C.B. Stevens, R.A. Frey, S.S. Hunter, R. Ashino, S. Kawamura, and D.L. Stenkamp, *Retinoic Acid Signaling Regulates Differential Expression of the Tandemly-*

Duplicated Long Wavelength-Sensitive Cone Opsin Genes in Zebrafish. PLoS Genet, 2015. **11**(8): p. e1005483.
40. Raine, J.C. and C.W. Hawryshyn, *Changes in thyroid hormone reception precede SWS1 opsin downregulation in trout retina.* J Exp Biol, 2009. **212**(17): p. 2781-8.
41. Gan, K.J. and I. Novales Flamarique, *Thyroid hormone accelerates opsin expression during early photoreceptor differentiation and induces opsin switching in differentiated TRalpha-expressing cones of the salmonid retina.* Dev Dyn, 2010. **239**(10): p. 2700-13.
42. Glaschke, A., J. Weiland, D. Del Turco, M. Steiner, L. Peichl, and M. Glosmann, *Thyroid hormone controls cone opsin expression in the retina of adult rodents.* J Neurosci, 2011. **31**(13): p. 4844-51.
43. Aramaki, M., X. Wu, H. Liu, Y. Liu, Y.W. Cho, M. Song, Y. Fu, L. Ng, and D. Forrest, *Transcriptional control of cone photoreceptor diversity by a thyroid hormone receptor.* Proc Natl Acad Sci U S A, 2022. **119**(49): p. e2209884119.
44. Trimarchi, J.M., S. Harpavat, N.A. Billings, and C.L. Cepko, *Thyroid hormone components are expressed in three sequential waves during development of the chick retina.* BMC Dev Biol, 2008. **8**: p. 101.
45. Brent, G.A., *Mechanisms of thyroid hormone action.* J Clin Invest, 2012. **122**(9): p. 3035-43.
46. Bianco, A.C. and P.R. Larsen, *Cellular and Structural Biology of the Deiodinases.* Thyroid, 2005. **15**: p. 777-786.
47. Peeters, R. and T.J. Visser, *Metabolism of Thyroid Hormone*, in *Endotext*. 2017, MDText.com, Inc: South Dartmouth, MA.
48. Bartalena, L. and J. Robbins, *Thyroid hormone transport proteins.* Clin Lab Med, 1993. **13**(3): p. 583-598.
49. Kogai, T. and G.A. Brent, *Thyroid Hormones (T4, T3)*, in *Endocrinology*, S. Melmed and P.M. Conn, Editors. 2005, Humana Press.
50. Arjona, F.J., E. de Vrieze, T.J. Visser, G. Flik, and P.H. Klaren, *Identification and functional characterization of zebrafish solute carrier Slc16a2 (Mct8) as a thyroid hormone membrane transporter.* Endocrinology, 2011. **152**(12): p. 5065-73.
51. Bianco, A.C., A. Dumitrescu, B. Gereben, M.O. Ribeiro, T.L. Fonseca, G.W. Fernandes, and B. Bocco, *Paradigms of Dynamic Control of Thyroid Hormone Signaling.* Endocr Rev, 2019. **40**(4): p. 1000-1047.
52. Hahm, J.B., A.C. Schroeder, and M.L. Privalsky, *The two major isoforms of thyroid hormone receptor, TRalpha1 and TRbeta1, preferentially partner with distinct panels of auxiliary proteins.* Mol Cell Endocrinol, 2014. **383**(1-2): p. 80-95.
53. Shibusawa, N., A.N. Hollenberg, and F.E. Wondisford, *Thyroid hormone receptor DNA binding is required for both positive and negative gene regulation.* J Biol Chem, 2003. **278**(2): p. 732-8.
54. Wu, Y., B. Xu, and R.J. Koenig, *Thyroid hormone response element sequence and the recruitment of retinoid X receptors for thyroid hormone responsiveness.* J Biol Chem, 2001. **276**(6): p. 3929-36.
55. Paquette, M.A., E. Atlas, M.G. Wade, and C.L. Yauk, *Thyroid hormone response element half-site organization and its effect on thyroid hormone mediated transcription.* PLoS One, 2014. **9**(6): p. e101155.
56. Oberste-Berghaus, C., K. Zanger, K. Hashimoto, R.N. Cohen, A.N. Hollenberg, and F.E. Wondisford, *Thyroid hormone-independent interaction between the thyroid hormone receptor beta2 amino terminus and coactivators.* J Biol Chem, 2000. **275**(3): p. 1787-92.
57. Shabtai, Y., N.K. Nagaraj, K. Batmanov, Y.-W. Cho, Y. Guan, C. Jiang, J. Remsberg, D. Forrest, and M.A. Lazar, *A coregulator shift, rather than the canonical switch, underlies thyroid hormone action in the liver.* Genes & Development, 2021. **35**.
58. Kojetin, D.J., E. Matta-Camacho, T.S. Hughes, S. Srinivasan, J.C. Nwachukwu, V. Cavett, J. Nowak, M.J. Chalmers, D.P. Marciano, T.M. Kamenecka, A.I. Shulman, M. Rance, P.R.

Griffin, J.B. Bruning, and K.W. Nettles, *Structural mechanism for signal transduction in RXR nuclear receptor heterodimers.* Nat Commun, 2015. **6**: p. 8013.
59. Cunningham, T.J. and G. Duester, *Mechanisms of retinoic acid signalling and its roles in organ and limb development.* Nat Rev Mol Cell Biol, 2015. **16**(2): p. 110-23.
60. da Silva, S. and C.L. Cepko, *Fgf8 Expression and Degradation of Retinoic Acid Are Required for Patterning a High-Acuity Area in the Retina.* Dev Cell, 2017. **42**(1): p. 68-81 e6.
61. Waxman, J.S. and D. Yelon, *Comparison of the expression patterns of newly identified zebrafish retinoic acid and retinoid X receptors.* Dev Dyn, 2007. **236**(2): p. 587-95.
62. Buchholz, D.R., *Xenopus metamorphosis as a model to study thyroid hormone receptor function during vertebrate developmental transitions.* Mol Cell Endocrinol, 2017. **459**: p. 64-70.
63. Brown, D.D., *The role of thyroid hormone in zebrafish and axolotl development.* Proc Natl Acad Sci U S A, 1997. **94**: p. 13011–13016.
64. Campinho, M.A., *Teleost Metamorphosis: The Role of Thyroid Hormone.* Front Endocrinol (Lausanne), 2019. **10**: p. 383.
65. Galindo, D., E. Sweet, Z. DeLeon, M. Wagner, A. DeLeon, C. Carter, S.K. McMenamin, and W.J. Cooper, *Thyroid hormone modulation during zebrafish development recapitulates evolved diversity in danionin jaw protrusion mechanics.* Evol Dev, 2019. **21**(5): p. 231-246.
66. Inui, Y. and S. Miwa, *Thyroid Hormone Induces Metamorphosis of Flounder Larvae.* Gen Comp Endocrinol, 1985. **60**: p. 450-454.
67. Holzer, G. and V. Laudet, *Thyroid hormones: a triple-edged sword for life history transitions.* Curr Biol, 2015. **25**(8): p. R344-7.
68. Bjornsson, B.T., S.O. Stefansson, and S.D. McCormick, *Environmental endocrinology of salmon smoltification.* Gen Comp Endocrinol, 2011. **170**(2): p. 290-8.
69. Cheng, C.L. and I.N. Flamarique, *Chromatic organization of cone photoreceptors in the retina of rainbow trout: single cones irreversibly switch from UV (SWS1) to blue (SWS2) light sensitive opsin during natural development.* J Exp Biol, 2007. **210**(Pt 23): p. 4123-35.
70. Shi, Y., Y. Shi, W. Ji, X. Li, Z. Shi, J. Hou, W. Li, and Y. Fu, *Thyroid Hormone Signaling Is Required for Dynamic Variation in Opsins in the Retina during Metamorphosis of the Japanese Flounder (Paralichthys olivaceus).* Biology (Basel), 2023. **12**(3).
71. Mader, M.M. and D.A. Cameron, *Effects of induced systemic hypothyroidism upon the retina: Regulation of thyroid hormone receptor alpha and photoreceptor production.* Mol Vis, 2006. **12**: p. 915-930.
72. Temple, S.E., E.M. Plate, S. Ramsden, T.J. Haimberger, W.M. Roth, and C.W. Hawryshyn, *Seasonal cycle in vitamin A1/A2-based visual pigment composition during the life history of coho salmon (Oncorhynchus kisutch).* J Comp Physiol A Neuroethol Sens Neural Behav Physiol, 2006. **192**(3): p. 301-13.
73. Enright, J.M., M.B. Toomey, S.Y. Sato, S.E. Temple, J.R. Allen, R. Fujiwara, V.M. Kramlinger, L.D. Nagy, K.M. Johnson, Y. Xiao, M.J. How, S.L. Johnson, N.W. Roberts, V.J. Kefalov, F.P. Guengerich, and J.C. Corbo, *Cyp27c1 Red-Shifts the Spectral Sensitivity of Photoreceptors by Converting Vitamin A1 into A2.* Curr Biol, 2015. **25**(23): p. 3048-57.
74. Hartong, D.T., E.L. Berson, and T.P. Dryja, *Retinitis pigmentosa.* Lancet, 2006. **368**(9549): p. 1795-809.
75. Fleckenstein, M., T.D.L. Keenan, R.H. Guymer, U. Chakravarthy, S. Schmitz-Valckenberg, C.C. Klaver, W.T. Wong, and E.Y. Chew, *Age-related macular degeneration.* Nat Rev Dis Primers, 2021. **7**(1): p. 31.
76. Gasparini, S.J., K. Tessmer, M. Reh, S. Wieneke, M. Carido, M. Volkner, O. Borsch, A. Swiersy, M. Zuzic, O. Goureau, T. Kurth, V. Busskamp, G. Zeck, M.O. Karl, and M. Ader, *Transplanted human cones incorporate into the retina and function in a murine cone degeneration model.* J Clin Invest, 2022. **132**(12).

77. Zhong, X., C. Gutierrez, T. Xue, C. Hampton, M.N. Vergara, L.H. Cao, A. Peters, T.S. Park, E.T. Zambidis, J.S. Meyer, D.M. Gamm, K.W. Yau, and M.V. Canto-Soler, *Generation of three-dimensional retinal tissue with functional photoreceptors from human iPSCs.* Nat Commun, 2014. **5**: p. 4047.
78. Eldred, K.C., S.E. Hadyniak, K.A. Hussey, B. Brenerman, P.W. Zhang, X. Chamling, V.M. Sluch, D.S. Welsbie, S. Hattar, J. Taylor, K. Wahlin, D.J. Zack, and R.J. Johnston, Jr., *Thyroid hormone signaling specifies cone subtypes in human retinal organoids.* Science, 2018. **362**(6411).
79. Saaddine, V. Narayan, and Vinicor. *Vision Loss: A Public Health Problem*. Vision Health Initiative 2019 December 19, 2022 [cited 2023 6/29/23].
80. Rein, D.B., P. Zhang, K.E. Wirth, P.P. Lee, T.J. Hoerger, N. McCall, R. Klein, J.M. Tielsch, S. Vijan, and i. Saaddine, *The Economic Burden of Major Adult Visual Disorders in the United States.* Arch Ophthalmol, 2006. **124**: p. 1754-1760.

Chapter 2: Long wavelength-sensing cones of zebrafish retina exhibit multiple layers of transcriptional heterogeneity

Ashley A. Farre*, Chi Sun*, Margaret R. Starostik, Samuel S. Hunter, Milton A. English, Audrey Duncan, Abirami Santhanam, Eyad Shihabeddin, John O'Brien, Anand Swaroop, and Deborah L. Stenkamp

(*co-first author)

Abstract

Understanding how photoreceptor genes are regulated is important for investigating retinal development and disease. While much is known about gene regulation in cones, the mechanism by which tandemly-replicated opsins, such as human long wavelength-sensitive and middle wavelength-sensitive opsins, are differentially regulated remains elusive. In this study, we aimed to further our understanding of transcriptional heterogeneity in cones that express tandemly-replicated opsins and the regulation of such differential expression using zebrafish, which express the tandemly-replicated opsins *lws1* and *lws2*. We performed bulk and single cell RNA-Seq of LWS1 and LWS2 cones, evaluated expression patterns of selected genes of interest using multiplex fluorescence in situ hybridization, and used exogenous thyroid hormone (TH) treatments to test selected genes for potential control by thyroid hormone: a potent, endogenous regulator of *lws1* and *lws2* expression. Our studies indicate that additional transcriptional differences beyond opsin expression exist between LWS1 and LWS2 cones. Bulk RNA-Seq results showed 95 transcripts enriched in LWS1 cones and 186 transcripts enriched in LWS2 cones (FC>2, FDR<0.05). In situ hybridization results also reveal underlying heterogeneity within the *lws1*- and *lws2*-expressing populations. This heterogeneity is evident in cones of mature zebrafish, and further heterogeneity is revealed in transcriptional responses to TH treatments. We found some evidence of coordinate regulation of *lws* opsins and other genes by exogenous TH in LWS1 vs LWS2 cones, as well as evidence of gene regulation not mediated by TH. The transcriptional differences between LWS1 and LWS2 cones are likely controlled by multiple signals, including TH.

Introduction

Cone photoreceptors of vertebrates express specific opsins that maximally detect specific wavelengths of light. The presence of multiple types of cones that express opsin proteins with different peak spectral tuning allows for color vision. Humans have three different types of cones (red-, green-, and blue-sensitive) that each express a specific cone opsin: long wavelength-sensitive (LWS), middle wavelength sensitive (MWS), and short wavelength sensitive (SWS) opsins, respectively [1]. The genes encoding the human LWS and MWS opsins are arranged in tandem on the X chromosome [2], and the mechanism by which they are regulated remains largely unknown, although several models have been suggested [3-5]. Mutations in these opsin genes have been associated with multiple visual disorders including color vision deficiencies, high myopia, X-linked cone dysfunction, and X-linked cone dystrophy [6-10].

Although mice remain the predominant model system in molecular and cellular biology, and have been instrumental for vision research, they lack tandemly replicated opsin genes. The only mammals known to share this gene structure with humans are other primates and bats [11], for which genetic and other experimental manipulations that would be useful for the study of gene expression are severely limited and/or practically difficult. The zebrafish, however, is a vertebrate model organism that does possess tandemly replicated opsins [12], and for which many genetic tools have been developed [13]. Further, the tandemly duplicated zebrafish *lws* opsin genes and the human *LWS/MWS* opsin genes evolved from a common ancestral long wavelength-sensing opsin gene. Therefore, the zebrafish provides an excellent opportunity to study gene expression in cones that express tandemly replicated opsins. Previous research using the zebrafish and other model organisms has shown that thyroid hormone (TH) is essential in determining cone subtype identity and patterning [14-18]. This appears to be true for humans as well, as shown for stem cell-derived retinal organoids [19]. Recent studies from our lab have also demonstrated that TH can promote the expression of some tandemly replicated opsins over others, a conserved phenomenon for both of the tandemly replicated cone opsin arrays in zebrafish. In both the *lws* and *rh2* (middle wavelength-sensitive in nonmammalian vertebrates) arrays, TH promoted the expression of the long wavelength-shifted member(s) of the array at the

expense of the more short-wavelength-shifted member(s) [14]. Further, treatment with exogenous TH can cause larval cones expressing one member of the *lws1/lws2* tandem array to "switch" and begin expressing another member of the array [14].

Larval, juvenile, and adult zebrafish have characteristic *lws* opsin spatiotemporal expression patterns. In larval zebrafish, *lws2* expression begins at 40 hours post-fertilization (hpf) in the central and dorsal retina while *lws1* expression begins at approximately 5 days post-fertilization (dpf) in the ventral region. In adults, ventral and nasal LWS cones express *lws1* while central and dorsal LWS cones express *lws2* [20, 21]. Larval and juvenile zebrafish made experimentally athyroid display abnormal *lws1* vs. *lws2* expression patterns, supporting endogenous roles for TH in the regulation of their differential expression [14].

In this study, we aimed to further our understanding of the cones that express tandemly replicated opsins and the regulation of opsin expression by performing bulk and single cell RNA-Seq of LWS1 and LWS2 cones. We then investigated spatial patterning of several transcripts found to be differential expressed, in adult whole retina, and in larval retinas with or without exogenous thyroid hormone treatment. Our goals were to determine whether LWS1 vs. LWS2 cone subtypes exhibit transcriptional differences beyond opsin expression, to probe potential mechanisms for opsin switching and differential tandemly replicated opsin expression, and to investigate the role of TH in regulating differences between cone subtypes that express tandemly replicated opsins. Our studies indicate that additional transcriptional differences exist between these cone subtypes beyond opsin expression, and reveal underlying heterogeneity within the *lws1*- and *lws2*-expressing populations. This heterogeneity is evident in cones of mature and larval zebrafish, and further heterogeneity is revealed in transcriptional responses to TH treatments.

Methods

Animals.

Zebrafish were propagated and maintained as described [22], on recirculating, monitored, and filtered system water, on a 14:10 light/dark cycle, at 28.5°C. Procedures involving animals were approved by the Animal Care and Use Committees of the University of Idaho and of the University of Texas Health Science Center at Houston. Wild-type (WT)

zebrafish were of a strain originally provided by Scientific Hatcheries (now Aquatica Tropicals, Plant City, FL) and AB (RRID:ZIRC_ZL1) from the Zebrafish International Resource Center at the University of Oregon. The *lws:PAC(H)* transgenic line harbors a PAC clone that encompasses the *lws* locus, modified such that a GFP-polyA sequence, inserted after the *lws1* promoter, reports expression of *lws1*, and an RFP (dsRedExpress)-polyA sequence, inserted after the *lws2* promoter, reports expression of *lws2* [21]. This line was the kind gift of Shoji Kawamura and the RIKEN international resource facility. The *thrb2:tdTomato* transgenic line expresses the tdTomato reporter under control of *the thyroid hormone receptor beta 2 promoter*, resulting in tdTomato in all adult LWS cones [23]. This line was the kind gift of Rachel Wong. In this study larval (4 dpf) and adult (0.5 – 1.5 years; both sexes) zebrafish were used.

Retinal Tissue Dissociation and Fluorescence-Activated Cell Sorting (FACS).

Dissociation and FACS were carried out as previously reported [24, 25], for bulk RNA-Seq and for qPCR. In brief, adult *lws:PAC(H)* and *thrb2:tdTomato* zebrafish were collected near the time of light onset but maintained in the dark (dark-adapted), euthanized with MS-222, and retinal tissues dissected away from other ocular tissues including the RPE and collected into cold RNAse-free phosphate-buffered saline (PBS). Retinas were dissociated for 10 min at 37°C in a filtered buffer containing papain, trypsin, neutral protease, catalase, and superoxide dismutase. The reaction was quenched with heat-inactivated fetal bovine serum, and samples resuspended in DNAseI for 10 min at room temperature. Samples were pelleted and resuspended in RNAse-free PBS prior to FACS. *Lws:PAC(H)* samples were sorted with a SONY Cell Sorter SH800 based upon GFP and RFP fluorescence, and collected into TRIzol LS or lysis buffer from the Machery-Nagel RNA extraction kit [25]. *Thrb2:tdTomato* samples were sorted using the same instrument and conditions, but based upon tdTomato fluorescence intensity and the scatter characteristics [25].

Bulk RNA-Sequencing (bulk RNA-Seq).

The quality of isolated RNA was evaluated using the Bioanalyzer 2100 RNA 6000 Nano assay (Agilent Technologies). For samples with a RIN score greater than 8.0, sequencing libraries were constructed according to the manufacturer's protocol using the

TruSeq® RNA Library Preparation Kit (Illumina) with 5µg total RNA as input whereby ribosomal RNA was removed by poly-A selection using Illumina. Illumina sequencing adapters were ligated to each sample. Ligated fragments were then amplified for 12 cycles using primers incorporating unique dual index tags. Libraries were sequenced at the National Eye Institute (NEI) on the Illumina HiSeq 2500 platform, and raw sequencing reads were demultiplexed by NEI. Raw bulk RNA-Seq reads were trimmed for Illumina adapters and quality using Trimmomatic v0.36 [26]. Trimmed reads were aligned to the zebrafish reference genome GRCz11 using STAR v2.5.2a [27] and Salmon v1.0.0 [28]. Approximately 1-3 million reads were mapped per sample library (3 libraries per condition) to zebrafish reference genome GRCz11, with the exception of one *lws1*:GFP+ library, which still provided minimal depth for downstream analyses , and so was included in subsequent analyses to increase statistical power. Additional quality control metrics were evaluated using FastQC v0.11.5 (http://www.bioinformatics.babraham.ac.uk/projects/fastqc/) and HTStream [29]. Data were imported into R (R Core Team, 2017, https://www.R-project.org/ v. 3.5.0) using tximport [30]. Differential expression (DE) analysis was then carried out using DESeq2 [31]. Log2FC, as well as a moderated Log2FC (to normalize for transcripts displaying very low levels of expression) were determined for *lws1*:GFP vs. *lws2*:RFP DE analyses. As additional strategies for identifying transcripts DE in LWS1 vs. LWS2 cones, DE analyses were also carried out for the entire LWS cone population (*thrb2*:tdTomato+) vs. *lws1*:GFP and vs. *lws2*:GFP. Gene ontology analyses were performed using gProfiler.

Retinal Tissue Dissociation and Single-Cell RNA-Seq (scRNA-Seq).

Single-cell library preparation and data analysis are fully described in Santhanam et al. (bioRxiv 2022.10.04.510882). In brief, two female and one male wild-type AB strain zebrafish, age 7 months, were euthanized with MS222 on ice and isolated retina-RPE preparations were pooled in a 3:1 mix of Leibovitz's L-15 medium (Gibco) and Earle's Balanced Salt Solution (EBSS; Gibco). Cells were dissociated with papain solution (50 U/mL; Worthington Biochemical) for 60 min at 28˚C with gentle trituration. Digestion was halted by addition of 2x volume of 0.1% BSA in L15: EBSS medium, and cells were counted and tested for viability. Cell samples were submitted for 3’ scRNA library preparation and sequencing through the Baylor College of Medicine Single Cell Genomics Core facility. The

single-cell library was prepared using a Chromium Next GEM Single Cell 3' Reagent Kit v2 (10x Genomics, Pleasanton, CA). The single-cell library was sequenced with Illumina HiSeq2500.

The single-cell library sequences were initially analyzed using the 10x Genomics CellRanger V2.1.1.0 pipeline. Sequences were aligned to the zebrafish reference genome GRCz11 using CellRanger count, and quality-checked using FASTQC V0.11.9. Over 93% of reads mapped successfully to the genome. The initial alignment and analysis were performed through the Texas Advanced Computing Center (TACC) Lonestar5 computing service. Subsequent analyses of aligned data used the Seurat V2.1.1 [32] package in R V3.6.1. The data were initially filtered to remove low-abundance genes (expressed in fewer than 10 cells), doublets and cells with >5% mitochondrial genes. The dataset contained between 200 and 4000 genes per cell, and 13,551 cells were sequenced/analyzed. PCElbowPlots were performed and 20 principal components were used for downstream analysis of each dataset. PC1 to PC20 were used to construct nearest neighbor graphs in the PCA space followed by Louvain clustering and non-linear dimensional reduction by TSNE to visualize and explore the clusters. Expression levels are expressed in a base 2 log scale.

Thyroid Hormone Treatments.

Stock solutions of tri-iodothyronine (T3) were prepared in DMSO (Sigma), and maintained at -20°C in the dark. Embryos were obtained from WT crosses, with the time of light onset considered the time of fertilization. 0.003% phenylthiourea (PTU) was added to system water at 10-12 hours post-fertilization (hpf) to inhibit melanin synthesis [13]. Prior to T3 treatment, embryos were dechorionated using fine forceps, and the 1000X T3 stock solution was added to system water for a final concentration of 100 nM (DMSO final concentration was 0.1%). Controls were treated with 0.1% DMSO. Treatments took place from 48 to 96 hpf, and solutions were refreshed every 24 hr [14].

RNA Extraction and Quantitative RT-PCR (qPCR).

Total RNA from larval (4 dpf) zebrafish tissues was extracted using the Machery-Nagel kit, and then the Superscript III/IV (Invitrogen) was used to synthesize cDNA template with random primers. Gene-specific primer pairs for qPCR are provided in Supplemental

Table S1. Amplification was performed on a StepOne Real-Time PCR system using SYBR Green or Power Track SYBR Green master mix (Applied Biosystems). Quantification of transcript abundance was relative to the reference transcript (*β-actin*), using the ddCT method. Graphing and statistics were performed in Excel. Sample groups were evaluated for normal distributions using the Shapiro-Wilk test. For comparisons showing normal distributions, p-values were calculated using Student's t-test, and for comparisons not showing normal distributions, p-values were calculated using Mann-Whitney tests.

Hybridization Chain Reaction (HCR) in situ Hybridization.

HCR procedures were carried out according to the manufacturer's instructions (Molecular Instruments) [33]. In brief, zebrafish tissues were fixed overnight in phosphate-buffered 4% paraformaldehyde at 4°C. Tissues were then washed in PBS, dehydrated in MeOH, and stored in MeOH at -20°C at least overnight. Tissues were rehydrated in a graded MeOH/PBS/0.1% Tween 20 series, permeabilized with proteinase K (larvae only), and post-fixed with 4% paraformaldehyde prior to hybridization. Hybridization was done overnight at 37°C. Tissues were washed with the manufacturer's wash buffer, and then 5XSSCT (standard sodium citrate with 0.1% Tween-20), and the amplification/chain reaction steps were performed following the manufacturer's protocol. Probe sets were designed and generated by Molecular Instruments and can be ordered directly from their website.

Confocal Microscopy.

Whole, HCR-processed, adult (0.5-1.5 years) retinas were mounted in glycerol and imaged with a 20X dry lens, 40X water-immersion lens, or 40x oil-immersion lens. 3 µm-step sizes were used for 20X images. Z-series for 40x images were taken with ≤1 µm step size. Whole larval eyes were removed from HCR-processed embryos, and the sclera removed by microdissection. Eyes were mounted in glycerol and imaged with a 20X dry lens using a Nikon-Andor spinning disk confocal microscope and Zyla sCMOS camera. A z-series encompassing the entire globe of the embryo eye was obtained with 3-µm step sizes, using Nikon Elements software. Z-stacks were flattened by max projection, and brightness/contrast adjusted in FIJI (ImageJ). cross sectional images for adult whole mounted retinas were obtained using the orthogonal view function in FIJI.

Presence/absence of *gngt2a* expression in dorsal regions of larval eyes was determined using whole eye stacks. Brightness/contrast were adjusted to determine presence/absence of signal when signal was dim. Presence within dorsal retina was defined as signal localized in the center of the region dorsal to the center of the lens. A proportion test was used to determine statistical significance.

HCR fluorescence intensity quantification was performed using FIJI, using the approach of Thiel et al. [34]. For each image the color channels were split, and background measurements were performed on the channel reporting expression of the gene of interest at 3 positions in the z dimension. Whole eyes were traced in the segmentation editor to create an "object" for measurement. The 3D intensity measure plugin was used to obtain "intensity sum," also known as integrated density, as well as total volume. The single channel reporting expression of the gene of interest was used as the "signal" for 3D analysis. The mean fluorescence intensity of the background was multiplied by the volume of the eye to determine total background. Corrected total fluorescence was calculated by subtracting total background from measured intensity sum [34].

Graphing and statistics were performed in Excel. Sample groups were evaluated for normal distributions using the Shapiro-Wilk test. For comparisons showing normal distributions, p-values were calculated using two-tailed Student's t-test, and for comparisons not showing normal distributions, p-values were calculated using Mann-Whitney tests. *** denotes $p<0.001$, ** denotes $p<0.01$, * denotes $p<0.05$.

Results

Transcriptome Analysis of LWS1 vs. LWS2 Cones: FACS-bulk-RNA-Seq.

To address the hypothesis that LWS1 and LWS2 cone subtypes of the zebrafish are distinct in transcriptional characteristics other than opsin expression, we aimed to identify any genes that are DE in these two cone populations of adult zebrafish. LWS1 vs. LWS2 cones of the *lws*:PAC(H) transgenic line were FACS-sorted based upon GFP vs. RFP fluorescence [25], and RNA isolated from the sorted cones was sequenced to discover their respective transcriptomes (Fig. 1A,B). The results of the dissociation, sorting, evaluation of purity, and RNA quality were reported earlier [25]. Based upon a false discovery rate

(FDR)<0.05, and absolute fold-change (FC)>2, 95 transcripts were enriched in GFP+ (LWS1) cones, representing ~0.6% of the LWS1 transcriptome (Fig. 1C; Table 1; Dataset 1. Note that Tables 1-2 and Datasets 1-3 show log2FC rather than absolute FC). Using the same cutoff criteria, 186 transcripts were enriched in RFP+ (LWS2) cones, representing ~1.2% of the LWS2 transcriptome (Fig. 1C; Table 2; Dataset 1). These analyses suggest that these cone subtypes are indeed highly similar, although with sufficient transcriptional differences other than opsin expression, to support our original hypothesis. A moderated Log2FC approach, to normalize for transcripts expressed at very low levels, returned fewer, but several of the same transcripts (Dataset 2; 19 genes in common with Dataset 1 as LWS1-enriched; 56 genes in common with Dataset 1 as LWS2-enriched). The entire dataset is publicly accessible (GEO accession #GSE232902; https://www.ncbi.nlm.nih.gov/geo/query/acc.cgi?acc=GSE232902).

Transcripts enriched in LWS1 cones included those with functions in phototransduction (*gngt2a*, encoding one of the γ subunits of transducin; [35]), circadian rhythms (*per1b*, *cry1bb*), cell adhesion (*plxna1a*, *ephrin-A1a*), and transcriptional regulation (*foxg1a*, *hmgb1b*, *rorcb*) (Table 1; Datasets 1 and 2). Notable LWS1-enriched transcripts included two with functions related to TH signaling (*nrip1a*, *thrab*), which is a powerful regulator of *lws1* vs. *lws2* expression [14]. A gene ontology (GO) analysis returned one overrepresented molecular function category (transcription factor binding), and several cellular process categories related to differentiation and neurogenesis (Fig. 1D). Transcripts enriched in LWS2 cones also included those with functions in phototransduction (*gngt2b*, *cngb3*), cell adhesion (*adgrl3.1*, *nptna*), and transcriptional regulation related to nuclear hormone signaling (*nr2f2*, *nr4a3*), although none with functions in circadian rhythms (Table 2; Datasets 1 and 2). GO analysis of LWS2-enriched transcripts will be discussed below. Therefore, in addition to the divergent λ_{max} of LWS1 vs. LWS2 cones [12], the two populations may have further distinctions in phototransduction kinetics, cell-cell contacts, and transcriptional regulation by nuclear hormone receptors.

Selected transcripts were analyzed from two additional sorting experiments by qPCR. The results from Sort #1 were previously reported, and validated the presence of *opn1lw1*, but absence of *opn1lw2* (along with two *rh2*-type opsin transcripts) in the GFP+ (LWS1)

cones, and the presence of *opn1lw2*, but absence of *opn1lw1* (along with two *rh2*-type opsin transcripts) in LWS2 cones [25]. Sort #2 verified depletion of *gngt2a*, *arr3a*, and *neurod1*, and enrichment of *opn1lw2* and *gngt2b* in LWS2 (RFP+) cones (Supplemental Fig. S1). Curiously, *opn1lw1* was not detected as DE by either the RNA-Seq analysis, or by qPCR of Sort #2 (Supplemental Fig. S1). Although we only rarely observe co-expression of GFP and RFP reporters in adult *lws*:PAC(H) retinas [21, 36, 37], we tested whether co-expression was more common for the native transcripts, using multiplex fluorescence in situ hybridization. These studies confirmed that a small fraction of the adult LWS cones indeed express both *lws* transcripts (Supplemental Fig. S1C). Further, we note that the fish used for the RNA-Seq studies were sacrificed in the morning, a time of reduced levels of cone opsin transcript expression [38], perhaps affecting the likelihood of detecting *lws1* as DE.

Another feature of the DE list that represents a possible limitation of the FACS-RNA-Seq approach is the abundance of DE transcripts encoding components of the proteasome (37 of the 185 transcripts enriched in LWS2 cones; Datasets 1 and 2). Correspondingly, GO analysis returned numerous overrepresented categories, including one KEGG category related to proteasomal function (Supplemental Fig. S2A) The “RFP” in *lws*:PAC(H) is dsRedExpress [21], which has been noted to mis-fold and/or aggregate [37], and engage cell stress pathways [39], and so this is a potential explanation for the enriched presence of proteasome components.

We therefore used an additional FACS-RNA-Seq approach and analysis, to validate our findings and identify more transcripts enriched in LWS1 vs. LWS2 cones. Both types of LWS cones were sorted from *thrb2*:tdTomato transgenic retinas, using the strategy reported in Sun et al. ([25]; Supplemental Fig. S2B, C). Subsequent RNA-Seq (GEO upload in progress) and DE analyses using the *thrb2*:tdTomato transcripts vs. the *lws1*:GFP or *lws2*:RFP transcripts returned lists of transcripts DE in LWS1 cones vs. all LWS cones, and in LWS2 cones vs. all LWS cones (Dataset 3; Supplemental Fig. S2D). Not surprisingly, the list of transcripts enriched in LWS2 cones vs. all LWS cones was dominated by components of the proteasome; however, both lists contained transcripts identified in the prior analysis as DE, and also returned some novel findings. The additional dataset is also publicly available

(GEO accession # GSE232902; https://www.ncbi.nlm.nih.gov/geo/query/acc.cgi?acc=GSE232902).

Transcriptome Analysis of LWS1 vs. LWS2 Cones: scRNA-Seq.

As a further means to assess transcriptional distinctions between LWS1 and LWS2 cones, we used scRNA-Seq of WT adult zebrafish retinas. TSNE plotting identified 16 distinct clusters from dissociated retinal cells (Fig. 2A), with cone identity assigned to cluster#5, based upon expression of known cone transcripts: opsin markers, *gnat2*, and *pde6c*. Within this cluster, individual cells could be identified based upon expression of *opn1lw1* (94 cells) or *opn1lw2* (199 cells) (Fig. 2B). These cells were localized in the TSNE space near each other, and some *lws2* transcript was present in some LWS1 cones, suggesting that cones co-expressing *lws1* and *lws2* were sampled in this study (Fig. 2). All transcripts identified within these cones included 573 in the *lws1+* cells (31 unique to *lws1+*), and 886 in the *lws2+* cones (13 unique to *lws2+*) (Dataset 4). The scRNA-Seq dataset is publicly accessible (GEO accession #GSE234661; https://www.ncbi.nlm.nih.gov/geo/query/acc.cgi?acc=GSE234661).

A DE analysis of *lws1+* cells vs. *lws1-* cells of the scRNA-Seq results provided another means of identifying transcripts enriched in LWS1 cones vs. other retinal cell types (Dataset 4). Transcripts enriched in LWS1 cones included many identified by the bulk RNA-Seq approach, such as *gngt2a*, *arr3a*, and *ablim3*, as well as those not in the bulk RNA-Seq DE lists, including *aanat21* and *si:busm1-57f23.11* (Fig. 2C; Dataset 4). Transcripts enriched in LWS2 cones vs. other retinal cell types included *gngt2b*, *thrb1*, and *six7*. The most consistently identified DE transcripts in LWS1 vs. LWS2 cones, using both approaches, were the two paralogs encoding γ subunits of cone transducin, with *gngt2a* enriched in LWS1 cones, and *gngt2b* enriched in LWS2 cones. Known expression patterns of these paralogs appeared to support some degree of cone subtype specificity, with *gngt2a* found in ventral/peripheral retina, and *gngt2b* found in dorsal/central larval retina [35], patterns shown to reflect those of *lws1* and *lws2*, respectively [20, 21, 40]. The mapping of *gngt2a* and *gngt2b* paralogs on the TSNE graph also suggested coordinated co-expression of these transcripts within specific LWS cone subtypes, although the *gngt2*s were also more broadly associated with other retinal cell type clusters (Fig. 2B).

We wished to further evaluate potential DE transcripts through curating a "short list" to prioritize for additional study (Table 3). Transcripts were prioritized based upon 1) appearing in more than one DE list; 2) evidence in the literature (or in the ZFIN database) of expression patterns consistent with DE in LWS1 vs. LWS2 cones; 3) levels of expression in the bulk RNA-Seq dataset suggesting the transcript would be detectable by *in situ* hybridization; 4) potential cone-specific functional relevance (phototransduction, circadian rhythm, cell adhesion); and 5) potential relevance in regulation of *lws1* vs. *lws2* expression (nuclear hormone signaling) [14, 36]. We noted that *si:busm1-57f23.1* within our short list, was also detected as significantly downregulated in a zebrafish *thrb* mutant [41]. We reasoned that other DE transcripts identified in *thrb-/-* vs. WT in this previous study may also be DE in LWS1 vs. LWS2 cones, and so added these to the short list.

Expression analysis of LWS1-enriched and LWS2-enriched transcripts in adult retinas.

We selected eight of these transcripts (Table 2; LWS1-enriched: *gngt2a*, *nrip1a*, *vax1*, *vax2*, *si:busm1*, *cry3a*. LWS2-enriched: *gngt2b*, *nr2f2*) to test two hypotheses: 1) LWS1 and LWS2 cones are functionally distinct (already supported by the outcomes of the RNA-Seq analyses); and 2) multiple genes are coordinately regulated in LWS cones by thyroid hormone. We also wished to use these transcripts to evaluate heterogeneity within the LWS cone subtypes, as such heterogeneity was noted by Aramaki et al. [42] for M opsin dominant vs. S opsin dominant cone types in mouse. Our initial approach was to focus upon the first hypothesis by evaluating expression patterns of these transcripts in whole adult wild-type retinas using multiplex in situs.

gngt2a and *gngt2b*. The genes *gngt2a* and *gngt2b* are paralogous and encode gamma subunits of the heterotrimeric g-protein transducin, an essential part of the phototransduction cascade [35]. Previous studies have shown that the expression domains of *gngt2a* and *gngt2b* correspond with the expression domains of *lws1* and *lws2*, respectively [20, 40]. Consistent with these studies, our RNA-Seq data show that *gngt2a* is enriched in LWS1 cones and *gngt2b* is enriched in LWS2 cones (Tables 1, 2; Datasets 1, 2, 4). While the majority of *gngt2a* and *gngt2b* expressing cones are found within zones of *lws1* and *lws2* expression, respectively, multiplex fluorescence in situs of whole mounted adult retinas show expression of *gngt2a* and (to a lesser extent) *gngt2b* beyond their respective corresponding *lws* domains

(Fig. 3A'; 4A'). The expression domain of *gngt2a* was particularly widespread, including nearly the entirety of the retina, although the fluorescence signal appeared stronger in ventral retina (Fig 3A'). The images also show expression of both *gngt2a* and *gngt2b* in non-LWS cones (Fig. 3D; 4D). Interestingly, the morphology and position of some of the *gngt2b*-expressing non-LWS cones suggests they may be UV (*sws1*-expressing) cones, as these cells are short, single cones (Fig. 4D).

nrip1a and *nr2f2*. The protein encoded by *nrip1a* is predicted to interact with nuclear hormone receptors [43, 44], and is expressed in the anterior nervous system of zebrafish embryos [45]. The bulk RNA-Seq of sorted LWS1 vs. LWS2 cones, and the analysis of the scRNA-Seq output, indicated that *nrip1a* transcript is enriched in LWS1 cones (Table 1, Datasets 1, 4). Multiplex in situs of adult whole retinas instead show widespread expression of *nrip1a* across the retina, without a ventrally-biased pattern, as would be predicted from the bulk-RNA-Seq (Fig. 5A'). The *nrip1a* transcript is indeed present in LWS cones of both types, and also in non-LWS cones (Fig. 5C). *Nrip1a* also appears to be expressed in cells of other retinal layers (Fig. 5C). *Nr2f2* encodes a nuclear hormone receptor with several known patterning roles within the nervous system and other organs [46], and is expressed within the photoreceptor layer of zebrafish embryos [45]. Our bulk RNA-Seq and scRNA-Seq results indicate that *nr2f2* transcript is enriched in LWS2 cones (Table 2; Datasets 1, 2,). Multiplex in situs of adult whole retina show a very slight bias in the *nr2f2* expression domain toward the dorsal half of the retina (Fig. 5A), similar to the *lws2* expression domain but with a less abrupt transition (Fig. 5D'). Further, our results show *nr2f2* is expressed in LWS cones (both LWS1 and LWS2) as well as in some cells of the INL having positions consistent with the identity of amacrine cells (Fig. 5F).

vax1 and *vax2*. These genes encode transcription factors needed for optic cup morphogenesis and closure of the choroid fissure [47] and are expressed in ventral regions of the embryonic zebrafish retina [48, 49]. Our bulk and scRNA-Seq data indicate that *vax1* is enriched in LWS1 cones (Table 1, Dataset 1). Multiplex in situ of adult zebrafish retinas verify that its expression domain is restricted to the ventral portion of the retina (Fig. 6A'). Interestingly, the *vax1* and *lws1* expression domains were very similar (Fig. 6A',D').

Resliced orthogonal projections show *vax1* expression in cells of the photoreceptor layer, including LWS1 cones, INL, and some cells of the GCL, with strongest signal localized to the INL (Fig. 6C). *Vax2* transcripts are also present in LWS1 cones, though not significantly enriched, based upon the output of our RNA-Seq analyses (Table 1; Dataset 1) (see also [40]). Whole mounted retinas processed for multiplex in situs show its expression is limited to a ventral portion of the retina (Fig. 6D'). Orthogonal views reveal expression of *vax2* in cells of the photoreceptor layer, including LWS1 cones, the INL, and the GCL, with most of the expression in the INL and GCL (Fig. 6F).

s*i:busm1-57f23.1*. The gene *si:busm1-57f23.1* encodes a protein that is predicted to be a secreted endopeptidase inhibitor [44], and in zebrafish embryos transcript is expressed in the photoreceptor layer of the retina [50]. Transcripts are predicted to be highly enriched in LWS cones of adult zebrafish, since a *thrb* mutant lacking LWS cones displays very low levels of expression in comparison with wildtype [41]. Our scRNA-Seq results expand on this information, suggesting that this gene is more highly expressed in LWS1 cones than in LWS2 cones (Dataset 4). While multiplex in situ images do not show an obvious bias in expression domain toward the LWS1 domain (Fig. 7A'), they confirm the presence of *si:busm1-57f23.1* transcript in cones (LWS cones and potentially some non-LWS cones; Fig. 7C). This gene also appears to be sporadically expressed by some cells of the INL, possibly amacrine cells (Fig. 7C).

cry3a. *Cry3a* encodes a cryptochrome circadian regulator, is expressed within the embryonic zebrafish retina [51], and is indicated by scRNA-Seq dataset to be enriched within LWS1 cones vs. LWS2 cones (Dataset 4). Images of adult retina multiplex in situs show this gene is diffusely expressed in the adult zebrafish retina and is present in all retinal layers (Supplemental Fig. S3).

In summary, multiplex in situ hybridization supported the findings from the bulk and scRNA-Seq indicating that the eight transcripts evaluated were indeed expressed in LWS cones. Further, the in situs supported that *gngt2a*, *vax1,* and *vax2*, but not *nrip1a*, *si:busm1-57f23.1,* and *cry3a* are enriched in LWS1 vs. LWS2 cones, and that *gngt2b* and *nr2f2* are enriched in LWS2 vs. LWS1 cones. Thus, we find further support for the hypothesis that LWS1 cones are transcriptionally distinct from LWS2 cones. In addition, we also observe

considerable heterogeneity within these two populations in expression of the predicted enriched transcripts.

Analysis of TH-mediated regulation of LWS1-enriched and LWS2-enriched transcripts.

We next used a TH treatment protocol demonstrated to increase *lws1* at the expense of *lws2*, in individual cones [14], to evaluate the response of the eight transcripts to TH, thereby testing our second hypothesis. This protocol involved treatment of zebrafish embryos at 48 hpf with 100 nM T3, or the DMSO vehicle, and collecting whole larvae at 96 hpf for measurement of relative abundance of transcript (qPCR) and changes in expression pattern (multiplex fluorescence in situ) as the experimental endpoints.

gngt2a and *gngt2b.* The pattern of expression of *gngt2a* in control, 96 hpf whole eyes appeared largely localized to the photoreceptor layer within ventral retina (Fig. 8 [35]), distinct from the results from adult retina (Fig. 3). Multiplex in situ hybridization using probe sets targeting *gngt2a*, *lws1*, and *lws2*, revealed that many cells in this layer and region expressed *gngt2a*, including those that were *lws1*+ and those that were *lws2*+ (Fig. 8A,C,E). Therefore, although *gngt2a* was consistently detected as enriched in adult *lws1*+ vs. *lws2*+ cones, the patterns of *gngt2a* and *lws1* at larval stages did not precisely align (Fig. 8A). Larval eyes that had been treated with 100 nM T3 showed dorsally expanded domains of *gngt2a* expression, along with dorsally expanded domains of *lws1* and restricted domains of *lws2* [14] (Fig. 8B,D,F). qPCR, however, showed no difference between treatment groups for relative abundance of *gngt2a* (Fig. 8H, $p=0.0967$). Further, quantitative fluorescence analysis showed no difference between treatment groups (Fig. 8I, $p=0.454$). Interestingly, however, the presence of *gngt2a* expression in the dorsal portion of the eye was significantly more likely to be found in T3 treated eyes (Fig. 8J, $p=0.013$). Therefore, it is likely that the expansion of the expression domain, despite being consistent and obvious, did not alter the average amount of *gngt2a* transcript in the whole eye. In total, *lws1* and LWS1 cone-enriched transcript *gngt2a* both appear to be upregulated, but to different degrees and in not exactly the same domains. This suggests that *lws1* and *gngt2a* are regulated in some way by TH but not in a precisely coordinated manner.

The expression domain of *gngt2b* in 96 hpf whole eyes also appeared localized to photoreceptors, but more widespread than that of *gngt2a*, and excluded from ventral retina

(Fig. 9A,C [35]), similar to what we observed in adult retina (Fig. 4) . Many cones co-expressed *lws2* and *gngt2b*, although there were also many *gngt2b*+ cells that were not *lws2*+ (Fig. 9E). The *gngt2b* domain was slightly reduced as a proportion of the eye in comparison with the *lws2* domain, but shared general pattern characteristics. These findings are consistent with the DE analyses of adult LWS1 vs. LWS2 cones. Eyes of larvae treated with T3, somewhat surprisingly, showed no reduction in size of the *gngt2b* expression domain (Fig. 9D). The fluorescence intensity, however, significantly decreased in the T3 condition, as did transcript abundance reported by qPCR (Fig. 9H,I, p=3.159E-05, 0.0191). The size of the *lws2* domain was reduced, and that of the *lws1* domain was enlarged, as expected (Fig. 9B; [14]), providing an internal control that the treatment was effective. Whole larval tissues analyzed by qPCR, and whole mounted eyes analyzed by quantitative fluorescence showed increased *lws1* due to T3 treatment (Fig. 9H,I). Collectively, these findings support the hypothesis that exogenous TH controls *lws1*, *lws2*, *gngt2a*, and *gngt2b* expression, but not in a topographically, and/or temporally coordinated manner.

nrip1a and *nr2f2.* The *nrip1a* transcript was predicted to be enriched in LWS1 cones, encodes a protein that interacts with nuclear hormone receptors [44], but adult whole retinas did not display an obvious bias in expression domain (Fig. 5). This transcript was abundantly expressed in the retina of 96 hpf larvae, and many cells were co-labeled for *lws1* and *lws2* (Fig. 10E,F). T3 treatment did not appear to alter the expression domain of *nrip1a*, although the domains of *lws1* increased, and *lws2* decreased, as expected (Fig. 10C,D). Abundance of transcript, however, increased significantly in response to T3 treatment (Fig. 10G, p=0.00152). Further, quantitative fluorescence analysis showed increased fluorescence in the T3 treated group, indicating that transcript abundance of *nrip1a* increased upon T3 treatment without altering its expression domain (Fig. 10H, p=0.014). The *nr2f2* transcript was predicted to be enriched in LWS2 cones and is a predicted nuclear hormone receptor. This transcript was abundantly expressed in multiple layers of adult retina and displayed a slight bias in expression signal in dorsal retina (Fig. 5). At 96 hpf, expression of this transcript also appeared to be higher in the dorsal portion of the retina, which is consistent with the RNA-Seq and adult *in situ* results (Fig. 10K,L). T3 treatment did not appear to alter the expression domain of this gene (Fig. 10K,L), and both qPCR and quantitative fluorescence analysis

results showed no significant difference between treatment groups (Fig. 10O,P, p=0.476, sample size too small for Mann-Whitney test).

vax1 and *vax2.* The *vax1* transcript was predicted to be enriched in LWS1 cones, encodes a transcription factor important in patterning the nervous system, and was expressed in the ventral region of adult retina in multiple retinal layers, with some cells coexpressing *lws1* (Fig. 6). T3 treatment did not appear to alter the expression domain of this gene (Fig. 11C,D), and qPCR results also showed no significant difference between treatment groups (Fig. 11G, p=0.123). The *vax2* transcript was predicted to be enriched in LWS1 cones, encodes a transcription factor important in patterning the nervous system, and was expressed in the ventral region of adult retina in multiple retinal layers, with some cells coexpressing *lws1* (Fig. 6). T3 treatment did not appear to alter the expression domain of this gene (Fig. 11J,K), and qPCR results also showed no significant difference between treatment groups (Fig. 11N, p=0.312).

si:busm1-57f23.1. The *si:busm1-57f23.1* transcript was identified as enriched in LWS1 cones by the scRNA-Seq, and is DE (reduced in expression) in *thrb* mutants vs. WT [27]. This transcript encodes a predicted extracellular protein with cysteine protease inhibitor activity, and adult retinas indeed show expression in LWS and some non-LWS cones (Fig. 7). Expression of *si:busm1-57f23.1* in 96 hpf larvae was localized to the photoreceptor layer, and many cells were co-labeled for *lws1* or *lws2* (Fig. 12A,B,C,D,E',F'). Eyes of larvae treated with T3 showed marked reduction in the expression domain of *si:busm1-57f23.1*, as well as reduction in the *lws2* domain and expansion of the *lws1* domain (Fig. 12B,D). Whole larval tissues analyzed by qPCR showed no statistically significant change in *si:busm1-57f23.1* expression due to T3 treatment (Fig. 12K, p= 0.244). We hypothesized that expression in non-retinal tissues may make the apparent downregulation seen in the in situs difficult to detect by qPCR in whole larvae. To check this, we performed whole larval HCR and imaged the entire larval head, including the brain and both eyes. We found that *si:busm1-57f23.1* is, indeed, expressed in the brain and spinal cord of 4 day old zebrafish (Fig. 12G,H). We then performed quantitative fluorescence analysis on the eyes alone and found that fluorescence trended down in the eyes of T3 treated embryos (Fig 12L, p= 0.0556).

cry3a. The *cry3a* transcript was one of many *cry* genes predicted to be LWS1 enriched. This gene encodes a transcription factor involved in circadian regulation. This transcript was diffusely expressed in the retina of the 96 hpf embryo without particular localization to the photoreceptor layer (Supplemental Fig. S3). T3 treatment did not appear to alter the expression domain of this gene (Supplemental Fig. S3), and qPCR results also showed no significant difference between treatment groups (Supplemental Fig. S3, p=0.335).

Taken together, the outcomes of larval TH treatments provide only modest support for the second hypothesis that LWS cone transcripts are coordinately regulated by TH. These studies supported that *gngt2a* and *nrip1a* are upregulated by T3, although not in the same spatiotemporal manner as *lws1* [9] while *vax1*, *vax2*, and *cry3a* are unaffected, and *si:busm1-57f23.1* appears downregulated in the retina by T3. Further, *gngt2b* is downregulated by T3, again not in the same spatiotemporal manner as *lws2* [9], while *nr2f2* is unaffected. The LWS cone population therefore appears to display considerable heterogeneity in transcriptional response to TH.

Discussion

In this study we have probed the transcriptomes of long wavelength-sensitive cone photoreceptors of the zebrafish to advance our understanding of cone subtypes toward applications related to retinal development, function, and disease. The main findings of our study are as follows: LWS1 and LWS2 cones differ transcriptionally beyond opsin expression, and these differences include transcripts involved in photoreceptor function and development. Further, these cone subtypes show within-type heterogeneity. We also found that some of these transcriptional differences may be regulated by exogenous thyroid hormone, but in a manner that appears distinct from TH regulation of *lws1* vs. *lws2*.

LWS1 and LWS2 cones differ at the transcriptional level beyond opsin expression.

In total, the bulk RNA-Seq results showed 95 transcripts enriched in LWS1 cones and 186 transcripts enriched in LWS2 cones, a finding that supports our first hypothesis that these cone subtypes differ beyond the level of opsin expression. To our knowledge, any such distinctions in the human LWS vs. MWS cone populations, other than opsin expression, have not been noted, although this is largely due to the challenges of detecting *LWS*-expressing vs.

MWS-expressing cones within a dataset [52]. The tandemly-replicated *LWS/MWS* opsin genes of primates display 98% homology at the level of transcript [53] and are difficult to distinguish using standard RNA-Seq approaches. Interestingly, the scRNA-Seq approach of Peng et al. [54] permitted this analysis for macaque cones, with the conclusion that these LWS and MWS cones are transcriptionally distinct only for the opsin genes, in contrast to our findings for the zebrafish.

Some of the transcripts enriched in zebrafish LWS1 vs. LWS2 cones suggest the possibility of further functional differences between the LWS cone subtypes. For example, the presence of the paralogous gamma transducin enriched in each cone subtype may reflect differences in phototransduction kinetics and/or recovery. However, to our knowledge such distinctions have not been experimentally tested. In addition, because multiple transcripts encoding factors involved in circadian rhythms were found to be enriched in LWS1 cones (*cry1bb*, *per3*, [Dataset 1] *cry1ba*, *aanat2*, *per2* [Dataset 4]), and no circadian related transcripts were enriched in LWS2 cones, LWS1 cones may have specialized functions in circadian rhythm. The majority of LWS1 cones are located within the ventral domain of the retina, exposed to direct sunlight, and therefore are in an ideal position to obtain circadian information [20, 40]. While the transcript tested using HCR *in situ* did not appear to be ventrally enriched, differences in sample collection timing may have been a factor (near lights-on for RNA-Seq, and midafternoon for adult whole retina collection), and retina-specific spatial expression data for the other circadian genes have not been reported in the literature.

Other differences in gene expression may give insight into the regulatory landscape of the retina. Multiple nuclear receptors and proteins that interact with nuclear receptors were predicted to be DE between LWS1 and LWS2 cones, including *nrip1a* and *nr2f2*. Given that ligands of nuclear hormone receptors (retinoic acid and TH) can regulate expression of *lws1* vs. *lws2* [14, 36], *nrip1a* and *nr2f2* may be considered candidates for participation in this regulation. The expression of *vax2* in LWS1 cones also proves interesting. *Vax2* is instrumental in regulating RA metabolism by altering the expression of RA-catabolizing and RA-synthesizing enzymes in developing mouse retina [55]. RA is known to be important in regulating cone opsin expression in multiple species [56, 57] including zebrafish, and

specifically for regulating *lws1* vs. *lws2* [36], and RA receptors are known to heterodimerize with TH receptors [58]. RA signaling takes place in ventral retina of juvenile zebrafish, spatially coinciding with a "transition zone" where LWS cones switch from *lws2* to *lws1* expression as the retina grows [36]. Further, experimentally athyroid juvenile zebrafish display only a small ventral patch of *lws1* expression, which also spatially coincides with the RA signaling domain [14]. As *vax2* is known to be present in the zebrafish retina long before LWS cone development [59], this gene may play an upstream role in *lws* regulation by spatially tuning RA levels which, in turn, impart dorsoventral location information to developing LWS cones along with TH. While the presence of *vax2* in larval zebrafish retina is not surprising and likely is involved in the regulation of many genes, *vax2* expression in adult zebrafish was unexpected as *vax2* is not expressed in adult mouse retina [60]. We speculate that *vax2* may be important in the maintenance of correct topography of cone subtypes in the adult zebrafish, perhaps even after regeneration [37].

TH regulates several LWS1 and LWS2 enriched transcripts.

We initially hypothesized that TH could be a master regulator of transcriptional differences between the LWS cone subtypes, LWS1 and LWS2. For this hypothesis to be true, DE genes would be coordinately regulated with *lws1* and *lws2* such that genes enriched in LWS1 cones would be upregulated by TH and genes enriched in LWS2 cones would be downregulated by TH. Our observations did not match this hypothesis. While *gngt2a* and *gngt2b* show some features of coordinated regulation with *lws1* and *lws2*, respectively, other transcripts such as *si:busm1* show the opposite – *si:busm1* was predicted to be enriched in LWS1 cones but appears downregulated by TH. *Nrip1a* is enriched in LWS1 cones and is upregulated by TH, similar to *lws1*, but its expression domain extends beyond the *lws1* domain and even beyond the photoreceptor layer. Other transcripts that are specifically enriched in LWS1 cones such as *vax1* and *vax2* display no transcriptional response to TH treatment. Therefore, TH is likely involved in regulation of transcripts other than *lws1* and *lws2*, but in a more complex manner than originally hypothesized, and perhaps independently of the *lws* opsin genes.

Transcriptional heterogeneity within the LWS cone population.

Transcriptional heterogeneity among photoreceptor subtypes was recently described in detail for the zebrafish as the "partitioning" of expression of paralogs of photoreceptor components that emerged through whole genome duplications [40]. For example, the authors took note of partitioning of a paralog of the gamma subunit of transducin, *gngt2a*, within LWS1 and RH2-4 cones [40], which express the most red-shifted members of the tandemly-replicated *lws* and *rh2* cone opsin gene arrays, respectively [12]. While our studies are largely consistent with this concept, the patterns of expression of the *gngt2* paralogs in cone subtypes appear more nuanced. Some LWS2 cones express *gngt2b*, but some express *gngt2a* or possibly both paralogs. Expression of *gngt2a* in adult retina is not limited to the ventral domain of LWS1 cones. Similarly, some but not all LWS1 cones express *vax1*. Some but not all LWS2 cones express *nr2f2*. For each of these LWS cone subtypes, there appears to be a great deal of transcriptional heterogeneity across the expanse of the retina.

Further heterogeneity is revealed within cone responses to treatment with exogenous TH - some but not all of these genes can be regulated by TH. Based on these observations, it appears that TH may be regulating these genes not because it is particularly regulating the entirety of LWS1 and LWS2 cone phenotype but rather because TH is an important regulator of spatial dynamics of gene expression in the zebrafish retina. Recent work in mouse supports this thyroid hormone-mediated spatial gradient regulation. It was found that *trβ2*, a TH receptor shared by mice and zebrafish, can control the expression and chromatin state of multiple cone genes that are expressed in a dorsoventral gradient in the mouse retina [42]. This influential study also reveals heterogeneity within populations of mouse cones that express both *sws1* and *mws* opsins, in support of the concept that not all cones expressing a particular opsin are identical [42]. The present study extends this concept to the *lws1*-expressing and *lws2*-expressing cone populations of the zebrafish. We aim to identify the TH receptor(s) that mediate the effects of TH in the zebrafish, as well as determine whether any are directly interacting with elements on the regulated gene.

While our approach was able to expand our understanding of LWS1 and LWS2 cone biology, we were limited in our ability to detect all of the potential transcriptional variability in these photoreceptors due to the limitations of sensitivity of bulk and scRNA-Seq. The bulk

RNA-Seq results were further restricted by the effectiveness of the cell sorting procedure, and by the presence of proteasome-related transcripts in the LWS2 cone samples. Therefore we leveraged the bulk RNA-Seq datasets with information derived from a scRNA-Seq approach. We evaluated eight transcripts for their spatial patterning and TH responses. It is possible that many of the other differentially expressed genes may be regulated by TH. Further, these evaluations were done at the transcript level and do not reveal protein expression and/or localization, which would add another layer of support to the hypothesis that LWS1 and LWS2 cones are functionally distinct beyond opsin expression. In the future, we plan to perform single cell RNA-Seq on control and TH treated retinas to determine widespread effects of TH on the retinal cell transcriptomes. Due to the similarity of the LWS1 and LWS2 cone transcriptomes, LWS cone studies might also benefit from a manual photoreceptor collection technique, as in Angueyra et al. [61], in order to increase the signal-to-noise ratio in the transcriptome data and reveal more potentially subtle gene expression differences.

Our results build upon our previous studies that showed *lws1* and *lws2* are regulated by TH [14] by suggesting that multiple genes within the cones expressing these tandemly replicated opsins are non-stochastically regulated, and that these genes may also be regulated by TH. Further, our findings add to the growing literature that shows TH is a major regulator of spatial patterning in the retina and that its role is conserved across multiple species.

References

1. Nathans, J., *The evolution and physiology of human color vision: insights from molecular genetic studies of visual pigments.* Neuron, 1999. **24**(2): p. 299-312.
2. Vollrath, D., J. Nathans, and R.W. Davis, *Tandem array of human visual pigment genes at Xq28.* Science, 1988. **240**(4859): p. 1669-72.
3. Peng, G.H. and S. Chen, *Active opsin loci adopt intrachromosomal loops that depend on the photoreceptor transcription factor network.* Proc Natl Acad Sci U S A, 2011. **108**(43): p. 17821-6.
4. Wang, Y., et al., *Mutually exclusive expression of human red and green visual pigment-reporter transgenes occurs at high frequency in murine cone photoreceptors.* Proc Natl Acad Sci U S A, 1999. **96**(9): p. 5251-6.
5. Hussey, K.A., S.E. Hadyniak, and R.J. Johnston, Jr., *Patterning and Development of Photoreceptors in the Human Retina.* Front Cell Dev Biol, 2022. **10**: p. 878350.
6. Ayyagari, R., et al., *Bilateral macular atrophy in blue cone monochromacy (BCM) with loss of the locus control region (LCR) and part of the red pigment gene.* Mol Vis, 1999. **5**: p. 13.
7. Gardner, J.C., et al., *X-linked cone dystrophy caused by mutation of the red and green cone opsins.* Am J Hum Genet, 2010. **87**(1): p. 26-39.
8. Michaelides, M., et al., *X-linked cone dysfunction syndrome with myopia and protanopia.* Ophthalmology, 2005. **112**(8): p. 1448-54.
9. Winderickx, J., et al., *Defective colour vision associated with a missense mutation in the human green visual pigment gene.* Nat Genet, 1992. **1**(4): p. 251-6.
10. Young, T.L., et al., *X-linked high myopia associated with cone dysfunction.* Arch Ophthalmol, 2004. **122**(6): p. 897-908.
11. Hofmann, C.M. and K.L. Carleton, *Gene duplication and differential gene expression play an important role in the diversification of visual pigments in fish.* Integr Comp Biol, 2009. **49**(6): p. 630-43.
12. Chinen, A., et al., *Gene duplication and spectral diversification of cone visual pigments of zebrafish.* Genetics, 2003. **163**(2): p. 663-75.
13. Niklaus, S. and S.C.F. Neuhauss, *Genetic approaches to retinal research in zebrafish.* J Neurogenet, 2017. **31**(3): p. 70-87.
14. Mackin, R.D., et al., *Endocrine regulation of multichromatic color vision.* Proc Natl Acad Sci U S A, 2019. **116**(34): p. 16882-16891.
15. Roberts, M.R., et al., *Making the gradient: thyroid hormone regulates cone opsin expression in the developing mouse retina.* Proc Natl Acad Sci U S A, 2006. **103**(16): p. 6218-23.
16. Boyes, W.K., et al., *Moderate perinatal thyroid hormone insufficiency alters visual system function in adult rats.* Neurotoxicology, 2018. **67**: p. 73-83.
17. Forrest, D. and A. Swaroop, *Minireview: the role of nuclear receptors in photoreceptor differentiation and disease.* Mol Endocrinol, 2012. **26**(6): p. 905-15.
18. Ng, L., et al., *A thyroid hormone receptor that is required for the development of green cone photoreceptors.* Nat Genet, 2001. **27**(1): p. 94-8.
19. Eldred, K.C., et al., *Thyroid hormone signaling specifies cone subtypes in human retinal organoids.* Science, 2018. **362**(6411).
20. Takechi, M. and S. Kawamura, *Temporal and spatial changes in the expression pattern of multiple red and green subtype opsin genes during zebrafish development.* J Exp Biol, 2005. **208**(Pt 7): p. 1337-45.
21. Tsujimura, T., T. Hosoya, and S. Kawamura, *A single enhancer regulating the differential expression of duplicated red-sensitive opsin genes in zebrafish.* PLoS Genet, 2010. **6**(12): p. e1001245.

22. Westerfield, M., *The Zebrafish Book: A Guide for the Laboratory Use of Zebrafish (Danio rerio)*. 5th ed. 2007, Eugene: University of Oregon Press.
23. Suzuki, S.C., et al., *Cone photoreceptor types in zebrafish are generated by symmetric terminal divisions of dedicated precursors.* Proc Natl Acad Sci U S A, 2013. **110**(37): p. 15109-14.
24. Sun, C., C. Galicia, and D.L. Stenkamp, *Transcripts within rod photoreceptors of the Zebrafish retina.* BMC Genomics, 2018. **19**(1): p. 127.
25. Sun, C., D.M. Mitchell, and D.L. Stenkamp, *Isolation of photoreceptors from mature, developing, and regenerated zebrafish retinas, and of microglia/macrophages from regenerating zebrafish retinas.* Exp Eye Res, 2018. **177**: p. 130-144.
26. Bolger, A.M., M. Lohse, and B. Usadel, *Trimmomatic: a flexible trimmer for Illumina sequence data.* Bioinformatics, 2014. **30**(15): p. 2114-20.
27. Dobin, A., et al., *STAR: ultrafast universal RNA-seq aligner.* Bioinformatics, 2013. **29**(1): p. 15-21.
28. Patro, R., et al., *Salmon provides fast and bias-aware quantification of transcript expression.* Nat Methods, 2017. **14**(4): p. 417-419.
29. Petersen, K.R., Streett, D.A., Gerritsen, A.T., Hunter, S.S., Settles, M.L. . *Super deduper, fast PCR duplicate detection in fastq files.* in *6th ACM Conference on Bioinformatics, Computational Biology and Health Informatics*. 2015.
30. Soneson, C., M.I. Love, and M.D. Robinson, *Differential analyses for RNA-seq: transcript-level estimates improve gene-level inferences.* F1000Res, 2015. **4**: p. 1521.
31. Love, M.I., W. Huber, and S. Anders, *Moderated estimation of fold change and dispersion for RNA-seq data with DESeq2.* Genome Biol, 2014. **15**(12): p. 550.
32. Butler, A., et al., *Integrating single-cell transcriptomic data across different conditions, technologies, and species.* Nat Biotechnol, 2018. **36**(5): p. 411-420.
33. Choi, H.M., V.A. Beck, and N.A. Pierce, *Next-generation in situ hybridization chain reaction: higher gain, lower cost, greater durability.* ACS Nano, 2014. **8**(5): p. 4284-94.
34. Thiel, W.A., et al., *Modulation of retinoid-X-receptors differentially regulates expression of apolipoprotein genes apoc1 and apoeb by zebrafish microglia.* Biol Open, 2022. **11**(1).
35. Lagman, D., et al., *Transducin duplicates in the zebrafish retina and pineal complex: differential specialisation after the teleost tetraploidisation.* PLoS One, 2015. **10**(3): p. e0121330.
36. Mitchell, D.M., et al., *Retinoic Acid Signaling Regulates Differential Expression of the Tandemly-Duplicated Long Wavelength-Sensitive Cone Opsin Genes in Zebrafish.* PLoS Genet, 2015. **11**(8): p. e1005483.
37. Stenkamp, D.L., D.D. Viall, and D.M. Mitchell, *Evidence of regional specializations in regenerated zebrafish retina.* Exp Eye Res, 2021. **212**: p. 108789.
38. Li, P., et al., *CLOCK is required for maintaining the circadian rhythms of Opsin mRNA expression in photoreceptor cells.* J Biol Chem, 2008. **283**(46): p. 31673-8.
39. Zhou, J., et al., *Cytotoxicity of red fluorescent protein DsRed is associated with the suppression of Bcl-xL translation.* FEBS Lett, 2011. **585**(5): p. 821-7.
40. Ogawa, Y. and J.C. Corbo, *Partitioning of gene expression among zebrafish photoreceptor subtypes.* Sci Rep, 2021. **11**(1): p. 17340.
41. Volkov, L.I., et al., *Thyroid hormone receptors mediate two distinct mechanisms of long-wavelength vision.* Proc Natl Acad Sci U S A, 2020. **117**(26): p. 15262-15269.
42. Aramaki, M., et al., *Transcriptional control of cone photoreceptor diversity by a thyroid hormone receptor.* Proc Natl Acad Sci U S A, 2022. **119**(49): p. e2209884119.
43. Grasedieck, S., et al., *The retinoic acid receptor co-factor NRIP1 is uniquely upregulated and represents a therapeutic target in acute myeloid leukemia with chromosome 3q rearrangements.* Haematologica, 2022. **107**(8): p. 1758-1772.

44. O'Leary, N.A., , Wright, M.W.,, Brister, J.R., Ciufo, S., Haddad, D., McVeigh, R., Rajput, B., Robbertse, B., Smith-White, B., Ako-Adje,i D., Astashyn, A., Badretdin, A., Bao, Y., Blinkova, O., Brover, V., Chetvernin, V., Choi, J., Cox, E., Ermolaeva, O., Farrell, C.M., Goldfarb, T., Gupta, T., Haft, D., Hatcher, E., Hlavina, W., Joardar, V.S., Kodali, V.K., Li, W., Maglott, D., Masterson, P., McGarvey, K.M., Murphy, M.R., O'Neill, K., Pujar, S., Rangwala, S.H., Rausch, D., Riddick, L.D., Schoch, C., Shkeda, A., Storz, S.S., Sun, H., Thibaud-Nissen, F., Tolstoy, I., Tully, R.E., Vatsan, A.R., Wallin, C., Webb, D., Wu, W., Landrum, M.J., Kimchi, A., Tatusova, T., DiCuccio, M., Kitts, P., Murphy, T.D., Pruitt, K.D., *Reference sequence (RefSeq) database at NCBI: current status, taxonomic expansion, and functional annotation.* . Nucleic Acids Research, 2016. **44**(D1): p. D733-745.
45. Thisse, B., Thisse, C., *Expression from: Unexpected Novel Relational Links Uncovered by Extensive Developmental Profiling of Nuclear Receptor Expression.*, Z.T.Z.I. Network, Editor. 2008.
46. Barske, L., et al., *Essential Role of Nr2f Nuclear Receptors in Patterning the Vertebrate Upper Jaw.* Dev Cell, 2018. **44**(3): p. 337-347 e5.
47. Take-uchi, M., J.D. Clarke, and S.W. Wilson, *Hedgehog signalling maintains the optic stalk-retinal interface through the regulation of Vax gene activity.* Development, 2003. **130**(5): p. 955-68.
48. Richardson, R., et al., *Transcriptome profiling of zebrafish optic fissure fusion.* Sci Rep, 2019. **9**(1): p. 1541.
49. Holly, V.L., et al., *Sfrp1a and Sfrp5 function as positive regulators of Wnt and BMP signaling during early retinal development.* Dev Biol, 2014. **388**(2): p. 192-204.
50. Hartmeyer, A., Thisse, B., Thisse, C., *Fast Release Clones: A High Throughput Expression Analysis. ZFIN Direct Data Submission* 2004.
51. Tsai, S.M., K.C. Chu, and Y.J. Jiang, *Newly identified Gon4l/Udu-interacting proteins implicate novel functions.* Sci Rep, 2020. **10**(1): p. 14213.
52. Lukowski, S.W., et al., *A single-cell transcriptome atlas of the adult human retina.* EMBO J, 2019. **38**(18): p. e100811.
53. Onishi, A., et al., *Variations in long- and middle-wavelength-sensitive opsin gene loci in crab-eating monkeys.* Vision Res, 2002. **42**(3): p. 281-92.
54. Peng, Y.R., et al., *Molecular Classification and Comparative Taxonomics of Foveal and Peripheral Cells in Primate Retina.* Cell, 2019. **176**(5): p. 1222-1237 e22.
55. Alfano, G., et al., *Vax2 regulates retinoic acid distribution and cone opsin expression in the vertebrate eye.* Development, 2011. **138**(2): p. 261-71.
56. Prabhudesai, S.N., D.A. Cameron, and D.L. Stenkamp, *Targeted effects of retinoic acid signaling upon photoreceptor development in zebrafish.* Dev Biol, 2005. **287**(1): p. 157-67.
57. Roberts, M.R., et al., *Retinoid X receptor (gamma) is necessary to establish the S-opsin gradient in cone photoreceptors of the developing mouse retina.* Invest Ophthalmol Vis Sci, 2005. **46**(8): p. 2897-904.
58. Berrodin, T.J., et al., *Heterodimerization among thyroid hormone receptor, retinoic acid receptor, retinoid X receptor, chicken ovalbumin upstream promoter transcription factor, and an endogenous liver protein.* Mol Endocrinol, 1992. **6**(9): p. 1468-78.
59. French, C.R., et al., *Gdf6a is required for the initiation of dorsal-ventral retinal patterning and lens development.* Dev Biol, 2009. **333**(1): p. 37-47.
60. Barbieri, A.M., et al., *A homeobox gene, vax2, controls the patterning of the eye dorsoventral axis.* Proc Natl Acad Sci U S A, 1999. **96**(19): p. 10729-34.
61. Angueyra, J.M., et al., *Transcription factors underlying photoreceptor diversity.* Elife, 2023. **12**.

Tables

Table 2.1. Selected genes differentially expressed (enriched) in LWS1 (GFP+) vs. LWS2 (RFP+) cones.

gene_name	gene_description	Log2FC	adj.P.Val
gngt2a	guanine nucleotide binding protein (G protein), gamma transducing activity polypeptide 2a	-1.36672	3.90E-12
nrip1a	nuclear receptor interacting protein 1a	-2.04606	1.69E-05
per1b	period circadian clock 1b	-1.04133	2.08E-05
cry1bb	cryptochrome circadian clock 1bb	-1.92388	3.12E-05
snap25a	synaptosomal-associated protein, 25a	-1.40065	0.000127
neurod1	neuronal differentiation 1	-1.3581	0.000382
taok2a	TAO kinase 2a	-1.03578	0.000645
foxg1a	forkhead box G1a	-2.25344	0.000732
ppef2b	protein phosphatase with EF-hand domain 2b	-1.82645	0.000732
hmgb1b	high mobility group box 1b	-1.2662	0.000749
znf395a	zinc finger protein 395a	-2.99349	0.000798
per3	period circadian clock 3	-1.16867	0.002191
plxna1a	plexin A1a	-1.29707	0.003367
efna1a	ephrin-A1a	-1.36806	0.005018
neurod4	neuronal differentiation 4	-1.90268	0.00563
acvr1ba	activin A receptor, type IBa	-1.67671	0.00563
thrab	thyroid hormone receptor alpha b	-1.17058	0.00563
pkp1b	plakophilin 1b	-1.56174	0.00644
nlgn4b	neuroligin 4b	-2.07195	0.011266
hmgb3a	high mobility group box 3a	-1.12235	0.01199
ntm	neurotrimin	-1.72035	0.022466
rorcb	RAR-related orphan receptor C b	-1.66891	0.030361
vax1	ventral anterior homeobox 1	-2.44783	0.034141
opn1lw1	opsin 1 (cone pigments), long-wave-sensitive 1	-1.72355	0.291626

Table 2.2. Selected genes differentially expressed (enriched) in LWS2 (RFP+) vs. LWS1 (GFP+) cones.

Name	Gene Description	Log2FC	adj.P.Val
psmb1	proteasome subunit beta 1	2.39001	1.09E-06
LOC562466	cyclic nucleotide-gated cation channel beta-3-like	1.729221	1.81E-05
calm1b	calmodulin 1b	2.011385	2.08E-05
adgrl3.1	adhesion G protein-coupled receptor L3.1	1.603454	0.000213
gngt2b	guanine nucleotide binding protein (G protein), gamma transducing activity polypeptide 2b	1.849842	0.000231
nptna	neuroplastin a	2.224251	0.002037
nr2f2	nuclear receptor subfamily 2, group F, member 2	1.693942	0.00244
sox4a	SRY (sex determining region Y)-box 4a	2.357806	0.005018
nr4a3	nuclear receptor subfamily 4, group A, member 3	2.099178	0.01027
ift27	intraflagellar transport 27 homolog (Chlamydomonas)	1.581392	0.011241
syt4	synaptotagmin IV	7.886233	0.02799
stox2a	storkhead box 2a	1.827619	0.028404

Table 2.3. Curated "short list" of transcripts DE in LWS1 (vs. LWS2) or LWS2 (vs. LWS1) prioritized for further study.

Name	Subtype Enriched	Predicted/Known function	Data predicting enrichment
gngt2a	LWS1	phototransduction	Dataset 1, 4
gngt2b	LWS2	phototransduction	Dataset 1, 2, 4
nrip1a	LWS1	nuclear receptor interacting	Dataset 1
nr2f2	LWS2	nuclear receptor	Dataset 1, 2
vax1	LWS1	transcription factor	Dataset 1
vax2	LWS1	transcription factor	Dataset 1
si:busm1	LWS1	endopeptidase inhibitor	Dataset 4
cry3a	LWS1	circadian rhythm	Dataset 4
six7	LWS1	transcription factor	Dataset 1, 4
irbp	LWS2	retinoid binding	Dataset 1
rbp41	LWS2	retinoid binding	Dataset 1, 4
sox4a	LWS2	transcription factor	Dataset 1
dio3b	LWS1	TH inactivator	Dataset 1, 2, 4

Figures

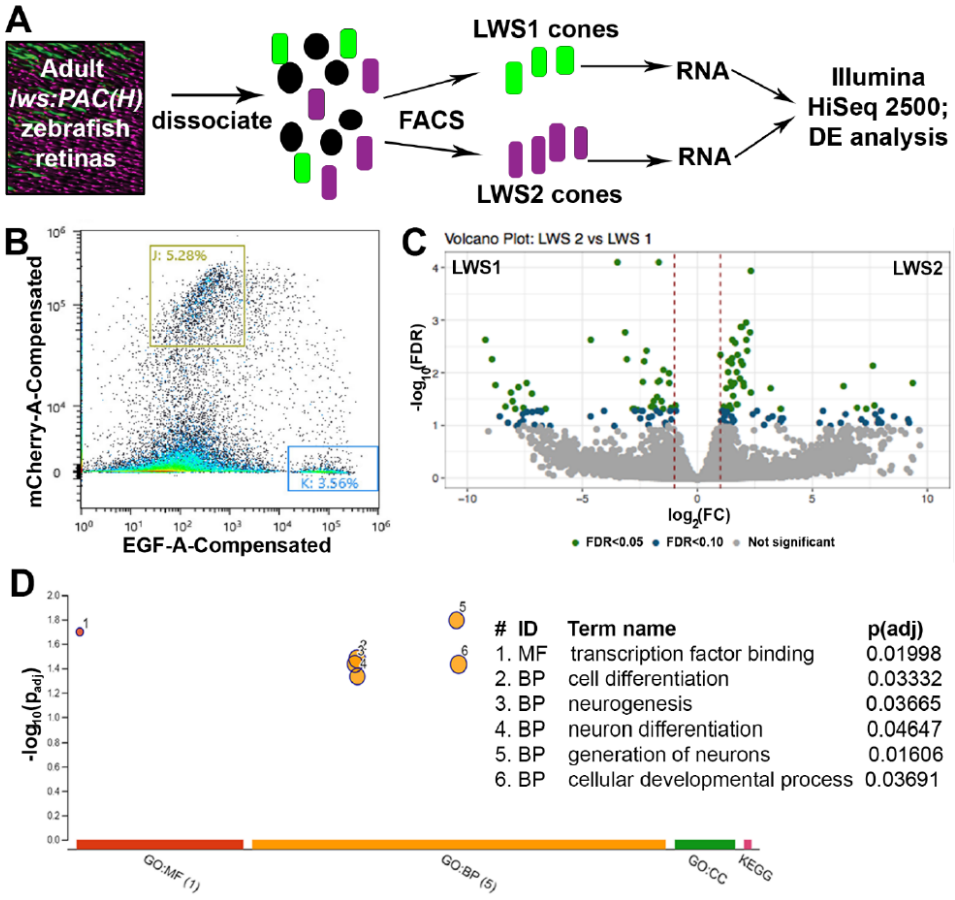

Figure 2.1: Comparative transcriptome analysis of LWS1 vs. LWS2 cones using FACS followed by bulk RNA-Seq. A) Schematic of dissociation and sequencing workflow. B) Representative (100,000 sorted events) sorting report for an *lws:PAC(H)* sample used in the study; red fluorescence intensity vs green fluorescence intensity. Gating strategy (boxes labeled J and K) for this sort resulted in the sorting percentages of events indicated. C) Volcano plot depicting transcripts differentially expressed (DE) in LWS1 (left side) vs LWS2 (right side) cones. Green symbols, transcripts DE at FDR < 0.05; blue symbols, transcripts DE at FDR < 1.0. D) Gene ontology (GO) analysis depicting GO categories overrepresented in the list of DE genes enriched in LWS1 (vs. LWS2) cones. MF, molecular function; BP, biological process.

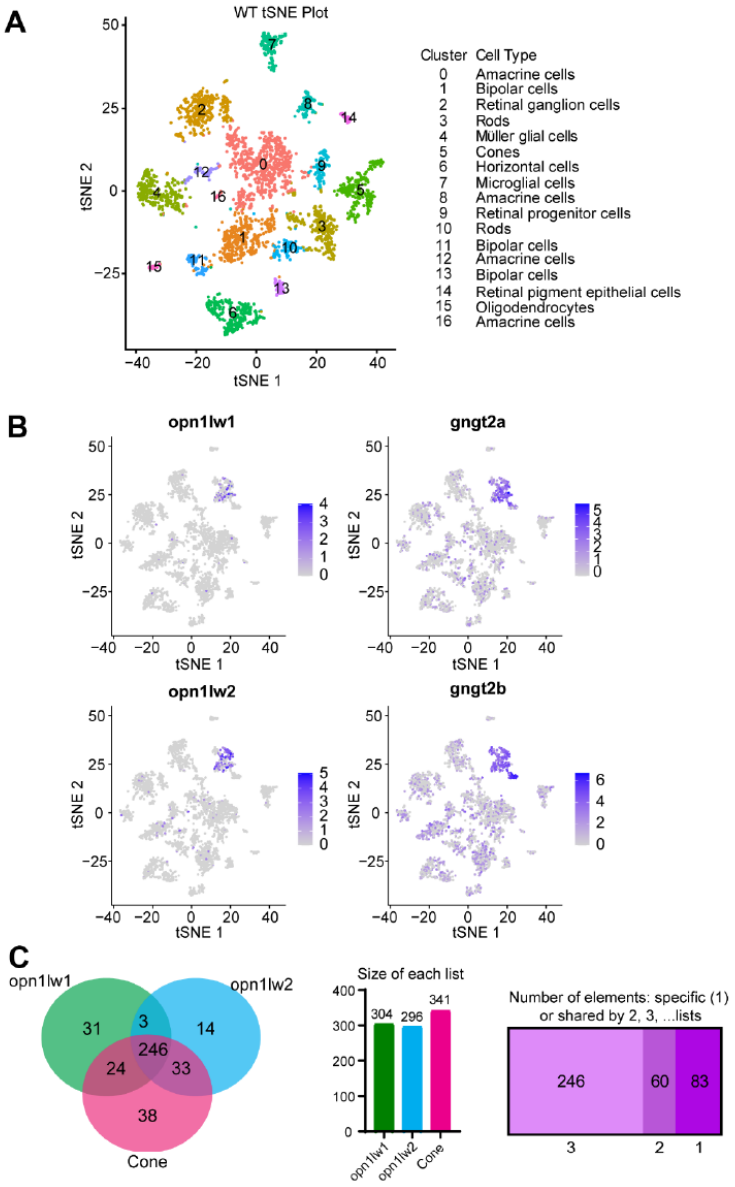

Figure 2.2: Single cell RNA-Seq and interrogation for transcripts enriched in LWS1 vs. LWS2 cones. A) Visualization of scRNA-Seq output using t-distributed stochastic neighbor embedding (TSNE) plots. Colors of plotted symbols correspond to retinal cell types as predicted by gene expression. B) Expression of *lws1* (*opn1lw1*), *lws2* (*opnlw2*), *gngt2a*, and *gngt2b* predominantly within the cone cluster of the TSNE plot. There is very little coincidence in *lws1* vs. *lws2* expression in individual cones, but greater coincidence for *gngt2a* and *gngt2b*. C) Venn diagram of genes specifically expressed by LWS1 cones, LWS2 cones, and the overall cone population. scRNA-Seq was able to identify transcripts unique to

each LWS cone subtype as well as those common to both. Individual lists of transcripts within each space of the Venn diagram are provided as Dataset 4.

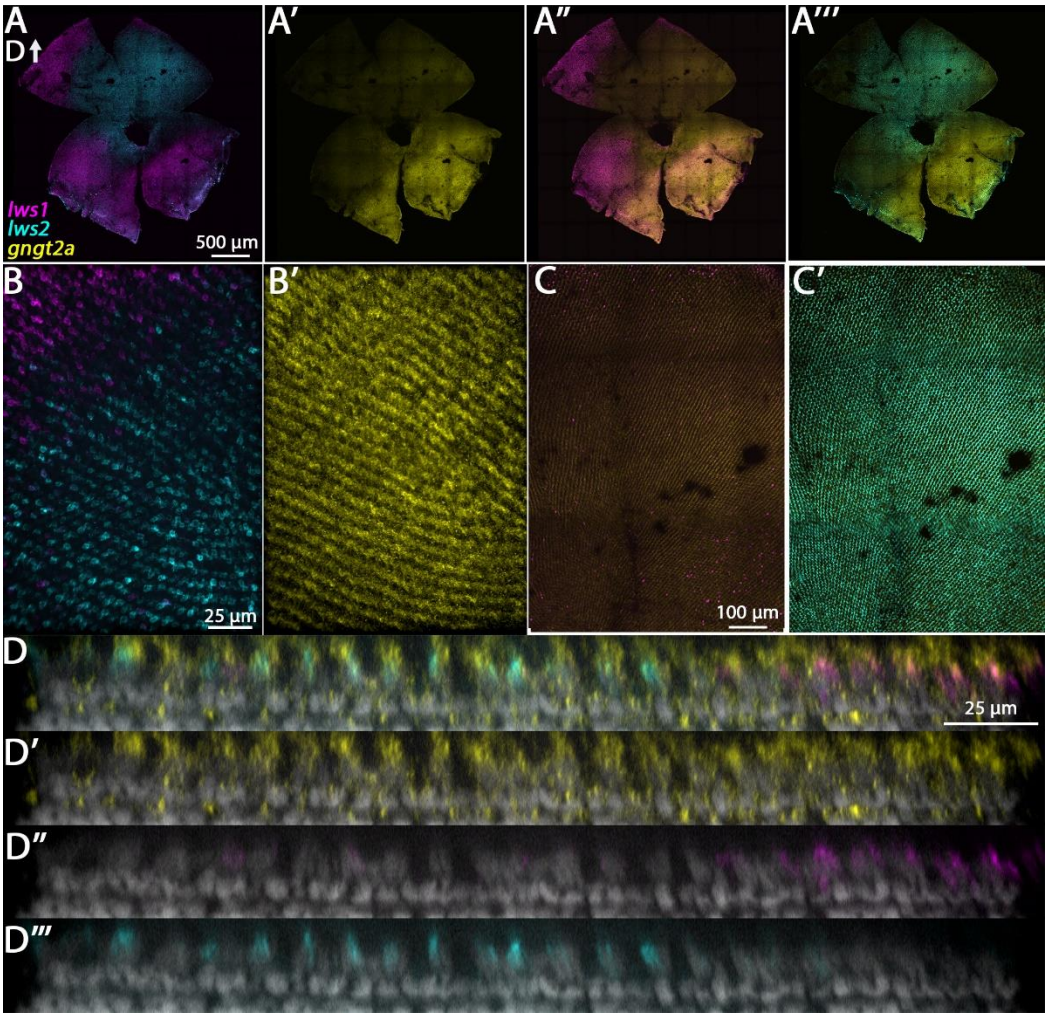

Figure 2.3: Expression of *gngt2a* in adult wildtype zebrafish retina using multiplex fluorescence in situ hybridization chain reaction (HCR). A) Expression of *lws1* (magenta) and *lws2* (cyan) in a representative whole retina (D, dorsal). A') Expression of *gngt2a* (yellow) in the same preparation, showing that signal intensity appears greatest in the *lws1*-expressing domain, but signal is not confined to this domain. A'') *gngt2a* and *lws1*. A''') *gngt2a* and *lws2*. B) 40x image of *lws1* and *lws2* expression in a region of transition from *lws1* to *lws2*. B') 40x image of *gngt2a* expression in the same region, indicating *gngt2a* is not restricted to *lws1*-expressing cones, nor to LWS cones in general. C) Selected enlarged region of A''showing *gngt2a* and *lws1*. D) Same region showing *gngt2a* and *lws2*. D-D''') Resliced orthogonal projections of B. D) All imaging channels merged. D') DAPI and *gngt2a*. D'') DAPI and *lws1*. D''') DAPI and *lws2*. *gngt2a* is co-expressed by *lws1*+ and *lws2*+ cones, as well as in non-LWS cones. Sample size=2.

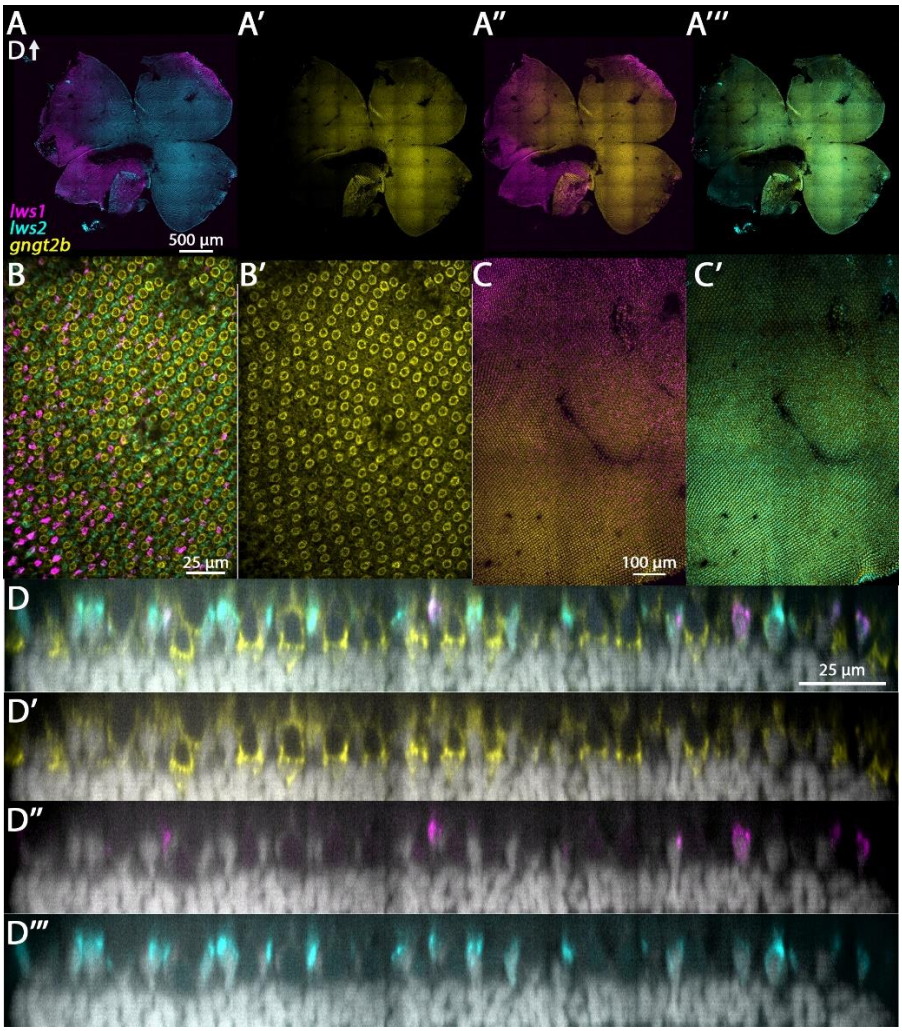

Figure 2.4: Expression of *gngt2b* in adult wildtype zebrafish retina using HCR. A) Expression of *lws1* (magenta) and *lws2* (cyan) in a representative whole retina. A') Expression of *gngt2b* (yellow) in the same preparation, showing that signal intensity appears greatest in the *lws2*-expressing domain. A'') *gngt2b* and *lws1*. A''') *gngt2b* and *lws2*. B) 40x image of *lws1*, *lws2*, and *gngt2b* expression in a region of transition from *lws1* to *lws2*, indicating *gngt2b* and *lws2* co-expression, and *gngt2b* expression in other populations of photoreceptors. B') 40x image of *gngt2b* expression, highlighting distinct subcellular expression domains of *gngt2b*. C) Selected enlarged region (transition zone) of A'' - *gngt2b* and *lws1*. D) Same region showing *gngt2b* and *lws2*. D-D''') Resliced orthogonal projections of B. D) All imaging channels merged. D') DAPI and *gngt2b*. D'') DAPI and *lws1*. D''') DAPI and *lws2*. D = dorsal. Sample size=2.

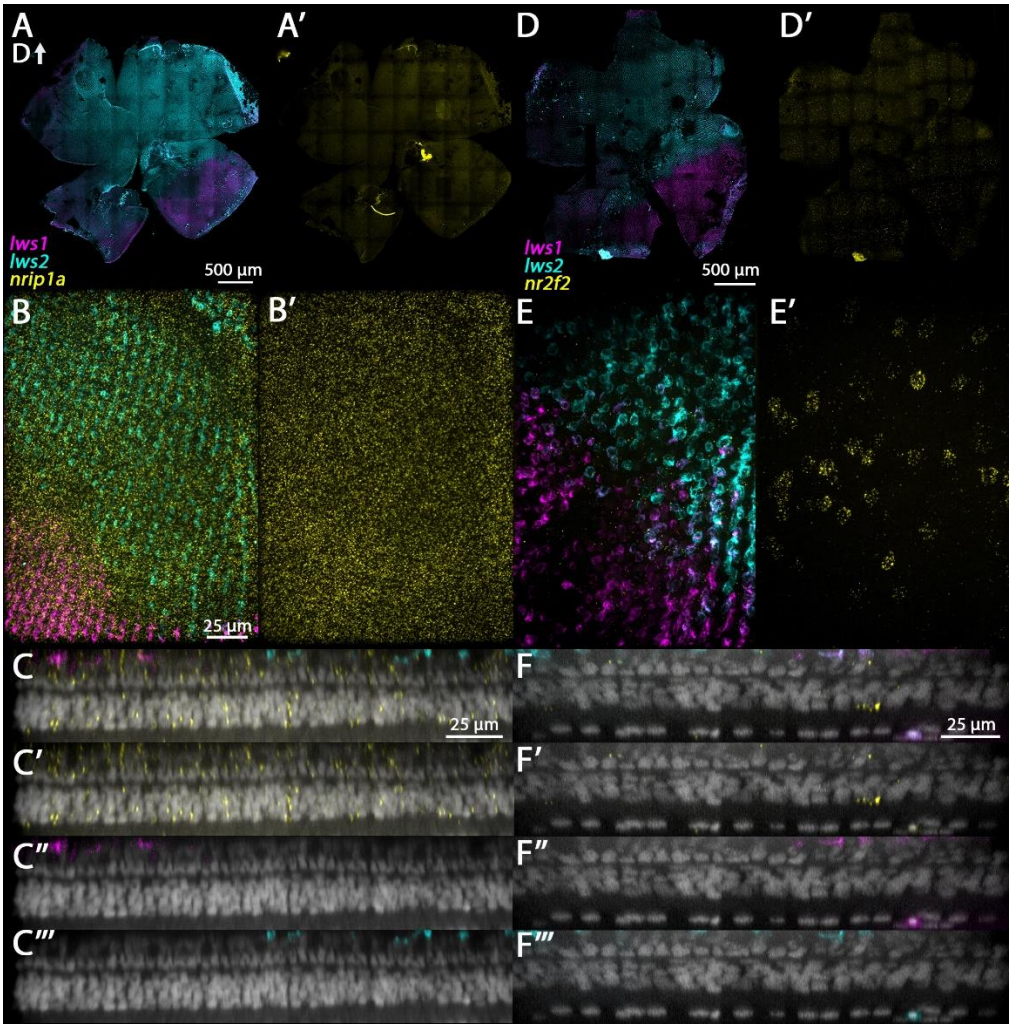

Figure 2.5: Expression of *nrip1a* and *nr2f2* in adult zebrafish retina. A-C’’’) *nrip1a*. D-F’’’) *nr2f2*. A) Expression of *lws1* (magenta) and *lws2* (cyan) in a representative whole retina. A’) *nrip1a* expression (yellow) in the same preparation, showing pan-retinal expression. B) 40x image of *lws1*, *lws2*, and *nrip1a* expression in a region of *lws1* to *lws2* transition. B’) *nrip1a* alone, in same region. C-C’’’) Resliced orthogonal projection of B. C) All imaging channels merged. C’) DAPI and *nrip1a*. C’’) DAPI and *lws1*. C’’’) DAPI and *lws2*. D) Expression of *lws1* (magenta) and *lws2* (cyan) in a representative whole retina. D’) *nr2f2* expression (yellow), showing slight bias in signal intensity toward dorsal retina. E) 40x image of *lws1*, *lws2*, and *nr2f2* expression in a region of *lws1* to *lws2* transition, at the level of cone inner segments. Scale same as in B. E’) *nr2f2* alone, in the same region, at the level of the deep INL. F-F’’’) Resliced orthogonal projection of E. F) All imaging channels merged. F’) DAPI and *nr2f2*. F’’) DAPI and *lws1*. F’’’) DAPI and *lws2*. D = dorsal. Sample size=2.

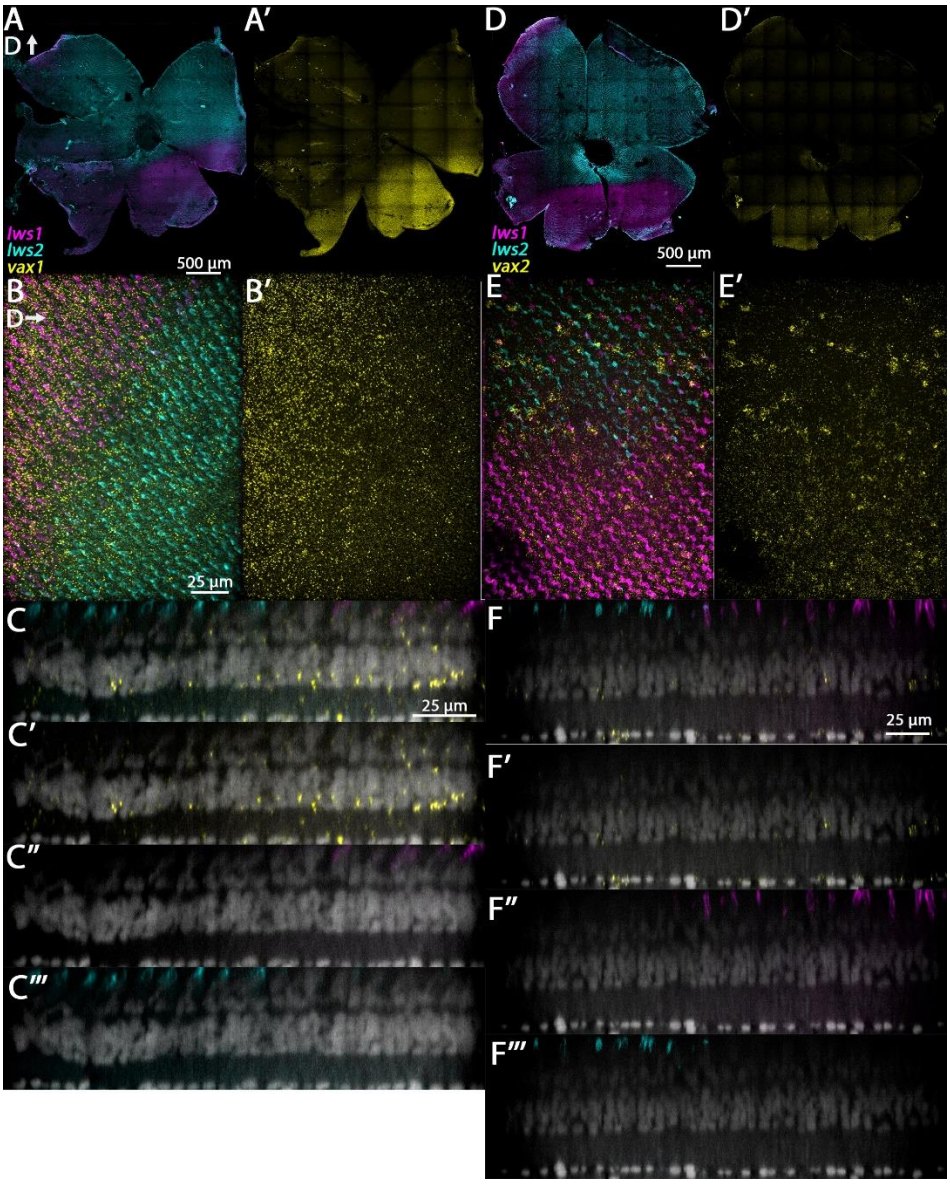

Figure 2.6: Expression of *vax1* and *vax2* in adult zebrafish retina. A-C’’’) *vax1*. D-F’’’) *vax2*. A) Expression of *lws1* (magenta) and *lws2* (cyan) in a representative whole retina. A’) *vax1* expression (yellow) in the same preparation, showing expression restricted to the *lws1*-expressing domain. B) 40x image of *lws1*, *lws2*, and *vax1* expression, in a region of *lws1* to *lws2* transition; orientation of B and B’ are such that dorsal is to the right. B’) 40x image of *vax1* alone, showing transition to *vax1* domain is less abrupt than the transition to the *lws1* domain. C-C’’’) Resliced orthogonal projections of B. C) All imaging channels merged. C’) DAPI and *vax1*. C’’) DAPI and *lws1*. C’’’) DAPI and *lws2*. D) Expression of *lws1* (magenta) and *lws2* (cyan) in a representative whole retina. D’) *vax2* expression (yellow) in the same

preparation, showing expression restricted to the *lws1*-expressing domain. E) 40x image of *lws1*, *lws2*, and *vax2* expression, in a region of *lws1* to *lws2* transition. E') 40x image of *vax2* alone in the same region, showing transition to *vax1* domain is less abrupt than the transition to the *lws1* domain. . F-F''') Resliced orthogonal projections of E. F) All imaging channels merged. F') DAPI and *nr2f2*. F'') DAPI and *lws1*. F''') DAPI and *lws2*. D = dorsal. Sample size=2.

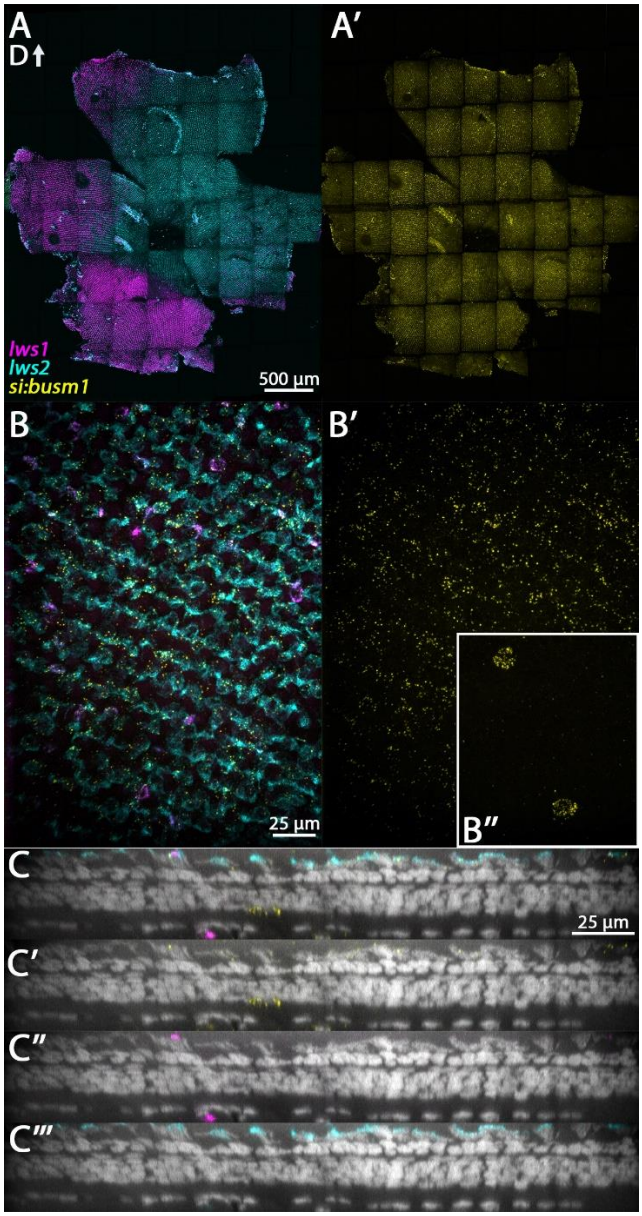

Figure 2.7: Expression of *si:busm1* in adult zebrafish retina. A) Expression of *lws1* (magenta) and *lws2* (cyan) in a representative whole retina. A') *si:busm1* expression (yellow) in the same preparation showing pan-retinal expression. B) 40x image of *lws1*, *lws2*, and *si:busm1* expression in a region of *lws1* to *lws2* transition. B') 40x image of *si:busm1* alone. Inset continues the field of view but at the level of the boundary between the inner nuclear layer and inner plexiform layer. C-C''') Resliced orthogonal projections of B. C) All imaging channels merged. C') DAPI and *si:busm1*. C'') DAPI and *lws1*. C''') DAPI and *lws2*. D = dorsal. Sample size=2.

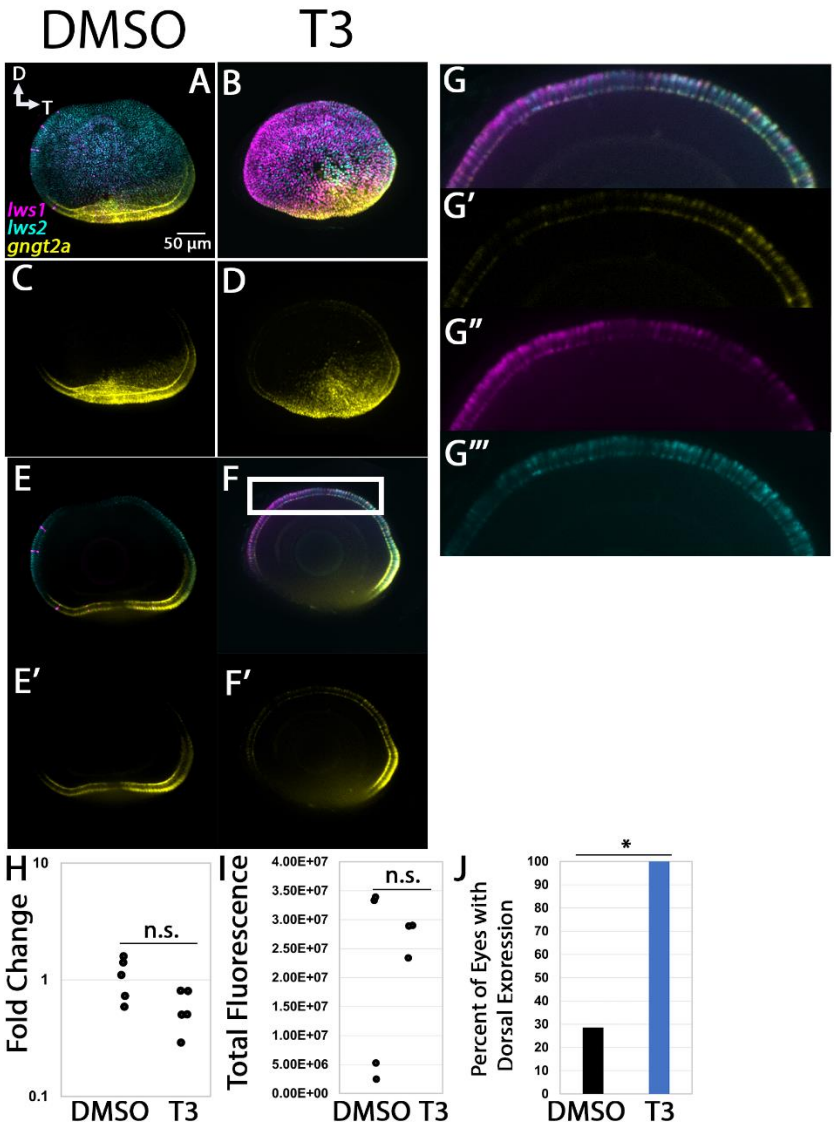

Figure 2.8: Expression of *gngt2a* in control (DMSO) and TH-treated (T3) larval zebrafish. A-D) Projections of representative whole, imaged eyes. Note reduced expression domain of *lws2* (cyan), and expanded expression domains of *lws1* (magenta) and *gngt2a* (yellow) in T3-treated (B, D) vs. controls (A, C); expanded domains do not appear to align, however. E-F') Single z slices obtained from the same preparations. G-G''') Enlarged images of region within box in F. G) All imaging channels merged. G') *gngt2a*. G'') *lws1*. G''') *lws2*. H) qPCR quantification of *gngt2a* transcript abundance in pooled samples of whole larvae, n=5 biological replicates per condition, p= 0.0967. I) 3D fluorescence intensity quantification, n=3 embryos per condition. J) percent of eyes with expression of *gngt2a* in dorsal retina, n = 7 (DMSO), 5 (T3), p=0.013. (proportion test). D = dorsal, T = temporal.

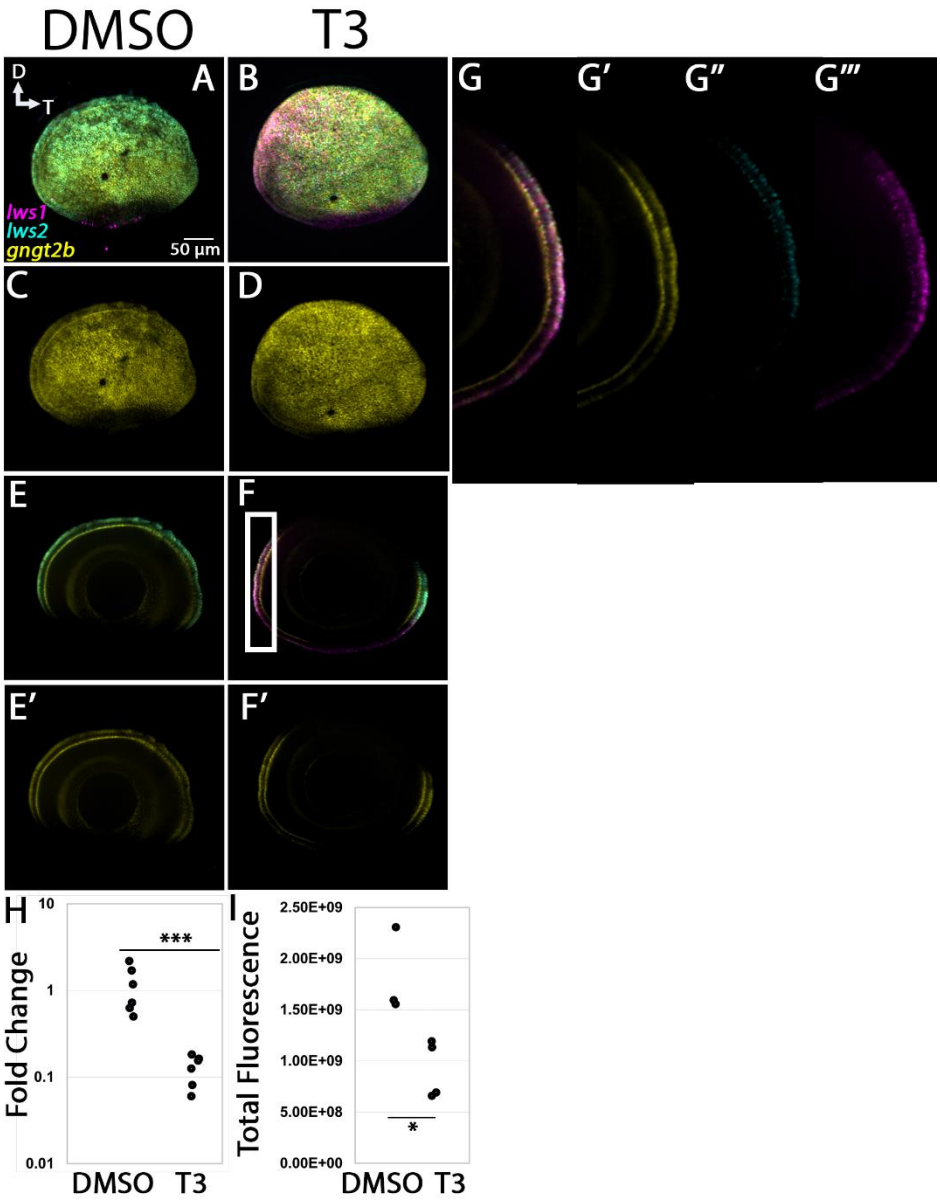

Figure 2.9: Expression of *gngt2b* in control (DMSO) and TH-treated (T3) larval zebrafish. A-D) Projections of representative whole, imaged eyes. Note reduced expression domain of *lws2* (cyan), and expanded expression domains of *lws1* (magenta) in T3-treated (B, D) vs. controls (A, C); the *gngt2b* (yellow) expression domain did not appear to change. E-F') Single z slices obtained from the same preparations. G-G''') Enlarged images of region within box in F. G) All imaging channels merged. G') *gngt2b* G'') *lws2* G''') *lws1* H) qPCR quantification of *gngt2b* transcript abundance in pooled samples of whole larvae, n=6 biological replicates per condition, p= 3.159E-05. I) 3D fluorescence intensity quantification, n=3 embryos (DMSO), 4 (T3). D=dorsal, T=temporal.

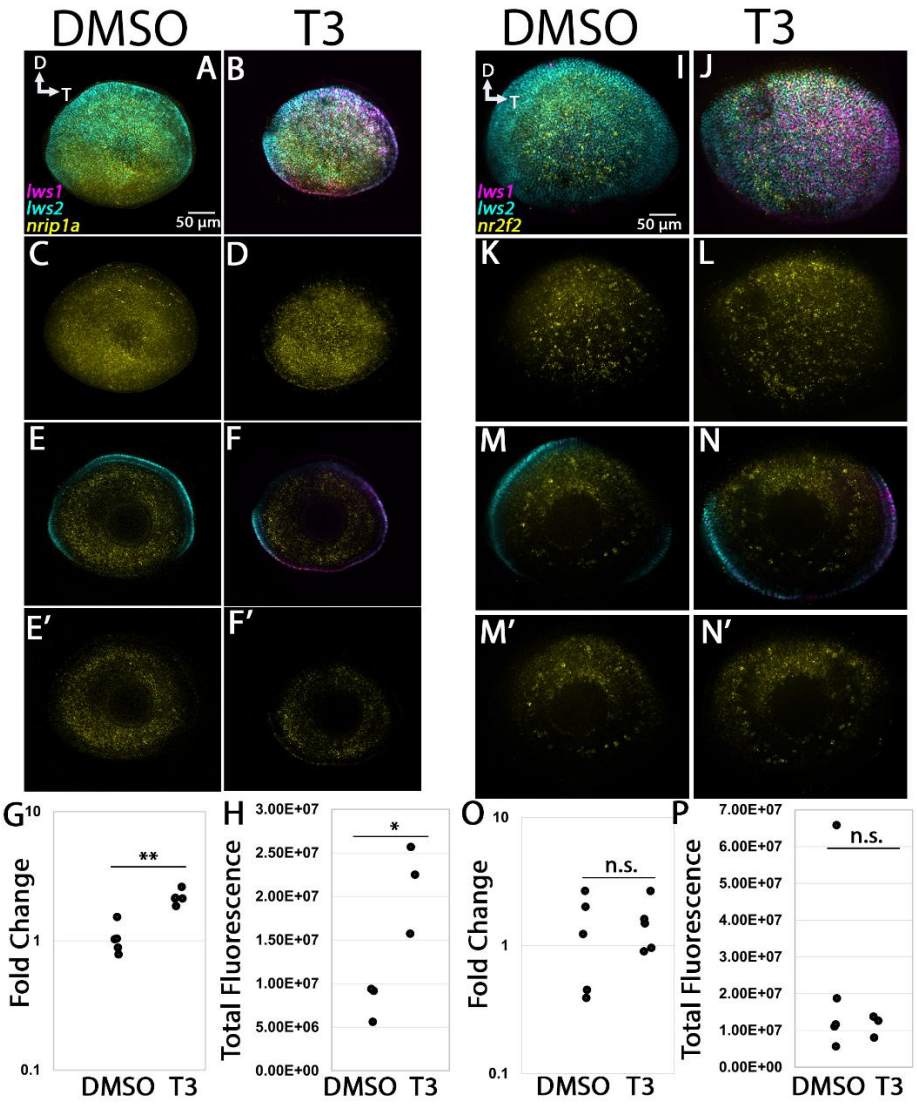

Figure 2.10: Expression of *nr2f2* and *nrip1a* in larval zebrafish. A-H) *nrip1a*. I-P) *nr2f2*. A-D, I-L) Projections of representative whole, imaged eyes. E-F', M-N') Single z slices obtained from the same preparations. Note reduced expression domain of *lws2* (cyan), and expanded expression domains of *lws1* (magenta) in T3-treated (B, D, J, L) vs. controls (A, C, I, K); the *nrip1a* (yellow, A-D) expression domain did not appear to change; the *nr2f2* (yellow, I-L) expression domain did not appear to change, however there appears to be slightly greater expression in the dorsal portion of the retina E,F) All imaging channels merged. E',F') *nrip1a* M,N) All imaging channels merged. M',N') *nr2f2* G) qPCR quantification of *nrip1a* transcript abundance in pooled samples of whole larvae, n = 5 biological replicates per condition, p= 0.476. H) 3D fluorescence intensity quantification for

nrip1a, n=5 embryos (DMSO), 3 (T3), sample size too small for Mann-Whitney test. O) qPCR quantification of *nr2f2* transcript abundance in pooled samples of whole larvae, n = 5 biological replicates per condition, p=0.00152 P) 3D fluorescence intensity quantification of *nr2f2*, n=3 embryos per condition, p=0.014 (t-test). D = dorsal, T = temporal.

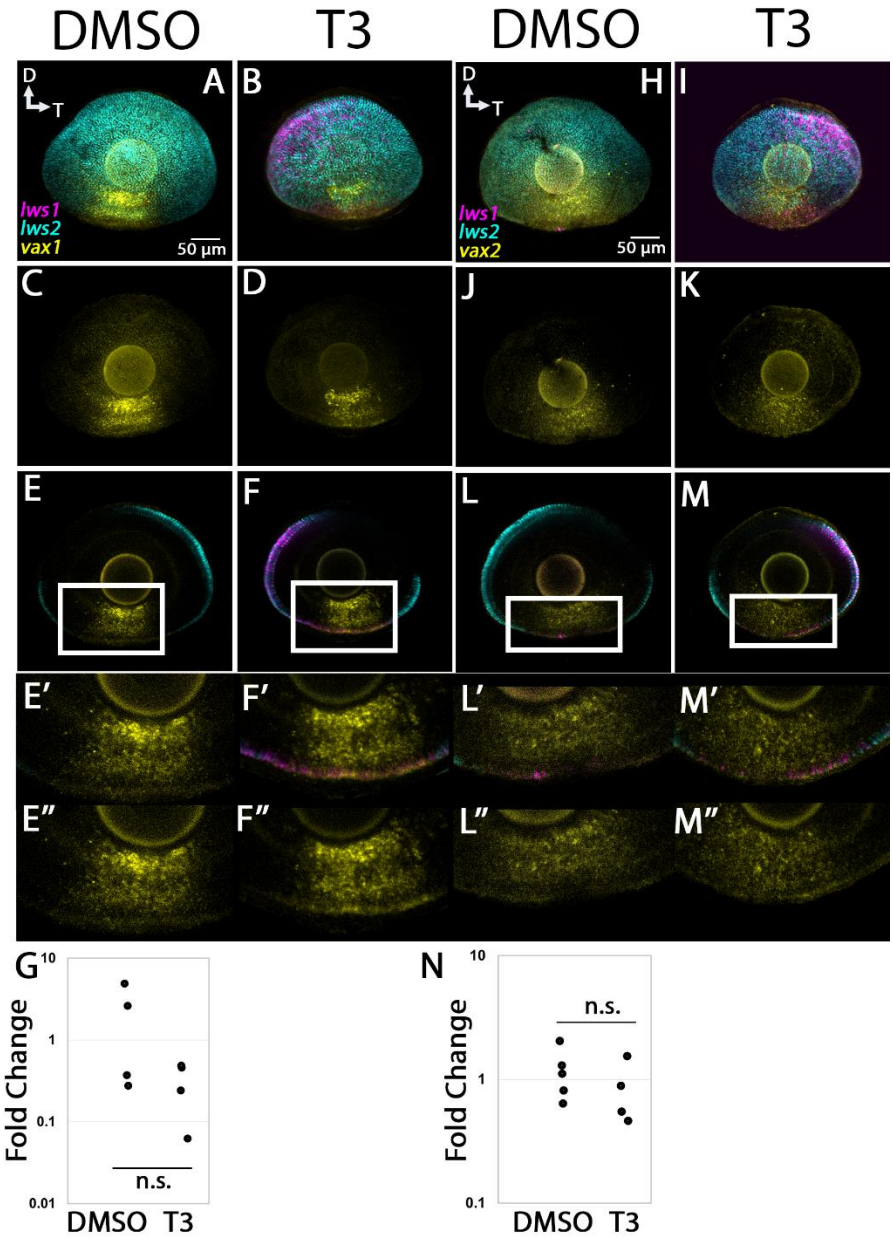

Figure 2.11: Expression of *vax1* and *vax2* in larval zebrafish. A-G) *vax1*. H-N) *nrip1a*. A-D, H-K) Projections of representative whole, imaged eyes . E-F'', L-M'') Single z slices obtained from the same preparations. Note reduced expression domain of *lws2* (cyan), and expanded expression domains of *lws1* (magenta) in T3-treated (B, D, I, K) vs. controls (A, C, H, J); the *vax1* (yellow, A-D) and *vax2* (yellow, H-K) expression domain did not appear to change. E'-F'') Enlarged images of regions within box of E, F, respectively. E',F') All imaging channels merged. E'', F'') *vax1* L'-M'') Enlarged images of regions within box of L, M, respectively. L',M') All imaging channels merged. L'',M'') *vax2* G) qPCR

quantification of *vax1* transcript abundance in pooled samples of whole larvae, n = 4 biological replicates per condition, p=0.123. N) qPCR quantification of *vax2* transcript abundance in pooled samples of whole larvae, n=5 biological replicates per condition, p= 0.312.

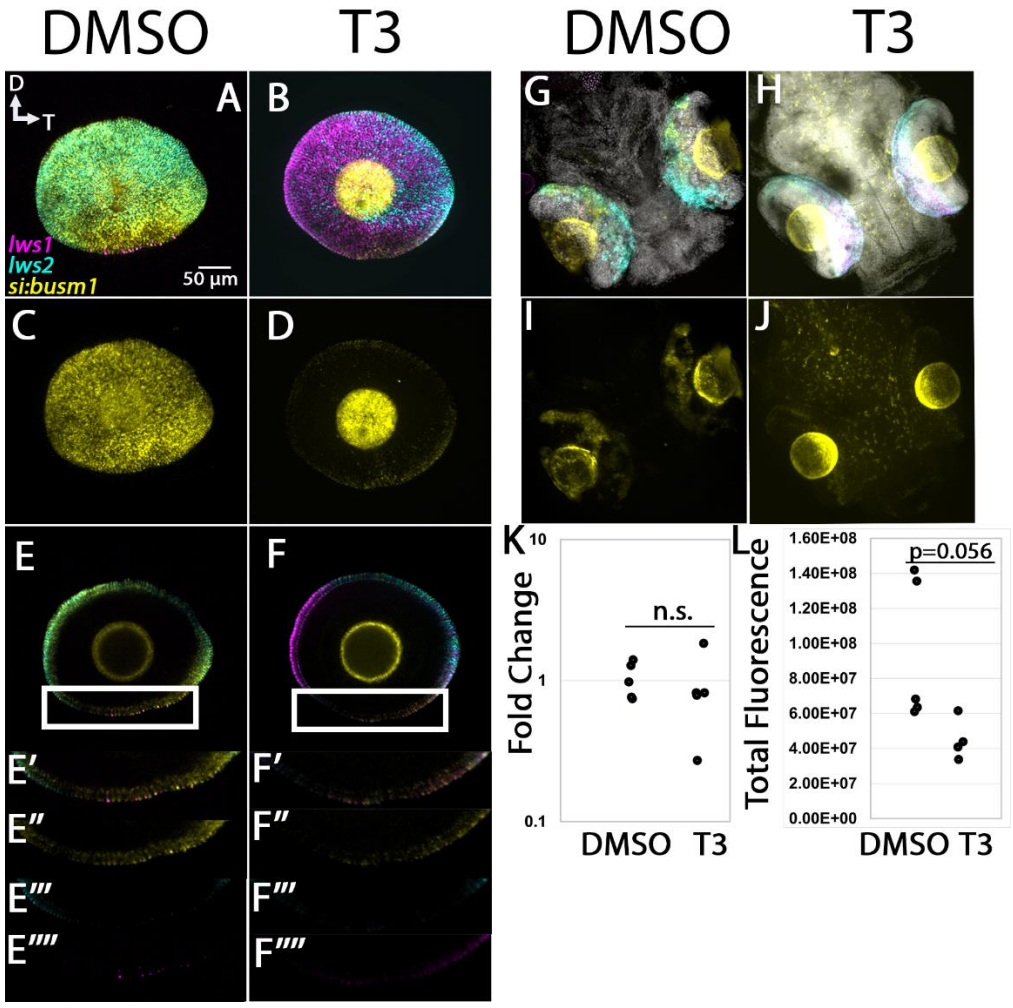

Figure 2.12: Expression of *si:busm1* in larval zebrafish. A-D) Projections of representative whole, imaged eyes . E-F’’’) Single z slices obtained from the same preparations. Note reduced expression domain of *lws2* (cyan), and expanded expression domains of *lws1* (magenta) in T3-treated (B, D) vs. controls (A, C); the *si:busm1* (yellow) expression domain appears greatly reduced in the treated condition (D). E’-E’’’) Enlarged images of region within box in E. E’) All imaging channels merged. E’’) *si:busm1* E’’’) *lws2* E’’’’) *lws1* F’-F’’’’) Enlarged images of region within box in F. F’) All imaging channels merged. F’’) *si:busm1* F’’’) *lws2* F’’’’) *lws1* G-J) Projections of whole embryo heads. K) qPCR quantification of *gngt2a* transcript abundance in pooled samples of whole larvae, n = 5 biological replicates, p= 0.244. L) 3D fluorescence intensity quantification, n=5 (DMSO), 4 (T3), p=0.056 (t-test). D = dorsal, T = temporal.

Supplemental Information

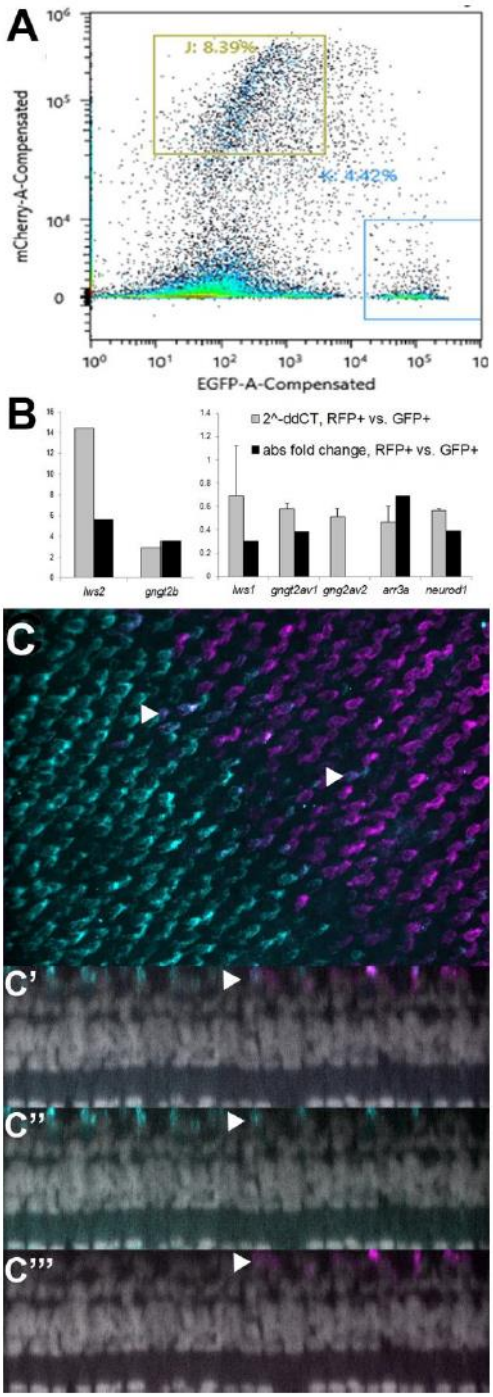

Supplemental Figure S2.1: qPCR validation of selected transcripts DE in LWS1 vs. LWS2 cones and evidence of some coexpression of *lws1* and *lws2* within LWS cones. A) Representative

(100,000 sorted events) sorting report for an *lws:PAC(H)* sample used for validation (referred to as “Sort #2” in text; results from “Sort #1” were reported in [1]; red fluorescence intensity vs green fluorescence intensity. Gating strategy (boxes labeled J and K) for this sort resulted in the sorting percentages of events indicated. B) Column graphs of qPCR results (2^ddCT; gray columns) and RNA-Seq fold change (black columns) for selected transcripts DE in LWS2 cones (left graph; increased transcript abundance in RFP+ vs. GFP+ cones) and in LWS1 cones (right graph; decreased transcript abundance in RFP+ vs. GFP+ cones). C) Multiplex fluorescence HCR in situ hybridization for *lws1* (magenta) and *lws2* (cyan) in a region of whole mounted retina displaying cones that express both transcripts (arrows). C’-C’’’) Resliced orthogonal projections of region in C showing all three color channels (DAPI, gray; *lws1*, magenta; *lws2*, cyan) (C’), DAPI and *lws2* only (C’’), DAPI and *lws1* only (C’’’).

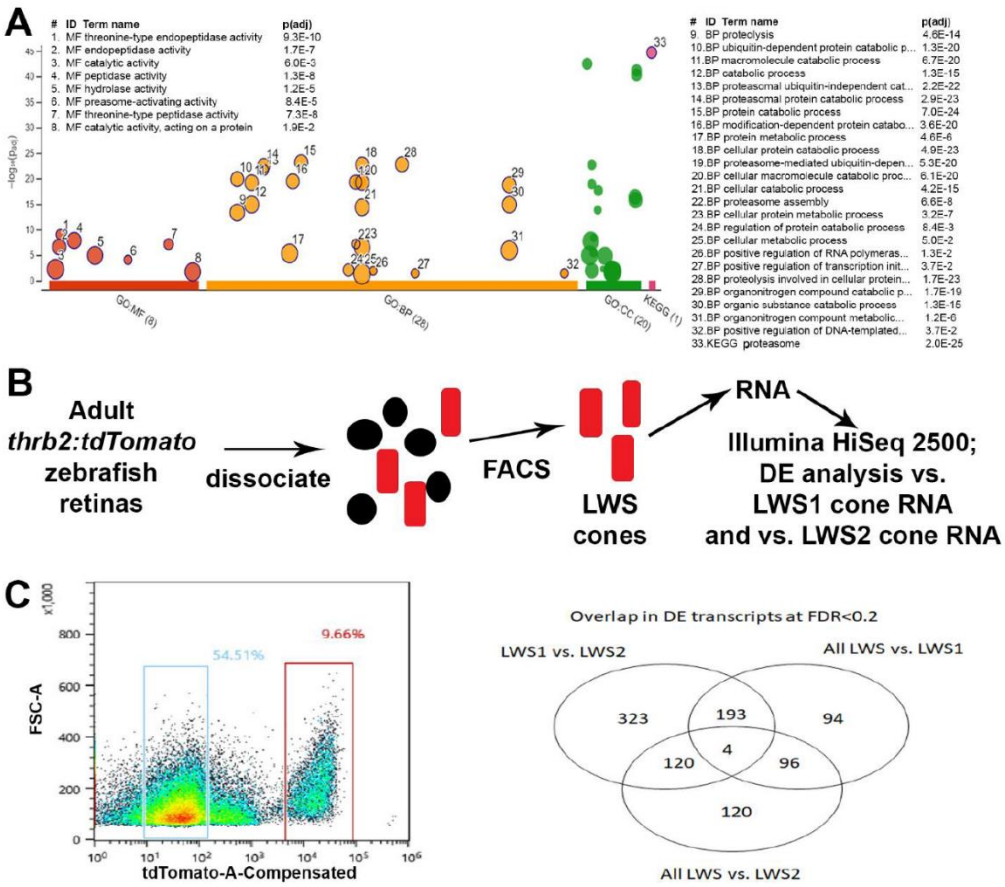

Supplemental Figure S2.2: A) Gene Ontology (GO) analysis depicting GO categories overrepresented in the list of DE genes enriched in LWS2 (vs. LWS1) cones. MF, molecular function; BP, biological process; CC, cellular component; KEGG, Kyoto encyclopedia of genes and genomes pathways. GO categories related to the proteasome dominate this analysis. B) Schematic of dissociation and sequencing workflow to obtain samples of LWS cones. C) Representative (100,000 sorted events) sorting report for an *thrb2:tdTomato* sample used in the study; red fluorescence intensity vs forward scatter. Gating strategy (red box) for this sort resulted in the sorting percentages of events indicated. D) Venn diagram of genes DE in LWS1 vs. LWS2 cones (from sort of *lws:PAC(H)* retinas), all LWS cones (from sort of *thrb2:tdTomato* retinas) vs. LWS1 cones (from sort of *lws:PAC(H)* retinas, and all LWS cones (from sort of *thrb2:tdTomato* retinas) vs. LWS2 cones (from sort of *lws:PAC(H)*). Approach identified transcripts DE in each LWS cone subtype as well as those common to both. Individual lists of transcripts within the overlapping regions of Venn diagram representing genes indicated as DE

in LWS2 cones (193 transcripts), and DE in LWS1 cones (120 transcripts) are provided in Dataset 3.

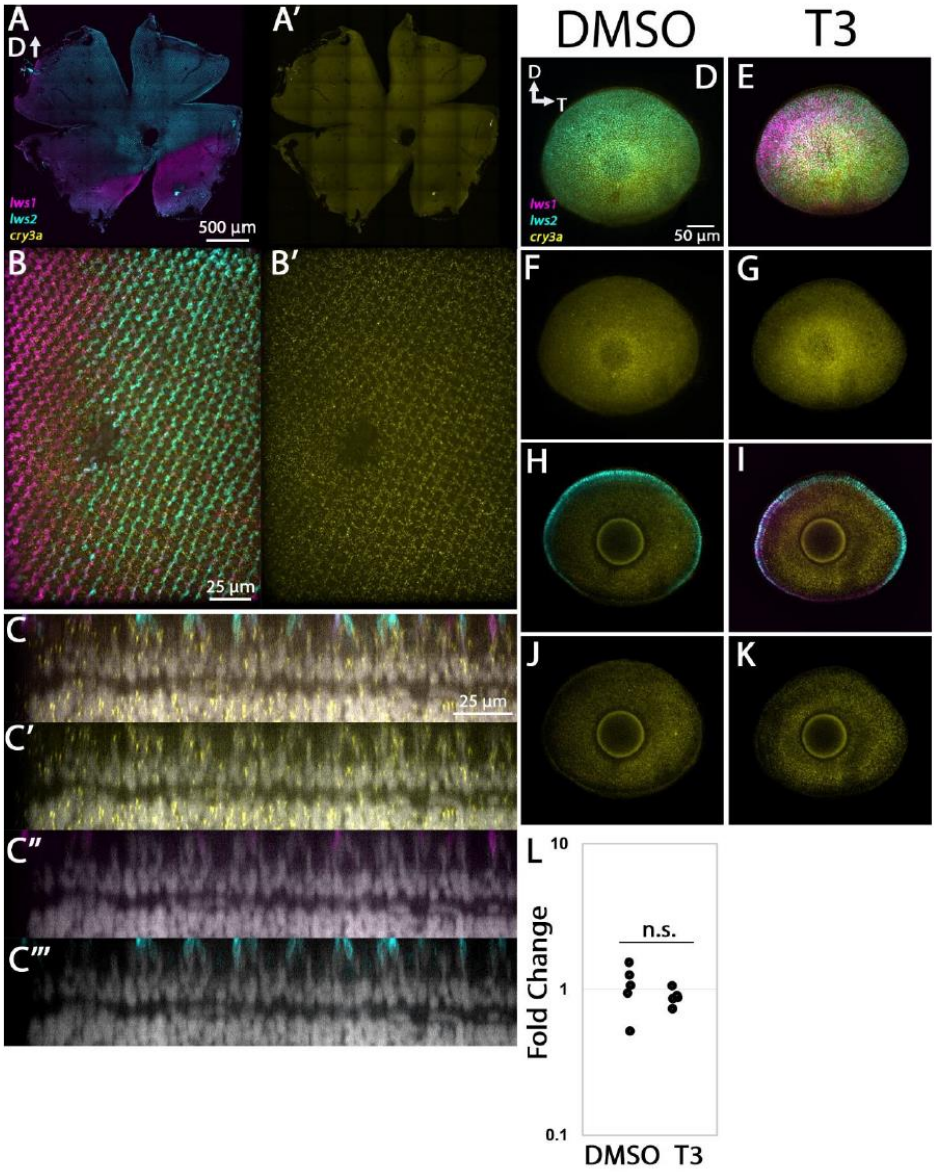

Supplemental Figure S2.3: Expression of *cry3a* in adult zebrafish retina (A-C), and in control (DMSO) and TH-treated (T3) larval zebrafish (D-K). A) Expression of *lws1* (magenta) and *lws2* (cyan) in a representative whole retina. A') *cry3a* expression (yellow) in the same preparation showing pan-retinal expression. B) 40x image of *lws1*, *lws2*, and *cry3a* expression in a region of *lws1* to *lws2* transition. B') 40x image of *cry3a* alone. C-C''') Resliced orthogonal projections of B. C) All imaging channels merged. C') DAPI and *cry3a*. C'') DAPI and *lws1*. C''') DAPI and *lws2*. D-G) Projections of representative whole, imaged eyes. Note reduced expression domain of *lws2* (cyan), and expanded expression domain of *lws1* (magenta) but *cry3a* expression (yellow)

appears unchanged in T3-treated (E, G) vs. controls (D, F). H-K) Single z slices obtained from the same preparations. L) qPCR quantification of *gngt2a* transcript abundance in pooled samples of whole larvae, n=5 biological replicates per condition, p= 0.335. D = dorsal, T = temporal.

Supplemental Table S2.1: Primers used for qPCR.

gene	forward primer	reverse primer
beta actin	GTACCACCAGACAATACAGT	CTTCTTGGGTATGGAATCTTGC
gngt2a	GTGACCTGTTGCCTCCATCG	TTTAGAGACAGGCTCTCTGGT
gngt2b	ATCCACAGTCAGGATGGCTCG	TCGGCAGATAAACCCTCCAC
nrip1a	TACGAGCCTCTCCGACTCTT	GACAGCCCTGTTCGGGTG
nr2f2	ACACAGTCAACCCCGACGAACC	TTTGTCCCCGCAAACCACGC
vax1	TCTGCAGCAAACCCCTCTAC	TCGTACCCTGTTCGTCCTTC
vax2	AGAGACGCCAAGGGCACTAT	GAAACCACACTTTCACCTGTGTC
si:busm1	AGGCGGTAGTTGTAGCAAGAAA	TTGCTCTGGGCTTGCTGTTA
cry3a	ATCATTGGCGTCCACTACCC	GGAGGCCAGAAGTCCAAGTC

Chapter 3: Phenotype Plasticity of Cone Photoreceptors in Adult Zebrafish Revealed by Thyroid Hormone Exposure

Ashley A. Farre, Preston Thomas, Johnson Huang, Rachael Poulsen, Emmanuel Owusu Poku, and Deborah L. Stenkamp

Abstract

Vertebrate color vision is possible due to the presence of multiple cone photoreceptor subtypes that are each maximally sensitive to different wavelengths of light. Thyroid hormone (TH) has been shown to be essential in the spatiotemporal patterning of cone subtypes in many species, including cone subtypes that express opsins that are encoded by tandemly replicated genes. TH has been shown to differentially regulate the tandemly replicated *lws* opsin genes in zebrafish, and exogenous treatments alter the expression levels of these genes in larvae and juveniles. In this study, we sought to determine whether gene expression in cone photoreceptors remains plastic to TH treatment in adults. We used a transgenic *lws* reporter line, multiplexed fluorescence hybridization chain reaction (HCR) *in situ* hybridization, and qPCR to examine the extent to which cone gene expression can be altered by TH in adults. Our studies revealed that opsin gene expression, and the expression of other photoreceptor genes, remains plastic to TH treatment in adult zebrafish. In addition to retinal plasticity, exogenous TH treatment alters skin pigmentation patterns in adult zebrafish after five days. Taken together, our results show a remarkable level of TH-sensitive phenotype plasticity in the adult zebrafish.

Introduction

Photoreceptors are the light-sensing neurons in the vertebrate retina. While rod photoreceptors are responsible for low-light, low-acuity vision, cone photoreceptors mediate high-acuity color vision. In many vertebrates, separate subpopulations of cones express distinct cone opsins: proteins that, together with a chromophore, form pigments that are maximally sensitive to specific wavelengths of light. The presence of multiple cone subtypes, each expressing a unique opsin and therefore sensitive to particular wavelengths of light, serves as the basis of color vision [1, 2].

Humans possess three cone subtypes (red-, green-, and blue-sensing) which express long wavelength sensitive (LWS), middle wavelength sensitive (MWS), and short wavelength sensitive (SWS) opsins, respectively [3] . The genes encoding the human LWS and MWS opsins are arranged in tandem on the X chromosome [4], and the mechanism by which they are regulated remains largely unknown. Several models for the regulation of the human *LWS* and *MWS* opsin genes have been suggested [5] [6, 7]; however, the study of tandemly replicated opsin genes is challenging due to the high sequence similarity of the primate LWS and MWS opsin proteins, mRNAs, and genes [8] and because the only non-human mammals known to express tandemly replicated opsins are other primates and bats [9]. Zebrafish, however, possess two sets of tandemly replicated opsins, the long wavelength sensing *lws* opsin genes (*lws1* and *lws2*) and the middle wavelength sensing *rh2* opsin genes (*rh2-1, rh2-2, rh2-3, rh2-4*) [10]. The zebrafish *lws* opsin genes and the human *LWS/MWS* opsin genes evolved from a common ancestral *LWS* opsin gene [9]. As such, the zebrafish serves as an excellent vertebrate model organism for the study of tandemly replicated opsin gene regulation.

Previous work using the zebrafish, other model organisms, and retinal organoids derived from human embryonic stem cells (ESC) or inducted pluripotent stem cells (iPSC) has shown that thyroid hormone (TH) is essential in determining cone subtype identity and patterning [11-17]. Recent studies from our lab demonstrated for the first time that TH regulates the expression of tandemly replicated opsin genes. For both the *lws* and *rh2* arrays, TH was shown to promote the expression of the long wavelength-shifted member(s) of the

array at the expense of the more short wavelength-shifted member(s), and the athyroid condition resulted in increased expression of the more short wavelength-shifted *lws2* at the expense of *lws1* [11]. These results added to a wide array of evidence showing TH has a conserved role in red-shifting retinal gene expression [18-22]. Further, treatment of zebrafish larvae with exogenous TH was shown to induce identified LWS2 cones to begin expressing *lws1* [11]. This phenomenon, which we refer to as "opsin switching" indicates that gene expression in individual larval LWS cones is plastic to TH treatment. Indeed, the expression of *lws1* and *lws2* in juveniles can also be altered by exogenous TH treatment, showing this plasticity remains at least through the juvenile stage [11].

The two LWS cone subtypes in the zebrafish, LWS1 and LWS2, are known to differ transcriptionally beyond opsin expression [17, 23]. We have shown that some of these differentially expressed transcripts are also plastic to TH treatment. For example, *gngt2a* and *gngt2b* are paralogous genes encoding gamma subunits of transducin (a heterotrimeric g-protein component of the phototransduction signaling cascade) and are enriched in LWS1 and LWS2 cones, respectively. *Gngt2b* is downregulated by TH treatment in larval zebrafish, as is *lws2*, while the expression domain of *gngt2a* expands in response to TH treatment, although transcript abundance does not change [17]. These results indicate that transcriptional heterogeneity between LWS cones beyond opsin expression is likely mediated in part by TH.

TH serves as an endocrine signal. The active form of TH is triiodothyronine (T3). Thyroxine (T4) is a less active form of thyroid hormone and can be converted to T3 in target tissues by the enzyme deiodinase 2 (Dio2). The thyroid gland primarily synthesizes T4, which is bound by carrier proteins and transported to tissues, where it enters cells through thyroid hormone transporters such as MCT8 [24-26]. T3 can bind to nuclear hormone receptors called TH receptors (TRs) to regulate gene expression. TRs can form homodimers or heterodimers with retinoid X receptors (RXRs), which bind retinoic acid [27, 28].

In this study, we aimed to determine the reach of TH-mediated transcriptional plasticity by investigating whether the cones of adult (0.5-1.5-year-old, reproductively mature) zebrafish remain plastic to TH treatment. While cone subtype patterning in juvenile

zebrafish is dynamic and likely regulated by both TH and retinoic acid (RA) signaling [11, 29], the pattern of cone subtypes in adult zebrafish is thought to be stable [30, 31]. T3 is present at detectable levels in the eyes of adult zebrafish, as is the T4 to T3-converting enzyme Dio2, indicating the possibility that TH may be involved in the homeostatic maintenance of cone subtype patterning in the adult zebrafish [32]. Other studies have shown that continued TH signaling is important to maintain skin pigment patterning in adult zebrafish [33]. It is unknown, however, whether exogenous TH treatment can change established cone subtype patterns in the adult zebrafish retina.

Our results in the current study indicate that cone subtype patterning in the retina is indeed plastic to exogenous TH treatment even in the adult zebrafish, and this plasticity occurs in as little as seven hours. We also found that the kinetics of the TH-induced changes in gene expression varied between transcripts. Specifically, the expression domain and transcript abundance of *lws1* changed more rapidly than those of other genes, including *lws2*. Additionally, we found that skin pigmentation patterns in adult zebrafish are also plastic to exogenous TH treatment. Taken together, our results show a remarkable level of TH-mediated plasticity in the adult zebrafish and underscore the importance of TH in maintaining homeostasis in cell patterning.

Methods

Animals.

Zebrafish were propagated and maintained according to Westerfield, on recirculating, monitored, and filtered system water, on a 14:10 light/dark cycle, at 28.5°C [34]. Procedures involving animals were approved by the Animal Care and Use Committee of the University of Idaho. Wild-type (WT) zebrafish were of a strain originally provided by Scientific Hatcheries. The *lws:PAC(H)* transgenic line harbors a PAC clone that encompasses the *lws* locus, modified such that a GFP-polyA sequence, inserted after the *lws1* promoter, reports expression of *lws1*, and an RFP (dsRedExpress)-polyA sequence, inserted after the *lws2* promoter, reports expression of *lws2* [35]. This line was the kind gift of Shoji Kawamura and the RIKEN international resource facility. Adult (0.5 – 1.5 years; both sexes) zebrafish were used.

Thyroid Hormone Treatments.

Stock solutions of tetra-iodothyronine (T4) were prepared in NaOH (Sigma), and maintained at -20°C in the dark. During treatments, adult zebrafish were maintained individually in 250 mL beakers in system water. 10,000X T4 stock solution was added to system water for a final concentration of 386 nM as in Suliman *et al.* 2014 [11, 36] (NaOH final concentration was 0.01% and did not alter system water pH). Controls were treated with 0.01% NaOH. For experiments lasting > one day, fish were fed once daily and treatment solution was completely replaced after feeding. Duration of treatments was seven hours, 12 hours, 24 hours, or five days (Figure S1) [11]. T4 (rather than T3 or a synthetic analog) was used as the experimental treatment to be consistent with other studies of TH treatment in postlarval fish [11, 22, 33, 37].

RNA Extraction and Quantitative RT-PCR (qPCR).

Total RNA from zebrafish eyes was extracted using the Machery-Nagel Nucleospin RNA kit, and then the Superscript III/IV (Invitrogen) was used to synthesize cDNA template with random primers. Gene-specific primer pairs for qPCR are provided in Supplemental Table S1. Amplification was performed on a StepOne Real-Time PCR system using SYBR Green or Power Track SYBR Green master mix (Applied Biosystems). Quantification of transcript abundance was relative to the reference transcript (*β-actin*), using the ddCT method. Graphing and statistics were performed in Excel. Sample groups were evaluated for normal distributions using the Shapiro-Wilk test. For comparisons showing normal distributions, p-values were calculated using Student's t-test, and for comparisons not showing normal distributions, p-values were calculated using Mann-Whitney tests. *** denotes $p<0.001$, ** denotes $p<0.01$, * denotes $p<0.05$.

Histological Processing

Fixation and preparation of adult PAC(H) eyes for tissue sectioning were performed as previously described [11, 29, 38, 39]. In brief, zebrafish were humanely euthanized, eyes were removed, and then were fixed with 4% paraformaldehyde overnight at 4°C, washed in increasing concentrations of sucrose, cryoprotected overnight at 4°C in phosphate-buffered

20% sucrose, embedded and frozen in a 2:1 solution of 20% sucrose: OCT medium (Sakura Finetek, Torrance, CA), and sectioned at 5 μm thick [40].

Hybridization Chain Reaction (HCR) in situ Hybridization.

HCR procedures were carried out according to the manufacturer's instructions (Molecular Instruments), with the exception that we did not incorporate a proteinase K treatment prior to the post-fixation step. In brief, zebrafish retinas were dissected and fixed overnight in phosphate-buffered 4% paraformaldehyde in phosphate-buffered saline (PBS) at 4°C. Tissues were then washed in PBS, dehydrated in MeOH, and stored in MeOH at -20°C at least overnight. Tissues were rehydrated in a graded MeOH/PBS/0.1% Tween 20 series, and post-fixed with 4% paraformaldehyde in PBS prior to hybridization. Hybridization was done overnight at 37°C. Tissues were washed with the manufacturer's wash buffer, and then 5XSSCT (standard sodium citrate with 0.1% Tween-20), and the amplification/chain reaction steps were performed following the manufacturer's protocol. Probe sets were designed and generated by Molecular Instruments and can be ordered directly from their website.

Confocal Microscopy.

Whole, fixed *lws:PAC(H)* adult retinas, cryosections of *lws:PAC(H)* eyes, and HCR-processed, adult (0.5-1.5 years) WT retinas were mounted in glycerol and imaged with a 20X dry lens using a Nikon-Andor spinning disk confocal microscope and Zyla sCMOS camera running Nikon Elements software, and 3 μm-step sizes were used for Z-series images. Z-stacks were flattened by max projection, and brightness/contrast adjusted in FIJI (ImageJ).

Analysis of Comparative Areas of Expression Domains.

Expression domains were traced using the freehand measurement tool in FIJI/ImageJ as described in Stenkamp *et al* 2021 [38]. Areas containing predominantly or exclusively GFP+ cones or RFP+ cones were measured within the individual fluorescence channels while areas containing "interspersed GFP+ and RFP+" cones were measured using both the red and green channels. Each area was traced in triplicate with the freehand selection tool in FIJI to ensure measurement reproducibility. Percentages were determined by dividing the number of pixels in each expression domain by the number of pixels in the entire retina [38].

The Shapiro-Wilk test was used to check for normal distribution. Differences between each measurement were tested using Student's T-test. Overall difference between control and treatment was tested using Fisher's Exact Test.

Brightfield Photography and Color Measurements.

Fish were anesthetized using MS-222 and placed on a sterilized portion of the lab bench. Fish were photographed using a Canon PowerShot SX70 HS, and each fish was photographed with and without flash, with a focal length between 40 and 60 mm. Stripe and interstripe colors of individual zebrafish were measured using the RGB spectrum tool in Adobe Photoshop [41].

Results

T4 treatment alters topography of lws1 and lws2 reporter patterning in adult lws:PAC(H) transgenic fish.

The *lws:PAC(H)* transgenic reports *lws1* expression with GFP and *lws2* expression with RFP. This line has been shown to recapitulate the characteristic pattern of *lws1* and *lws2* mRNA-expressing cones in the adult zebrafish, in which *lws1* is expressed in the ventral and nasal periphery, with some expression in the dorsal periphery, and *lws2* is expressed centrally and dorsally [31, 35]. Further, the *lws1* and *lws2* reporters reproduce the response of the native transcripts to TH [11]. In larval zebrafish, native *lws1* mRNA and the GFP reporter of *lws1* in *lws:PAC(H)* show increases in size of their expression domains in response to 100nM TH treatment while native *lws2* mRNA and the RFP reporter of *lws2* in *lws:PAC(H)* domains decrease [11]. Previous studies have shown that treatment of athyroid juvenile *lws:PAC(H)* zebrafish with T4 rescues GFP (*lws1*) expression, indicating that the reporter construct remains plastic to TH treatment at the juvenile stage, similar to the behavior of the native *lws* array [11]. As such, we reasoned it would be appropriate to investigate plasticity using the *lws:PAC(H)* reporter line.

Confocal imaging and subsequent expression domain area analysis showed that after five days of treatment with T4, the GFP (*lws1*) expression domain significantly expanded in comparison to controls (Fig. 1A-F). In control retinas, the GFP domain was found to include

approximately 60 % of the retina, while in TH treated retinas, the GFP domain covered over 90% of the retina (Fig. 1I). In contrast, the RFP (*lws2*) domain remained similar in both groups (approximately 60 %, Fig. 1J). This resulted in an increased region of interspersed and/or coexpressing GFP+ and RFP+ cones (Fig. 1K). Five-micron tissue sections (Fig. 5G, H) showed that in retinas from T4-treated fish, the majority of RFP expressing cells also expressed GFP (Fig 1H’’’). This coexpression could indicate that both members of the transgenic array were being transcribed or that only GFP was transcribed, but RFP (protein) had not yet been degraded. In order to distinguish between these possibilities, our next studies focused on monitoring endogenous mRNA.

Five days of T4 treatment induce widespread cone transcriptional changes.

Confocal imaging of retinas that underwent HCR *in situ* for *lws1* and *lws2* revealed that after five days of T4 treatment, the *lws1* expression domain expanded to a similar extent seen in the *lws:PAC(H)* reporter transgenic (Fig. 2A-F). Interestingly, *lws2* transcript was undetectable by HCR after five days of T4 treatment (Fig. 2E). Because our previous study identified the increase in *lws1*-expressing cones as the result of individual cones switching opsins [11], and because our current results obtained from the *lws:PAC(H)* transgenics showed widespread coexpression of GFP reporting *lws1* and RFP reporting *lws2*, we interpret that the expanded *lws1* domain and lack of *lws2* transcript was likely due to opsin switching. In other words, cone photoreceptors that previously expressed *lws2* have switched to express solely *lws1*. These results also suggest that the GFP:RFP coexpression seen in the *lws:PAC(H)* fish (Fig 1D) was likely due to slow degradation of the dsRedExpress reporter. Further, qPCR data showed that after five days of T4 treatment, *lws1* transcript abundance increased, while *lws2* transcript abundance decreased, in agreement with the HCR confocal images (Fig 2G).

We next analyzed other genes known to exhibit altered transcriptional abundance after TH treatment. We found that the abundance of *gngt2b*, encoding a gamma subunit of transducin associated with LWS2 cones and other cone subtypes in the central retina [23, 42], and known to be downregulated by T3 treatment in larvae, decreased after five days of T4 treatment of adults (Fig 2G) [17]. This finding suggests that cone photoreceptor genes other

than those encoding opsins remain plastic to the effects of TH even in adulthood. We also analyzed *gngt2a*, encoding a paralogous gamma subunit associated with LWS1 cones [17, 42], and showing altered expression domain following T3 treatment in larvae, though not changing in transcript abundance [17]. In T4 treated adults, abundance of this transcript was not altered (Fig. S2). The *rh2* array is another set of tandemly replicated opsins in zebrafish [10], and the members of this array are known to be affected by TH treatment in larval and juvenile fish [11, 17]. We found that, in keeping with larval and juvenile data, exogenous T4 treatment of the adults resulted in decreased *rh2-1* transcript abundance. Interestingly, while *rh2-2* is upregulated by exogenous T3 in larvae and unchanged in the juvenile by T4, we found that exogenous treatment of T4 downregulated *rh2-2* in the adult (Fig 2G). While the expression domains of the *lws* and *rh2* opsins shift through the juvenile stage, the expression domain of *rh2-2* is particularly dynamic as the fish ages [31]. In the embryo, *rh2-2* is expressed both centrally and peripherally. In the juvenile, *rh2-2* is expressed in the dorsal periphery and ventral mid-periphery, and in adults, *rh2-2* is expressed centrally [31]. Previous work has shown how cis elements of the *rh2* array underly expression domains of the *rh2* genes in adult zebrafish [35]. Our results here provide additional insight into how TH may also be involved in tuning the expression of *rh2* genes, and that this tuning effect may change over the zebrafish lifespan.

T4 treatment induces widespread cone transcriptional changes in as little as 24 hours.

We then tested whether shorter treatments would also generate changes in transcription of cone genes. Interestingly, the results of the 24-hour treatment were similar to those of the five-day experiment, suggesting that gene expression in cone photoreceptors responds rapidly to changes in T4 levels (Fig. 3A-F). We found that after 24 hours of T4 treatment, the *lws1* expression domain expanded to cover the entire retina and *lws2* expression became undetectable by HCR (Fig. 3D-F). The 24-hour qPCR results were also similar to the five-day results, showing that the transcript abundance of *lws1* increased after treatment while the abundance of *lws2, gngt2b, rh2-1 and rh2-2* transcripts significantly decreased (Fig. 3G), while that of *gngt2a* did not change (Supplemental Fig. S2).

Twelve hours or less of T4 treatment alters lws1 expression, but not the expression of other T4-regulated transcripts.

Confocal imaging of retinas that underwent HCR *in situ* revealed that after 12 hours of T4 treatment, the *lws1* expression domain expanded to a similar extent seen in five day and 24-hour treatment groups (Fig. 4A-F). In contrast, however, the *lws2* expression domain remained similar to that of controls (Fig. 4B,E). We found that most of the cells in which *lws2* mRNA was detected also showed *lws1* expression (Fig. 4D). Because mRNA half-lives in vertebrates exhibit a wide range, from minutes to several hours) , these results could indicate that many LWS cones actively transcribe both opsin genes after 12 hours of T4 treatment, or that the cones have switched to express *lws1* while *lws2* mRNAs remain [43, 44]. The specific half-lives of cone opsin mRNAs have not yet been determined, to our knowledge. Our qPCR results corroborate our *in situ* data, showing a significant increase in *lws1* transcript abundance but no change in *lws2* transcript abundance (Fig. 4G). Further, the transcript abundance of the other genes we investigated (*gngt2b, gngt2a, rh2-1, rh2-2*) also did not change (Fig. 4G; Supplemental Fig. S2). These results suggest that 12 hours is not sufficient for all T4-mediated transcriptional changes to be made in adult retina. This could indicate that an insufficient amount of T4 was able to enter the retina to induce the same level of changes as seen in the 24-hour treatment; however, as T3 levels in a particular cell can be specifically regulated by local deiodinase enzymes [24], this would require further study to determine. Alternatively, these results could indicate that *lws1* responds to TH through a direct mechanism while other genes respond through slower (indirect) mechanism, or that in general there are temporally different transcriptional control responses at different loci. Interestingly, in larvae, 24 hours of treatment, from 2-3 days post-fertilization (dpf) with 100nM T3 produced similar results to the adult 12-hour treatment, in which *lws1* levels increased while *lws2* levels did not change, but by 48 hours of larval treatment (2-4 dpf), *lws2* levels decreased [11]. The faster rate of TH-induced changes in adults could be due to the higher concentration of TH in the system water (100nM for larvae vs 386nM for adults), or other factors such as changes in the temporal controls of TH response between larvae and adults.

Confocal imaging of adult retinas that underwent HCR *in situ* revealed that after seven hours of T4 treatment, the *lws1* expression domain expanded to a similar extent seen in the previous treatment groups and the *lws2* expression domain remained similar to that of controls (Fig. 5A-F). We found that most of the cones in which *lws2* mRNA was detected also showed *lws1* expression (Fig. 5D). Our qPCR results corroborate these data, showing a significant increase in *lws1* transcript abundance but no change in *lws2* transcript abundance (Fig. 5G). Further, the transcript abundance of the other genes we investigated by qPCR (*gngt2b, gngt2a, rh2-1, rh2-2*) also did not change (Fig. 5G; Supplemental Fig. S2). These results suggest that seven hours is not sufficient to generate all T4 mediated changes in adult cone transcription.

The results from the 12 and seven-hour experiments show that the kinetics of T4 treatment and changes in gene expression within adult retinas are complex. Since zebrafish have two loci for each specific opsin gene (all are on autosomes), the coexpression could be achieved either by the expression of both genes on each locus, or by the expression of one gene from one locus and the other gene from the second locus. Alternatively, it is possible that *lws2* was not being transcribed and the mRNA from hours before has not yet been degraded. Other factors, including a temporal difference in the mechanisms controlling *lws1* vs *lws2* expression could also underly this observation.

Exogenous T4 treatment of adult zebrafish alters skin pigmentation.

The adult zebrafish exhibits a characteristic pattern of dark stripes consisting of melanophores (darkly pigmented cells) and iridophores (iridescent cells) alternating with light interstripes containing xanthophores (yellow/orange pigmented cells) and iridophores [45]. Previous work by others has shown that thyroid hormone is instrumental in determining the pigmentation patterns present in zebrafish skin and maintaining proper pigmentation patterns in adulthood [33]. It was shown that ablating the thyroid of larval zebrafish resulted in significant skin pigmentation changes after six months, particularly an increased number of melanophores and wider stripes [33]. Additionally, a genetically hyperthyroid mutant (*opallus*) showed an increased number of xanthophores and decreased number of melanophores [33]. The *opallus* mutant experiences hyperthyroidy from a very early age.

Therefore, we saw the opportunity to test whether the adult pigmentation patterns of euthyroid zebrafish were plastic to more “acute” hyperthyroidy through treatment of adults with T4.

We found that WT zebrafish exhibited striking skin pigmentation changes after five days of TH treatment. We observed that in T4-treated fish, the dark stripes appeared to lighten and appear green (Fig. 6A,B), and the fish appeared qualitatively similar to the *opallus* mutant [33]. Using photoshop assisted spectroscopy, there appeared to be trends toward differences in stripe color but not interstripe color (Fig 5 C). This change did not occur in the control group. These results suggest that skin pigmentation in zebrafish is plastic to external signals even at the adult stage, and that specific TH levels are required to maintain homeostasis in skin pigmentation.

Discussion

Our results show that cone subtype patterning in the retina is plastic to exogenous TH treatment even in the adult zebrafish, and this plasticity occurs in as little as seven hours. When adult fish were treated with T4 for 24 hours or longer, the expression of several genes was affected. *Lws1* expression increased while the expression of *lws2, gngt2b, rh2-1,* and *rh2-2* decreased. Further, we found that when adult fish were treated with T4 for 12 hours or less, *lws1* expression increased but the expression of the other transcripts tested did not change. Additionally, we found that exogenous T4 treatment for five days dramatically alters skin pigmentation in adult zebrafish. Because the appearance of the T4-treated fish was similar to that of the adult *opallus* mutants, and the *opallus* mutants exhibit increased xanthophore numbers and decreased melanophore numbers [33], it is likely that the T4 treatment also increased xanthophore numbers and decreased melanophore numbers. Our results provide further evidence that homeostatic TH levels are required for zebrafish to maintain normal melanophore and xanthophore populations.

We focused this study upon selected cone photoreceptor transcripts (*lws1, lws2, gngt2a, gngt2b, rh2-1, and rh2-2*), and found these remain plastic to TH treatment in the adult zebrafish. However, the plasticity of other transcripts such as *rh2-3* and *rh2-4* or *sws1* and *sws2* remains unknown. As T3 levels in a particular cell can be specifically tuned by

local deiodinase enzymes, it is possible that cells in various regions of the retina effectively received different amounts of TH [24]. Additionally, data for our seven hour experiment were collected at a different time of day than our other experiments (Supplemental Fig. S1). As zebrafish opsin expression exhibits circadian changes, with opsins expressed at low levels in the morning and high levels in the evening [46-49], this represents a confounding variable in our evaluation of the seven hour treatment results. In pigmentation analysis, our methods were limited to photography and Photoshop-assisted spectroscopy. Analyses using pigment cell counts or spectrometry would strengthen these results.

The present study adds to the extensive literature examining the role of TH in altering cone phenotypes in fish. TH signaling has been shown to be important during smoltification, a post-embryonic life stage transition that occurs in salmonids as juvenile fish change habitat [50]. This transition is accompanied by changes in skin pigmentation (lightening) and cone photoreceptor subtype patterning (redshifting) [51-53]. In both coho salmon and rainbow trout, TH signaling is associated with a UV to blue shift in opsin expression [19, 52]. TH signaling also underlies changes in opsin expression during metamorphoses in multiple flounder species [54, 55]. Further, TH has been shown to induce the expression of *cyp27c1*, an enzyme that converts vitamin A1 to vitamin A2, and thereby redshifting pigment sensitivity [11, 22, 56]. In coho salmon, a chromophore shift naturally occurs and is associated with seasonal variables [57]. Interestingly, there is some evidence that TH-induced plasticity in photoreceptor gene expression may be conserved in humans. Cakir et al. (2015) found that adult patients treated for hypothyroidism showed significant improvement in their color contrast sensitivity, indicating that cone gene expression in the adult human retina may also be plastic to TH levels [58]. The ability of TH to alter gene expression in the photoreceptors of an adult organism could inform therapeutic approaches to disorders involving cone photoreceptors, or in determining optimal protocols for retinal organoid development or other photoreceptor replacement strategies.

Based on results from our previous studies in larval zebrafish, our data suggest that the cones coexpressing *lws1* and *lws2* identified in our 12 and seven hour experiments are likely undergoing opsin switching [11]. While the exact nuclear hormone receptors responsible for controlling *lws1* vs *lws2* gene expression remain unknown, TH receptor beta

2 (*thrb2*) is a reasonable candidate for this role. *Thrb2* is required for red cone development in zebrafish [56, 59, 60] and sequences having predicted TH receptor binding activity have been identified near the *lws1* and *lws2* genes [11]. Additionally, overexpression of *thrb2* in zebrafish cones and bipolar cells has been shown to redshift the sensitivity of the retina, with the maximal response amplitude occurring at 650 nm (the wavelength at which the Lws1 opsin is most sensitive) compared to controls which showed a maximal response amplitude at 490 nm (a wavelength at which Rh2-2, 3, and 4 are most sensitive [61]. The complex kinetics of TH-mediated changes in adult photoreceptor gene expression could be mediated by the ability of the Thrb2 receptor (or other nuclear hormone receptor) to function in a manner that differs from the canonical model of nuclear hormone receptor action, in which the presence of ligand leads to recruitment of coactivators and the absence of ligand leads to recruitment of corepressors at genes that are positively regulated by TH [28]. Indeed, it has been shown that both liganded and unliganded forms of Thrb2 can promote transcription of positively regulated genes [62], although the activity level of liganded receptor is higher. Further, *thrb1*, a splice variant of *thrb2* has been shown to control gene expression by altering ratios of coactivators and corepressors, rather than recruiting either coactivators or corepressors [63]. The results shown here emphasize the necessity for the identification and study of the transcription factors that regulate tandemly replicated opsin genes.

In addition to regulating cone opsin gene expression and the spectral properties of the opsin chromophore, TH has been shown to regulate multiple photoreceptor transcripts, including multiple transcripts that are differentially expressed in LWS1 and LWS2 cones such as *gngt2b* [17]. Recent work has shown that zebrafish cone subpopulations exhibit inter-population transcriptional heterogeneity and intra-population heterogeneity, with *gngt2b* as an example of a transcript that varies in expression between the LWS cone subtypes, and within the cone subtypes [17, 23]. Other work has implicated *thrb2* in regulating multiple genes that are expressed in spatial gradients in mouse retina [64]. Taken together, these results implicate TH as an important regulator of transcriptional heterogeneity in cone populations. Because the non-opsin, LWS2-enriched gene *gngt2b* exhibited plasticity to TH treatment in adult fish, it is possible that additional cone-expressed genes also remain

sensitive to TH treatment in the adult. Therefore, TH may be involved in regulating transcriptional heterogeneity among and between cone subpopulations in adult zebrafish.

TH signaling is an important regulator of life history transitions in fish [50] and other vertebrates such as frogs [65]. Many of these life stage transitions are accompanied by a change in habitat or ecological niche, requiring different visual system capabilities [51, 54, 55, 65]. Zebrafish also undergo TH-mediated changes in jaw morphology, pigmentation, and feeding strategy as they change from larvae to juveniles [66-68]. The plasticity we observed in adults, however, cannot be directly explained as relevant to a life history change, as we used adult, reproductively mature zebrafish. This plasticity could instead indicate that TH signaling serves as an ongoing mechanism for maintaining cone subtype patterning in adults. Indeed, TH gradients in adult mice are involved in maintaining cone subtype patterning [12]. As zebrafish possess the ability to regenerate their retinas after injury, the plasticity of adult cones could also be important in reestablishing some elements of cone subtype patterning in the regenerating retina [38, 39]. There is evidence that zebrafish maintain surprisingly normal topographic patterns of *lws1* vs *lws2* after extensive damage to retinal neurons and subsequent retinal regeneration [38], and TH signaling may underlie this phenomenon. Plasticity within the visual system of cichlids experimentally exposed to different lighting conditions has been demonstrated , although the underlying mechanism(s) are not known [69]. It is possible that non-captive zebrafish utilize an endocrine mechanism to adjust their visual system to changing environmental conditions, such as increases in turbidity [70].

The present study builds upon our previous work showing that TH regulates the expression of the *lws* and *rh2* opsins in larval and juvenile zebrafish by determining the extent to which the zebrafish retina is plastic to TH, and reveals an interesting difference in the TH response kinetics of *lws1* and other cone photoreceptor genes. We found that skin pigmentation in adult zebrafish also remains plastic to exogenous TH treatment, showing an overall plasticity to TH that is reminiscent of TH-mediated postlarval photoreceptor and pigmentation changes seen in salmonids. This work adds to the body of literature showing TH as an important regulator of retinal development and cone subtype patterning, as well as an essential driver of retina and pigment phenotype changes in fish

References

1. Bartel, P., T. Yoshimatsu, F.K. Janiak, and T. Baden, *Spectral inference reveals principal cone-integration rules of the zebrafish inner retina.* Curr Biol, 2021. **31**(23): p. 5214-5226 e4.
2. Baden, T. and D. Osorio, *The Retinal Basis of Vertebrate Color Vision.* Annu Rev Vis Sci, 2019. **5**: p. 177-200.
3. Jeremy Nathans, D.T., David S. Hogness, *Molecular Genetics of Human Color Vision: The Genes Encoding Blue, Green, and Red Pigments.* Science, 1986. **232**.
4. Vollrath, D., J. Nathans, and R.W. Davis, *Tandem Array of Human Visual Pigment Genes at Xq28.* Science, 1988. **240**: p. 1669-1672.
5. Peng, G.H. and S. Chen, *Active opsin loci adopt intrachromosomal loops that depend on the photoreceptor transcription factor network.* Proc Natl Acad Sci U S A, 2011. **108**(43): p. 17821-6.
6. Wang, Y., P.M. Smallwood, M. Cowan, D. Blesh, A. Lawlers, J. Nathans, and P.M.S. YANSHU WANG*, MITRA COWAN‡,DIANE BLESH‡,ANN LAWLER§, AND JEREMY NATHANS, *Mutually exclusive expression of human red and green visual pigment-reporter transgenes occurs at high frequency in murine cone photoreceptors.* Proc Natl Acad Sci U S A, 1999. **96**: p. 5251–5256.
7. Hussey, K.A., S.E. Hadyniak, and R.J. Johnston, Jr., *Patterning and Development of Photoreceptors in the Human Retina.* Front Cell Dev Biol, 2022. **10**: p. 878350.
8. Onishi, A., S. Koike, M. Ida-Hosonuma, H. Imai, Y. Shichida, OsamuTakenaka, A. Hanazawa, H. Komatsu, A. Mikami, S. Goto, B. Suryobroto, A. Farajallah, P. Varavudhi, C. Eakavhibata, K. Kitahara, and T. Yamamori, *Variations in long- and middle-wavelength-sensitive opsin gene loci in crab-eating monkeys.* Vis Res, 2002. **42**: p. 281-292.
9. Hofmann, C.M. and K.L. Carleton, *Gene duplication and differential gene expression play an important role in the diversification of visual pigments in fish.* Integr Comp Biol, 2009. **49**(6): p. 630-43.
10. Chinen, A., T. Hamaoka, Y. Yamada, and S. Kawamura, *Gene Duplication and Spectral Diversification of Cone Visual Pigments of Zebrafish.* Genetics, 2003. **163**: p. 663–675.
11. Mackin, R.D., R.A. Frey, C. Gutierrez, A.A. Farre, S. Kawamura, D.M. Mitchell, and D.L. Stenkamp, *Endocrine regulation of multichromatic color vision.* Proc Natl Acad Sci U S A, 2019. **116**(34): p. 16882-16891.
12. Roberts, M.R., M. Srinivas, D. Forrest, G.M.d. Escoba, and T.A. Reh, *Making the gradient: Thyroid hormone regulates cone opsin expression in the developing mouse retina.* Proc Natl Acad Sci U S A, 2006. **103**(16): p. 6218–6223.
13. Boyes, W.K., L. Degn, B.J. George, and M.E. Gilbert, *Moderate perinatal thyroid hormone insufficiency alters visual system function in adult rats.* Neurotoxicology, 2018. **67**: p. 73-83.
14. Forrest, D. and A. Swaroop, *Minireview: the role of nuclear receptors in photoreceptor differentiation and disease.* Mol Endocrinol, 2012. **26**(6): p. 905-15.

15. Ng, L., J.B. Hurley, B. Dierks, M. Srinivas, C. Saltó, B. Vennström, T.A. Reh, and D. Forrest, *A thyroid hormone receptor that is required for the development of green cone photoreceptors.* Nature Genetics, 2001. **27**: p. 94-98.
16. Eldred, K.C., S.E. Hadyniak, K.A. Hussey, B. Brenerman, P.W. Zhang, X. Chamling, V.M. Sluch, D.S. Welsbie, S. Hattar, J. Taylor, K. Wahlin, D.J. Zack, and R.J. Johnston, Jr., *Thyroid hormone signaling specifies cone subtypes in human retinal organoids.* Science, 2018. **362**(6411).
17. Farre, A., C. Sun, M. Starostik, S. Hunter, M. English, A. Duncan, A. Santhanam, E. Shihabeddin, J. O'Brien, A. Swaroop, and D.L. Stenkamp, *Long wavelength-sensing cones of zebrafish retina exhibit multiple layers of transcriptional heterogeneity.* Front Cell Neurosci, 2023.
18. Gan, K.J. and I. Novales Flamarique, *Thyroid hormone accelerates opsin expression during early photoreceptor differentiation and induces opsin switching in differentiated TRalpha-expressing cones of the salmonid retina.* Dev Dyn, 2010. **239**(10): p. 2700-13.
19. Raine, J.C. and C.W. Hawryshyn, *Changes in thyroid hormone reception precede SWS1 opsin downregulation in trout retina.* J Exp Biol, 2009. **212**(17): p. 2781-8.
20. Houbrechts, A.M., L. Vergauwen, E. Bagci, J. Van Houcke, M. Heijlen, B. Kulemeka, D.R. Hyde, D. Knapen, and V.M. Darras, *Deiodinase knockdown affects zebrafish eye development at the level of gene expression, morphology and function.* Mol Cell Endocrinol, 2016. **424**: p. 81-93.
21. Glaschke, A., J. Weiland, D. Del Turco, M. Steiner, L. Peichl, and M. Glosmann, *Thyroid hormone controls cone opsin expression in the retina of adult rodents.* J Neurosci, 2011. **31**(13): p. 4844-51.
22. Enright, J.M., M.B. Toomey, S.Y. Sato, S.E. Temple, J.R. Allen, R. Fujiwara, V.M. Kramlinger, L.D. Nagy, K.M. Johnson, Y. Xiao, M.J. How, S.L. Johnson, N.W. Roberts, V.J. Kefalov, F.P. Guengerich, and J.C. Corbo, *Cyp27c1 Red-Shifts the Spectral Sensitivity of Photoreceptors by Converting Vitamin A1 into A2.* Curr Biol, 2015. **25**(23): p. 3048-57.
23. Ogawa, Y. and J.C. Corbo, *Partitioning of gene expression among zebrafish photoreceptor subtypes.* Sci Rep, 2021. **11**(1): p. 17340.
24. Bianco, A.C. and P.R. Larsen, *Cellular and Structural Biology of the Deiodinases.* Thyroid, 2005. **15**: p. 777-786.
25. Kogai, T. and G.A. Brent, *Thyroid Hormones (T4, T3)*, in *Endocrinology*, S. Melmed and P.M. Conn, Editors. 2005, Humana Press.
26. Arjona, F.J., E. de Vrieze, T.J. Visser, G. Flik, and P.H. Klaren, *Identification and functional characterization of zebrafish solute carrier Slc16a2 (Mct8) as a thyroid hormone membrane transporter.* Endocrinology, 2011. **152**(12): p. 5065-73.
27. Roberts, M.R., A. Hendrickson, C.R. McGuire, and T.A. Reh, *Retinoid X receptor (gamma) is necessary to establish the S-opsin gradient in cone photoreceptors of the developing mouse retina.* Invest Ophthalmol Vis Sci, 2005. **46**(8): p. 2897-904.
28. Warnmark, A., E. Treuter, A.P. Wright, and J.A. Gustafsson, *Activation functions 1 and 2 of nuclear receptors: molecular strategies for transcriptional activation.* Mol Endocrinol, 2003. **17**(10): p. 1901-9.

29. Mitchell, D.M., C.B. Stevens, R.A. Frey, S.S. Hunter, R. Ashino, S. Kawamura, and D.L. Stenkamp, *Retinoic Acid Signaling Regulates Differential Expression of the Tandemly-Duplicated Long Wavelength-Sensitive Cone Opsin Genes in Zebrafish.* PLoS Genet, 2015. **11**(8): p. e1005483.
30. Tsujimura, T., T. Hosoya, and S. Kawamura, *A single enhancer regulating the differential expression of duplicated red-sensitive opsin genes in zebrafish.* PLoS Genet, 2010. **6**(12): p. e1001245.
31. Takechi, M. and S. Kawamura, *Temporal and spatial changes in the expression pattern of multiple red and green subtype opsin genes during zebrafish development.* J Exp Biol, 2005. **208**(Pt 7): p. 1337-45.
32. Houbrechts, A.M., J. Delarue, I.J. Gabriels, J. Sourbron, and V.M. Darras, *Permanent Deiodinase Type 2 Deficiency Strongly Perturbs Zebrafish Development, Growth, and Fertility.* Endocrinology, 2016. **157**(9): p. 3668-81.
33. McMenamin, S.K., E.J. Bain, A.E. McCann, L.B. Patterson, D.S. Eom, Z.P. Waller, J.C. Hamill, J.A. Kuhlman, J.S. Eisen, and D.M. Parichy, *Thyroid hormone–dependent adult pigment cell lineage and pattern in zebrafish.* Science, 2014. **345**(6202): p. 1356-1361.
34. Westerfield, M., *The Zebrafish Book. A Guide for the Laboratory Use of Zebrafish (Danio rerio)*. Vol. 385. 2000, Unversity of Oregon Press.
35. Tsujimura, T., A. Chinen, and S. Kawamura, *Identification of a locus control region for quadruplicated green-sensitive opsin genes in zebrafish.* Proc Natl Acad Sci U S A, 2007. **104**(31): p. 12813–12818.
36. Suliman, T. and I. Novales Flamarique, *Visual pigments and opsin expression in the juveniles of three species of fish (rainbow trout, zebrafish, and killifish) following prolonged exposure to thyroid hormone or retinoic acid.* J Comp Neurol, 2014. **522**(1): p. 98-117.
37. W Ted Allison, T.J.H., Craig W Hawryshyn, Shelby E Temple, *Visual pigment composition in zebrafish: Evidence for a rhodopsin-porphyropsin interchange system.* Vis Neurosci, 2004. **21**(6): p. 945-952.
38. Stenkamp, D.L., D.D. Viall, and D.M. Mitchell, *Evidence of Regional Specializations in Regenerated Zebrafish Retina.* Exp Eye Res, 2021. **212**.
39. McGinn, T.E., D.M. Mitchell, P.C. Meighan, N. Partington, D.C. Leoni, C.E. Jenkins, M.D. Varnum, and D.L. Stenkamp, *Restoration of Dendritic Complexity, Functional Connectivity, and Diversity of Regenerated Retinal Bipolar Neurons in Adult Zebrafish.* J Neurosci, 2018. **38**(1): p. 120-136.
40. Stevens, C.B., D.A. Cameron, and D.L. Stenkamp, *Plasticity of photoreceptor-generating retinal progenitors revealed by prolonged retinoic acid exposure.* BMC Dev Biol, 2011. **11**(51).
41. Wright, K. and H. Herro, *Photoshop® Assisted Spectroscopy: An Economical and NonDestructive Method for Tracking Color Shift.* Topics Photogr Preserv, 2015. **16**: p. 148-155.
42. Lagman, D., A. Callado-Perez, I.E. Franzen, D. Larhammar, and X.M. Abalo, *Transducin duplicates in the zebrafish retina and pineal complex: differential specialisation after the teleost tetraploidisation.* PLoS One, 2015. **10**(3): p. e0121330.

43. Chan, L.Y., C.F. Mugler, S. Heinrich, P. Vallotton, and K. Weis, *Non-invasive measurement of mRNA decay reveals translation initiation as the major determinant of mRNA stability.* Elife, 2018. **7**.
44. Yang, E., E. van Nimwegen, M. Zavolan, N. Rajewsky, M. Schroeder, M. Magnasco, and J.E. Darnell, Jr., *Decay rates of human mRNAs: correlation with functional characteristics and sequence attributes.* Genome Res, 2003. **13**(8): p. 1863-72.
45. McGowan, K.A. and G.S. Barsh, *Evolution: How the zebrafish got its stripes.* Elife, 2016. **5**.
46. Li, P., S. Temple, Y. Gao, T.J. Haimberger, C.W. Hawryshyn, and L. Li, *Circadian rhythms of behavioral cone sensitivity and long wavelength opsin mRNA expression: a correlation study in zebrafish.* J Exp Biol, 2005. **208**(Pt 3): p. 497-504.
47. Li, P., S.S. Chaurasia, Y. Gao, A.L. Carr, P.M. Iuvone, and L. Li, *CLOCK is required for maintaining the circadian rhythms of Opsin mRNA expression in photoreceptor cells.* J Biol Chem, 2008. **283**(46): p. 31673-8.
48. Zang, J., C. Grimm, M. Gesemann, J. Keim, M. Samardzija, and S. Neuhauss, *Circadian regulation of vertebrate cone photoreceptor function.* Elife, 2021.
49. Sawant, O.B., A.M. Horton, O.F. Zucaro, R. Chan, V.L. Bonilha, I.S. Samuels, and S. Rao, *The Circadian Clock Gene Bmal1 Controls Thyroid Hormone-Mediated Spectral Identity and Cone Photoreceptor Function.* Cell Rep, 2017. **21**(3): p. 692-706.
50. Holzer, G. and V. Laudet, *Thyroid hormones: a triple-edged sword for life history transitions.* Curr Biol, 2015. **25**(8): p. R344-7.
51. Bjornsson, B.T., S.O. Stefansson, and S.D. McCormick, *Environmental endocrinology of salmon smoltification.* Gen Comp Endocrinol, 2011. **170**(2): p. 290-8.
52. Cheng, C.L., K.J. Gan, and I.N. Flamarique, *Thyroid hormone induces a time-dependent opsin switch in the retina of salmonid fishes.* Invest Ophthalmol Vis Sci, 2009. **50**(6): p. 3024-32.
53. Cheng, C.L. and I.N. Flamarique, *Chromatic organization of cone photoreceptors in the retina of rainbow trout: single cones irreversibly switch from UV (SWS1) to blue (SWS2) light sensitive opsin during natural development.* J Exp Biol, 2007. **210**(Pt 23): p. 4123-35.
54. Shi, Y., Y. Shi, W. Ji, X. Li, Z. Shi, J. Hou, W. Li, and Y. Fu, *Thyroid Hormone Signaling Is Required for Dynamic Variation in Opsins in the Retina during Metamorphosis of the Japanese Flounder (Paralichthys olivaceus).* Biology (Basel), 2023. **12**(3).
55. Mader, M.M. and D.A. Cameron, *Effects of induced systemic hypothyroidism upon the retina: Regulation of thyroid hormone receptor alpha and photoreceptor production.* Mol Vis, 2006. **12**: p. 915-930.
56. Volkov, L.I., J.S. Kim-Han, L.M. Saunders, D. Poria, A.E.O. Hughes, V.J. Kefalov, D.M. Parichy, and J.C. Corbo, *Thyroid hormone receptors mediate two distinct mechanisms of long-wavelength vision.* Proc Natl Acad Sci U S A, 2020. **117**(26): p. 15262-15269.
57. Temple, S.E., E.M. Plate, S. Ramsden, T.J. Haimberger, W.M. Roth, and C.W. Hawryshyn, *Seasonal cycle in vitamin A1/A2-based visual pigment composition*

during the life history of coho salmon (Oncorhynchus kisutch). J Comp Physiol A Neuroethol Sens Neural Behav Physiol, 2006. **192**(3): p. 301-13.
58. Cakir, M., B. Turgut Ozturk, E. Turan, G. Gonulalan, I. Polat, and K. Gunduz, *The effect of hypothyroidism on color contrast sensitivity: a prospective study.* Eur Thyroid J, 2015. **4**(1): p. 43-7.
59. Suzuki, S.C., A. Bleckert, P.R. Williams, M. Takechi, S. Kawamura, and R.O. Wong, *Cone photoreceptor types in zebrafish are generated by symmetric terminal divisions of dedicated precursors.* Proc Natl Acad Sci U S A, 2013. **110**(37): p. 15109-14.
60. Deveau, C., X. Jiao, S.C. Suzuki, A. Krishnakumar, T. Yoshimatsu, J.F. Hejtmancik, and R.F. Nelson, *Thyroid hormone receptor beta mutations alter photoreceptor development and function in Danio rerio (zebrafish).* PLoS Genet, 2020. **16**(6): p. e1008869.
61. Nelson, R.F., A. Balraj, T. Suresh, L.J. Elias, T. Yoshimatsu, and S.S. Patterson, *The Developmental Progression of Eight Opsin Spectral Signals Recorded from the Zebrafish Retinal Cone Layer Is Altered by the Timing and Cell Type Expression of Thyroxin Receptor beta2 (trbeta2) Gain-Of-Function Transgenes.* eNeuro, 2022. **9**(6).
62. Oberste-Berghaus, C., K. Zanger, K. Hashimoto, R.N. Cohen, A.N. Hollenberg, and F.E. Wondisford, *Thyroid hormone-independent interaction between the thyroid hormone receptor beta2 amino terminus and coactivators.* J Biol Chem, 2000. **275**(3): p. 1787-92.
63. Shabtai, Y., N.K. Nagaraj, K. Batmanov, Y.-W. Cho, Y. Guan, C. Jiang, J. Remsberg, D. Forrest, and M.A. Lazar, *A coregulator shift, rather than the canonical switch, underlies thyroid hormone action in the liver.* Genes & Development, 2021. **35**.
64. Aramaki, M., X. Wu, H. Liu, Y. Liu, Y.W. Cho, M. Song, Y. Fu, L. Ng, and D. Forrest, *Transcriptional control of cone photoreceptor diversity by a thyroid hormone receptor.* Proc Natl Acad Sci U S A, 2022. **119**(49): p. e2209884119.
65. Buchholz, D.R., *Xenopus metamorphosis as a model to study thyroid hormone receptor function during vertebrate developmental transitions.* Mol Cell Endocrinol, 2017. **459**: p. 64-70.
66. Brown, D.D., *The role of thyroid hormone in zebrafish and axolotl development.* Proc Natl Acad Sci U S A, 1997. **94**: p. 13011–13016.
67. Campinho, M.A., *Teleost Metamorphosis: The Role of Thyroid Hormone.* Front Endocrinol (Lausanne), 2019. **10**: p. 383.
68. Galindo, D., E. Sweet, Z. DeLeon, M. Wagner, A. DeLeon, C. Carter, S.K. McMenamin, and W.J. Cooper, *Thyroid hormone modulation during zebrafish development recapitulates evolved diversity in danionin jaw protrusion mechanics.* Evol Dev, 2019. **21**(5): p. 231-246.
69. Nandamuri, S.P., M.R. Yourick, and K.L. Carleton, *Adult plasticity in African cichlids: Rapid changes in opsin expression in response to environmental light differences.* Mol Ecol, 2017. **26**(21): p. 6036-6052.
70. Escobar-Camacho, D., M.E.R. Pierotti, V. Ferenc, D.M.T. Sharpe, E. Ramos, C. Martins, and K.L. Carleton, *Variable vision in variable environments: the visual system of an invasive cichlid (Cichla monoculus) in Lake Gatun, Panama.* J Exp Biol, 2019. **222**(Pt 6).

Figures

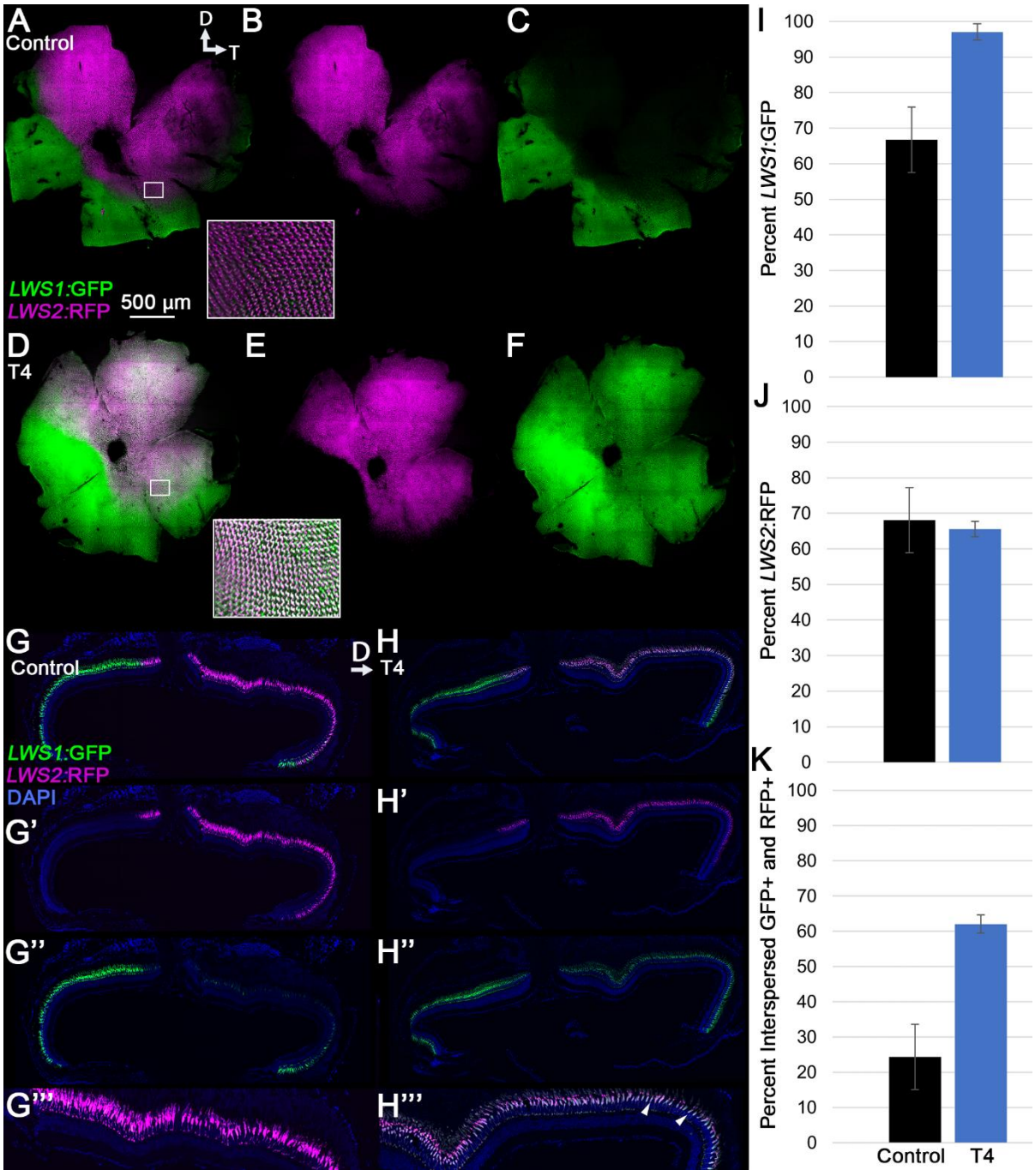

Figure 3.1: Topography of *lws1* and *lws2* reporter patterning in adult *lws:PAC(H)* transgenic fish, in which GFP reports *lws1* expression and RFP reports *lws2* expression. A-F) Projections of representative whole, imaged retinas from fish treated with NaOH (control, A-C) or T4 (treated, D-F) for five days. Insets show indicated regions enlarged by 700%. A,D) All imaging channels merged.

B,E) *lws2*:RFP. C,F) *lws1*:GFP. Note expanded GFP expression domain in response to T4 (D-F). G-H) Projections of representative sectioned retinas from fish treated with NaOH (control, G-G’’’) or T4 (treated, H-H’’’). G,H) All imaging channels merged. G’,H’) *lws2*:RFP. G’’,H’’) *lws1*:GFP. G’’’,H’’’) enlarged image of *lws2*:RFP-containing region. Arrows indicate cells coexpressing GFP and RFP. I-K) Analysis of areas of expression domains, n=3 for each group. I) Percent of retina occupied by GFP+ cells (p=0.0068, t-test). J) Percent of retina occupied by RFP+ cells (p=0.6910, t-test). K) Percent of retina occupied by GFP+ and RFP+ cells interspersed or coexpressing (p=0.0033, t-test). Error bars indicate confidence intervals. Fisher’s Exact Test was used to test for overall differences: p= 0.0034 with a 3x2 contingency table. D=dorsal, T=temporal.

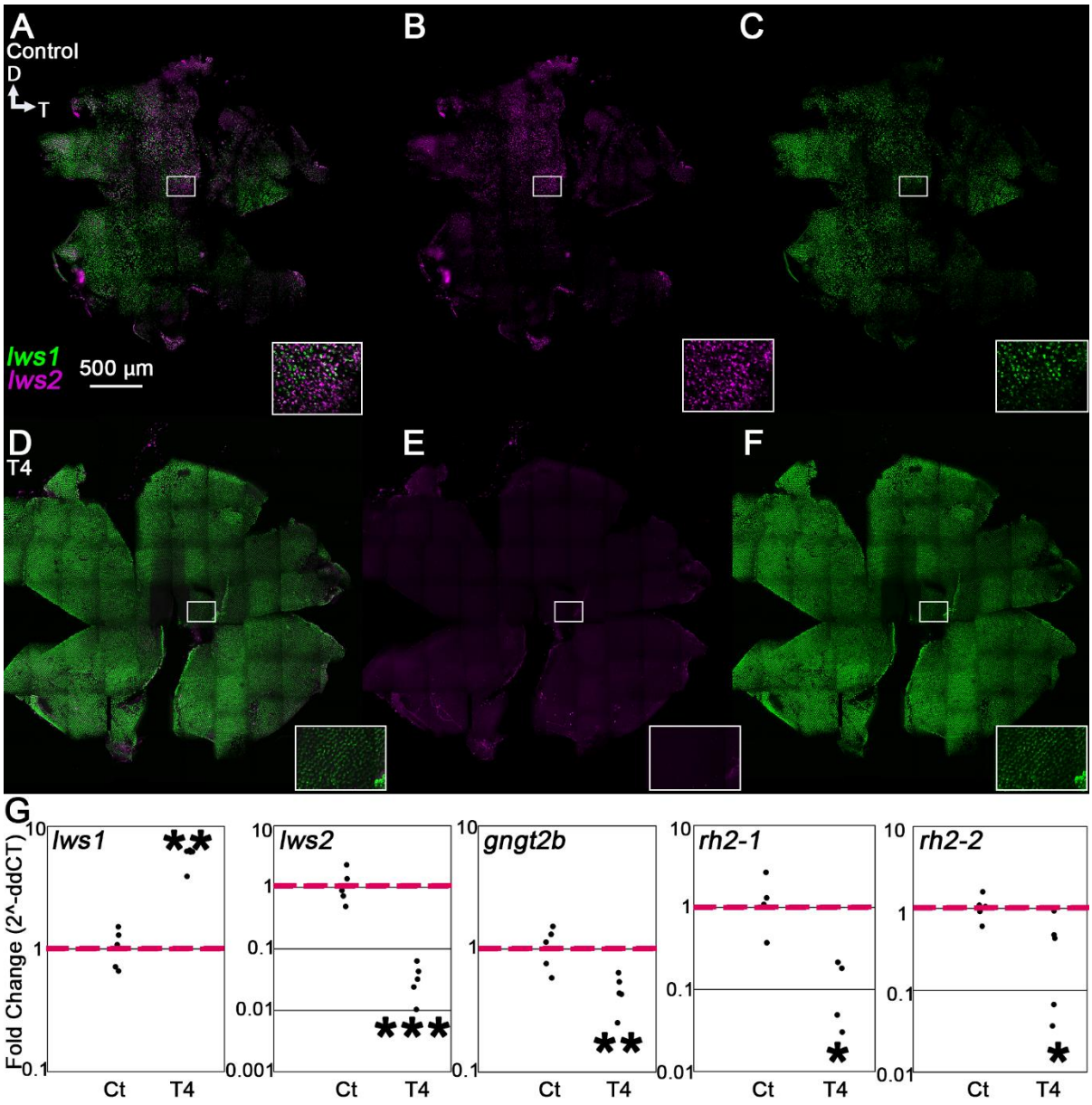

Figure 3.2: Plasticity of cone transcripts in response to five days of T4 treatment. A-F) Projections of representative whole, imaged retinas from fish treated with NaOH (control, A-C) or T4 (treated, D-F) followed by HCR *in situ*. Insets show indicated regions enlarged by 350%. A,D) All imaging channels merged. B,E) *lws2* C,F) *lws1*. Note expanded *lws1* domain and lack of *lws2* mRNA in T4-treated retina. G) qPCR of whole adult eyes. *lws1*) n=5, p=0.0079 (Mann-Whitney). *lws2*) n=5, p=1.2749E-05 (test?). *gngt2b*) n=5, p=0.0025 (t-test). *rh2-1*) n=4, p=0.0168 (t-test). *rh2-2*) n=5, p=0.0355 (t-test). D=dorsal, T=temporal.

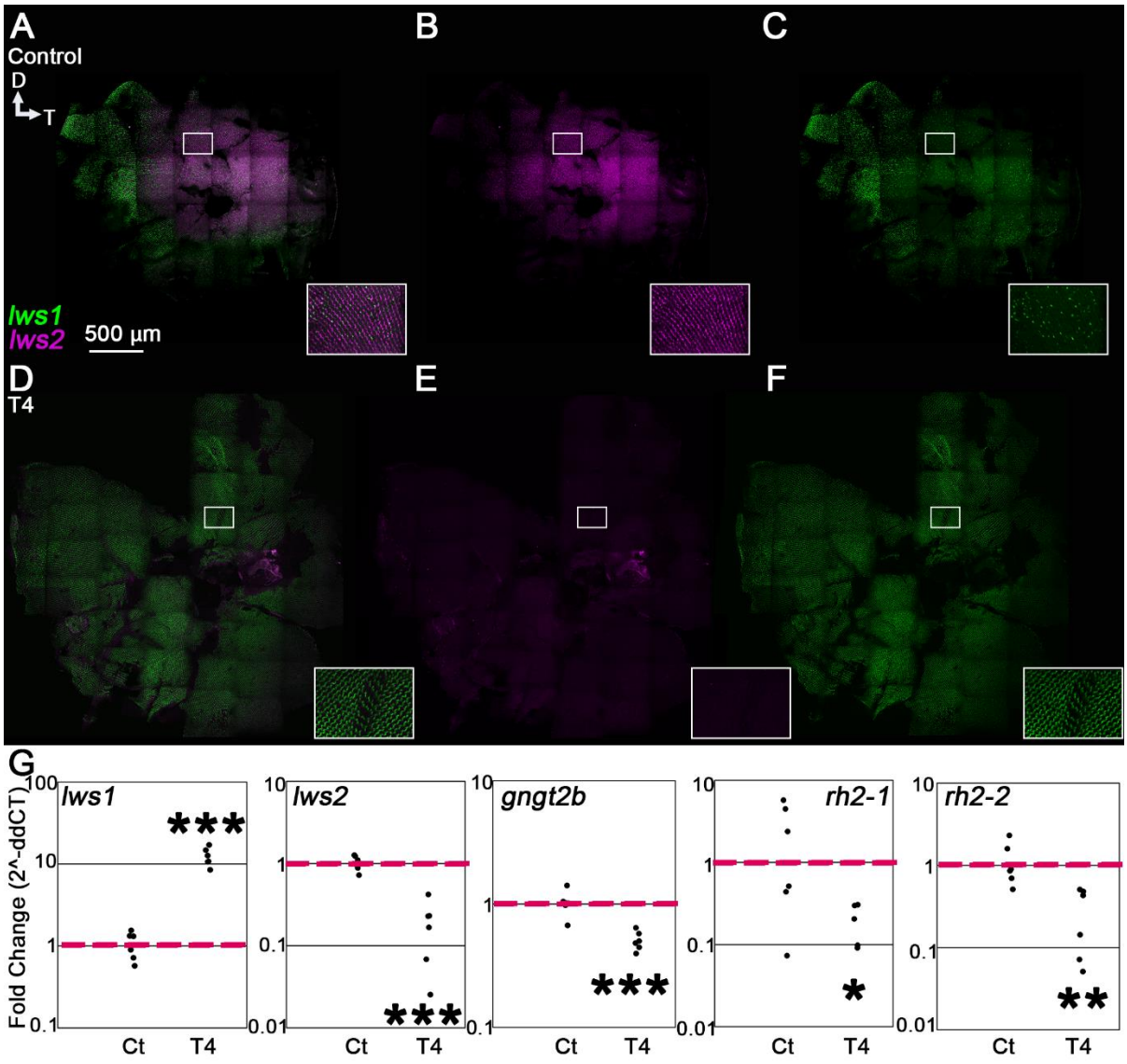

Figure 3.3: Plasticity of cone transcripts in response to 24-hour T4 treatment. A-F) Projections of representative whole, imaged retinas from fish treated with NaOH (control, A-C) or T4 (treated, D-F) followed by HCR *in situ*. Insets show indicated regions enlarged by 350%. A,D) All imaging channels merged. B,E) *lws2* C,F) *lws1*. Note expanded *lws1* domain and lack of *lws2* mRNA in T4-treated retina. G) qPCR of whole adult eyes, n=6 for each group. *lws1*) p=1.3235E-07 (t-test). *lws2*) p=0.0008 (t-test). *gngt2b*) p=0.0002 (t-test). *rh2-1*) p=0.0233 (t-test). *rh2-2*) p=0.0065 (t-test). D=dorsal, T=temporal

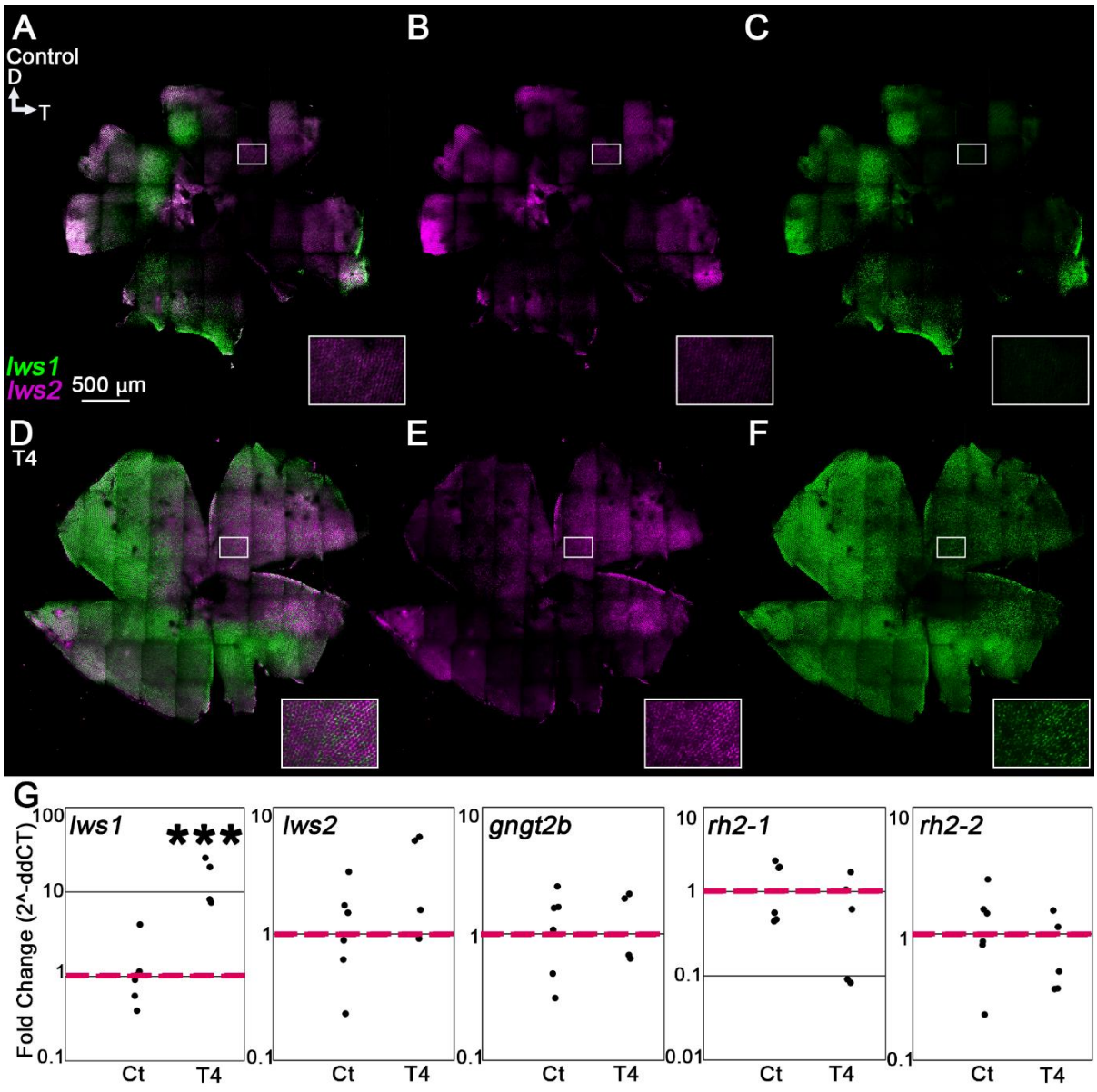

Figure 3.4: Plasticity of cone transcripts in response to 12-hour T4 treatment. A-F) Projections of representative whole, imaged retinas from fish treated with NaOH (control, A-C) or T4 (treated, D-F) followed by HCR *in situ*. Insets show indicated regions enlarged by 350%. A,D) All imaging channels merged. B,E) *lws2* C,F) *lws1*. Note expanded *lws1* domain and colocalization of *lws1* and *lws2* mRNA in T4-treated retina. G) qPCR of whole adult eyes. *lws1*) n=6 (control), 4 (treated); p=0.0006 (t-test). *lws2*) n=6 (control), 4 (treated); p=0.1424 (t-test). *gngt2b*) n=6 (control), 4 (treated); p=0.7863 (t-test). *rh2-1*) n=6 (control), n=5 (treated); p=0.1860 (t-test). *rh2-2*) n=6 (control), n=5 (treated); p=0.3820 (t-test). D=dorsal, T=temporal.

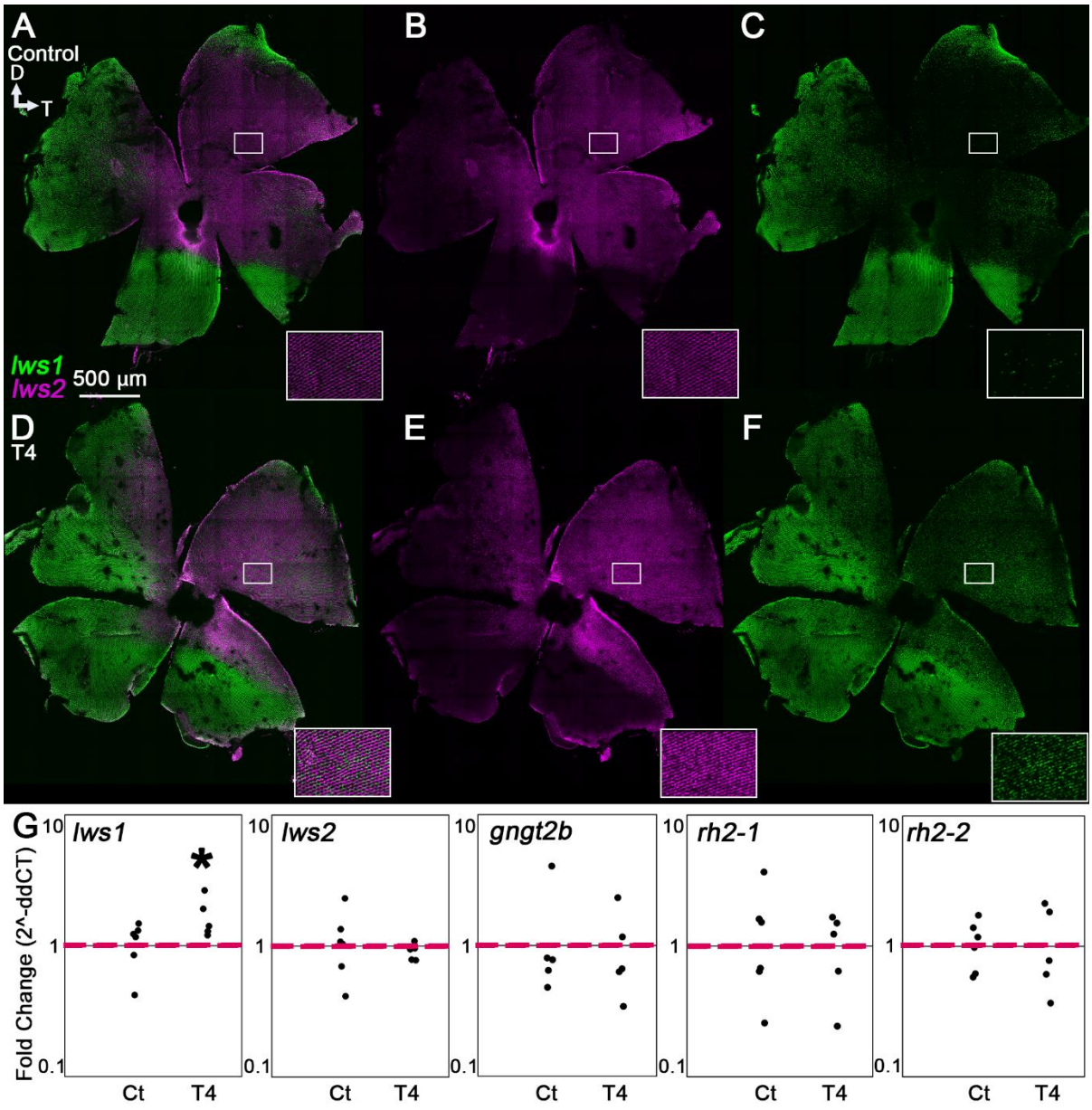

Figure 3.5: Plasticity of cone transcripts in response to 7-hour T4 treatment. A-F) Projections of representative whole, imaged retinas from fish treated with NaOH (control, A-C) or T4 (treated, D-F) followed by HCR *in situ*. Insets show indicated regions enlarged by 350%. A,D) All imaging channels merged. B,E) *lws2* C,F) *lws1*. Note expanded *lws1* domain and colocalization of *lws1* and *lws2* mRNA in T4-treated retina. G) qPCR of whole adult eyes. *lws1*) n=6 (control), 5 (treated); p=0.0373 (t-test). *lws2*) n=6 (control), 5 (treated); p=0.3173 (Mann-Whitney). *gngt2b*) n=5 (both treatments); p=0.8277 (t-test). *rh2-1*) n=6 (control), n=5 (treated); p=0.8246 (t-test). *rh2-2*) n=6 (control), n=5 (treated); p=0.8941 (t-test). D=dorsal, T=temporal.

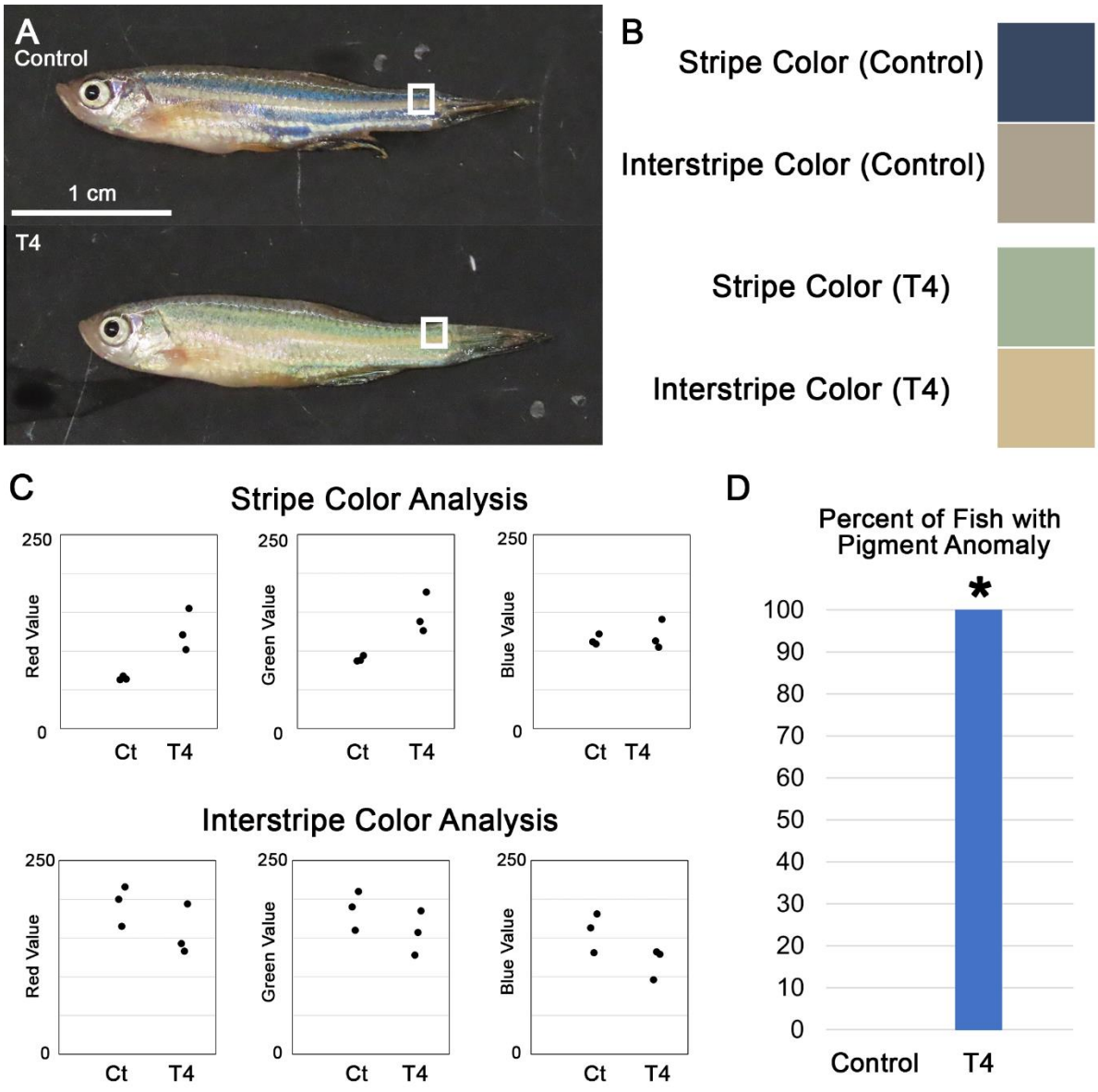

Figure 3.6: Five day T4 treatment of adult zebrafish alters skin pigmentation. A) Brightfield photographs of representative fish. B) Examples of representative stripe and interstripe colors of control and treated fish. Colors were sampled from regions denoted by rectangles in A. C) Color analysis of stripe and interstripe Red, Green, and Blue scale values, n=3. Values denote "redness," "greenness," and "blueness" on a scale from 0 to 255. High red values indicate high redness. Low red values indicate green, low green values indicate red, low blue values indicate orange. Note trend of higher red and green values in stripes of T4-treated fish. D) Percentages of fish in control and treated groups with altered pigmentation compared to untreated wildtype. All T4-treated fish showed altered skin pigmentation while all control fish showed normal pigmentation, p=0.0143 (proportion test).

Supplemental Information

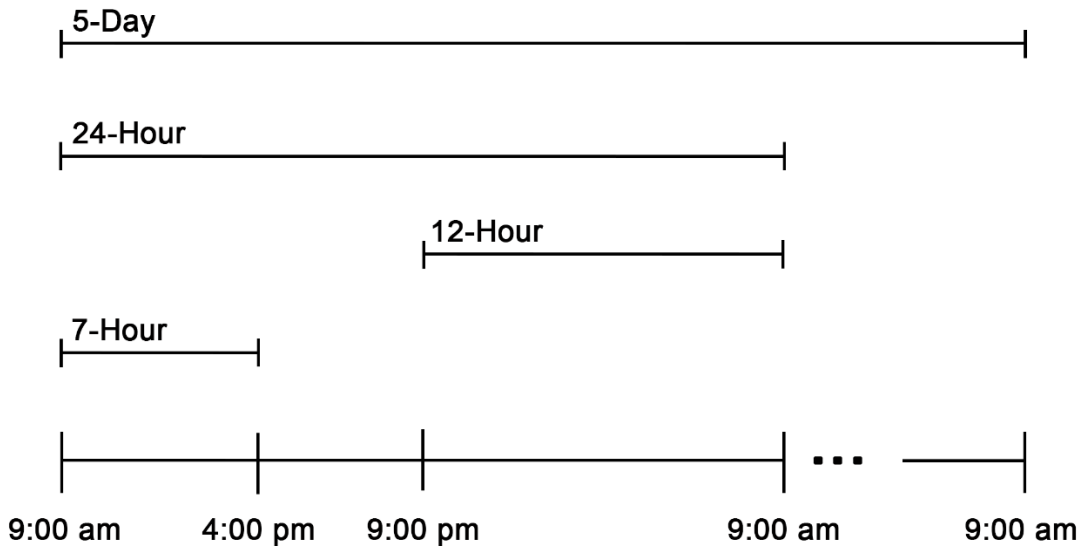

Figure S3.1: Timeline of adult treatments. 5-day and 24-hour treatments began at 9:00 am and ended at 9:00 am. 12-hour treatments began at 9:00 pm and ended at 9:00 am. 7-hour treatments began at 9:00 am and ended at 4:00 pm.

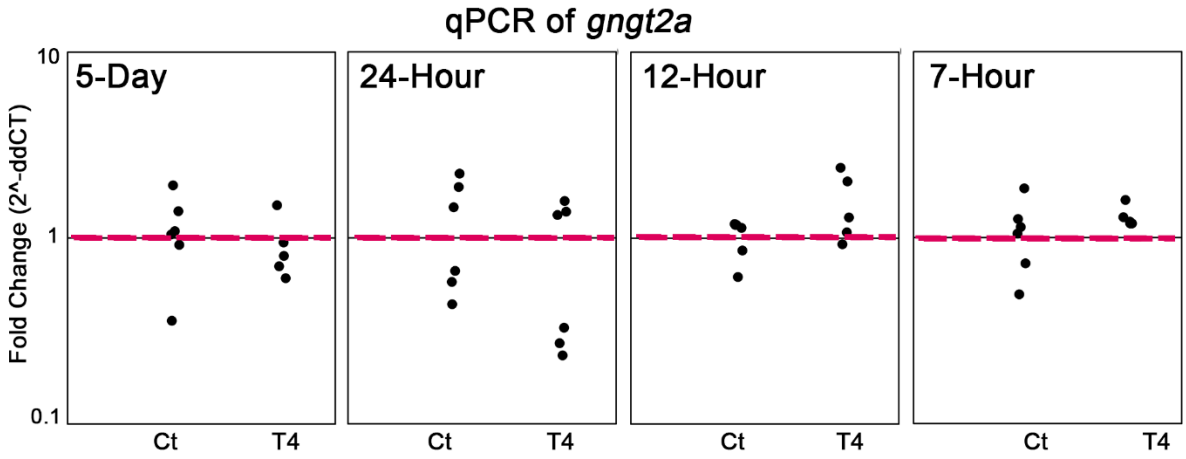

Figure S3.2: *Gngt2a* expression in control and treated adult zebrafish. qPCR of whole adult eyes. Note that transcript abundance of *gngt2a* (a transcript enriched in LWS1 cones compared to LWS2 cones) did not change in any condition, matching previous results in larvae. 5-day) n=6 (control), 5 (treated); p=0.617475 (t-test). 24-hour) n=6 (both treatments); p=0.329755 (t-test). 12-hour) n=6 (control), 5 (treated); p=0.23404 (Mann-Whitney). 7-hour) n=6 (control), 5 (treated); p=0.258549 (t-test).

Supplemental Table S3.1: Primers Used for qPCR

Gene	Forward primer	Reverse Primer
beta actin	GTACCACCAGACAATACAGT	CTTCTTGGGTATGGAATCTTGC
gngt2a	GTGACCTGTTGCCTCCATCG	TTTAGAGACAGGCTCTCTGGT
gngt2b	ATCCACAGTCAGGATGGCTCG	TCGGCAGATAAACCCTCCAC
lws1	CCCACACTGCATCTCGACAA	AAGGTATTCCCCATCACTCCAA
lws2	AGAGGGAAGAACTGGACTTTCAGA	TTCAGAGGAGTTTTGCCTACATATGT
rh2-1	CAGCCCAGCACAAGAAACTC	AGAGCAACCTGACCTCCAAGT
rh2-2	TTTTTGGCTGGTCCCGATACA	CAGGAACGCAGAAATGACAGC

Supplemental Table S3.2: Probe Sets Used for HCR

Gene	NCBI Accession Number	Probe Set Size
lws1	NM_001313715.1	13
lws2	NM_001002443.2	9

Chapter 4: Progress report on human 3D retinal organoids: Introducing a multifaceted approach for analyzing opsin expression

Ashley A. Farre, Emmanuel Owusu Poku, Blake Baker, Valeria Canto-Soler, Deborah L. Stenkamp

Abstract

Photoreceptors are the cells in the retina that detect light. Photoreceptor degeneration is associated with disorders that cause blindness, and damaged or degenerated photoreceptors cannot grow back. Cell replacement strategies, therefore, represent a promising option for helping patients with advanced retinal degeneration. Human retinal organoids represent potential sources of cells for retinal transplantation. Retinal organoids are derived from human induced pluripotent stem cells and are three-dimensional, laminated retinal structures that contain functioning photoreceptors and other retinal cell types in layers similar to those found in the normal vertebrate retina. Previous unpublished work has shown that thyroid hormone and retinoic acid can alter opsin expression in retinal organoids. Here, we build upon these findings. We tested a new treatment method for organoids and determined the effects on opsin expression. We also present a strategy for rigorously testing opsin expression in retinal organoids, using qPCR, hybridization chain reaction *in situ*, and droplet digital PCR approaches. Ultimately, this work represents an update on our progress toward establishing a protocol that can lead to the creation of 3D retinal organoids with optimal numbers of L, M, and S cones for cell transplantation interventions.

Introduction

Visual impairment is the most prevalent cause for disability in the industrialized world [1]. Photoreceptor degeneration is associated with several blinding disorders, such as retinitis pigmentosa and age-related macular degeneration [2, 3]. Since the mammalian nervous system lacks regenerative capabilities, damaged or degenerated photoreceptors cannot grow back [4]. Cell replacement strategies, therefore, represent a promising option for helping patients with advanced retinal degeneration. Human retinal organoids represent potential sources of cells for retinal transplantation, and a recent study has shown that retinal organoid-derived human photoreceptors incorporate into the degenerating mouse retina and establish functional synaptic connections, lasting for up to 6 months in the recipient retina [5]. Transplantation of modified photoreceptors has also been shown to restore visual function, even vision-mediated behavior, in mouse models of late-stage retinal degeneration [6]. In both studies, the visual improvements were shown to be the result of functional integration rather than material transfer [5, 6].

Retinal organoids are three-dimensional, laminated retinal structures that contain functioning photoreceptors and other retinal cell types in layers similar to the structure in a normal human retina [7-13]. To make retinal organoids, human iPSCs are induced to form neuroepithelial cells [14]. Using transient supplementation of signals such as bone morphogenic protein 4 (BMP4), the neuroepithelial cells can be directed toward the retinal progenitor fate [15]. When supplied with media containing additional retinal differentiation signals, the retinal progenitor cells will differentiate into retinal cell types which spontaneously arrange into a laminated retinal structure [14, 15]. In addition to providing material for cell replacement in human retinal disease, retinal organoids have proven advantageous in investigating the development of the human retina, allowing. Recently, work in retinal organoids has shown that thyroid hormone receptor beta 2 (*thrb2*) is important in promoting L/M cone fate as opposed to S cone fate in the human retina [16].

Humans have three types of cone photoreceptors: blue-sensing *SWS*, green-sensing *MWS*, and red-sensing *LWS* [17]. The human *LWS* and *MWS* are arranged in tandem on the X chromosome in a head-to-tail arrangement, and as such they are known as tandemly

replicated opsin genes [18]. Because males only possess one X chromosome, and one X is inactivated in female cells, transcription of these opsins occurs at only one locus. The human *LWS* and *MWS* genes are located downstream of a locus control region (LCR) which has shown to interact with the promoters of *LWS* and *MWS* [19]. Beyond the importance of the LCR, not much is known about the regulation of *LWS* and *MWS* expression. Zebrafish also possess tandemly replicated opsin genes in the *lws* array and the *rh2* array [20]. Further, human *LWS* and *MWS* opsin genes and the zebrafish *lws1* and *lws2* genes both evolved from an ancestral *lws* opsin gene [21]. Indeed, the only mammals that possess tandemly replicated opsin genes are primates and bats, making zebrafish an excellent option for studying the regulation of tandemly replicated opsin genes [21].

In addition to determining L/M vs S cone fate in human retinal organoids, thyroid hormone (TH) has been shown to differentially regulate *lws1* and *lws2* expression in the zebrafish [22]. Evidence from mouse, human organoids, and zebrafish indicates a strong potential for TH to have a conserved role in redshifting opsin gene expression [16, 22, 23]. The L and M cone opsins are nearly identical, with their transcripts sharing approximately 98% sequence similarity [24]. Currently, there is no widely accepted method to differentiate L and M opsin by immunofluorescence or by *in situ* hybridization. As such, rigorous validation of results claiming to analyze *LWS* vs *MWS* opsin gene expression is important. This study shows our plans for a multifaceted strategy for testing and validating *LWS* vs *MWS* opsin expression in human retinal organoids.

Previous results from our lab are summarized in Table 1. Using qPCR primers validated by amplicon sequencing, our data have shown that at 90 days, triiodothyronine (T3, the active form of TH), increases the transcript abundance of L opsin, M opsin, and S opsin while RA decreases M opsin abundance (Table 1). At 120 days, T3 increases the transcript abundance of L opsin and decreases the transcript abundance of M opsin, S opsin, and rhodopsin while RA decreases the transcript abundance of M opsin, S opsin, and rhodopsin (Table 1). At 150 days, T3 alters opsin expression in the same way as it does at 120 days while RA begins to downregulate L opsin, and upregulate S opsin, continues to downregulate M opsin and has no effect on rhodopsin. At 150 days, T3 alters opsin expression the same way as it does at 90 and 120 days, and RA shows similar effects on opsins as it does at 150

days, excepting its effect on rhodopsin, which is upregulated by RA at 150 days (Table 1). At 180 days, T3 had the same effect on opsin expression as it did at 120 and 150 days. RA had similar effects on opsin expression as it did in 150 day organoids; however, at 180 days it began to promote rhodopsin expression rather than having no effect (Table 1). These results implicate T3 and RA in differentially regulating human L/M opsin transcript abundance.

While our original treatment protocol was effective at altering opsin transcript abundance, we wanted to further optimize our experiments. The original T3 protocol disrupted lamination and surface topography of the organoids at older in vitro stages, making HCR *in situ* challenging (data not shown). The control and RA treatment protocols, however, did not disrupt organoid lamination. Previous studies have shown that lower concentrations of T3 (such as 20nM) also do not disrupt organoid lamination [16]. Additionally, our original treatment protocol introduced T3 earlier (63d) than the predicted time of onset of thyroid hormone metabolism and signaling in the human fetus [25]. As such, we wanted to delay concentration and timing of T3 treatment in our new studies, in order to more closely mimic human development and preserve retinal organoid structure.

Overall, we wished to further explore the effects of T3 and RA treatment. We collected more results at 180 days, investigated the effect of combinatorial T3/RA treatments on opsin expression, and altered treatment timing and concentration, toward establishing an optimal protocol that can lead to the creation of 3D retinal organoids with optimal numbers of L, M, and S cones for cell transplantation interventions.

Methods

Differentiation method and treatment conditions for three-dimensional retinal organoids.

The protocol for differentiation of three-dimensional retinal organoids was performed as described previously [7]. The control (CT) condition did not include any exposure to RA or T3, other than the small amounts present in serum and supplements, but did include treatment with 0.1% DMSO, the vehicle used for other conditions, from 63d until termination of experiments. In method 1: the RA condition involved exposure to 1µM RA 63-90d, and then 0.5µM RA from 90d until termination of experiments. The T3 condition involved

exposure to 500nM T3 from 63d until termination of experiments. The RA/T3 condition involved exposure to 1µM RA 63-90d, and then 500nM T3 from 63 days until termination of experiments. Previously, we collected the organoids at 90d, 120d, 150d, and 180d. For new data shown here, organoids were collected at 180d. Abundance of cone opsin transcripts was determined using qPCR. Primer sequences are provided within Table 1.

For method 2 differentiation conditions were similar to those of method 1. In the T3 condition, 100 nM T3 was used starting at 90 days instead of 63 days. In the RA/T3 condition, 20 nM T3 was used and T3 was added at 90 days instead of 63 days. Organoids were collected at 120d and 180d.

R*NA extraction and quantitative reverse transcriptase PCR (qPCR).*

Total RNA from each treatment group of pooled (3) whole retina cups was extracted using the Machery-Nagel kit, and was used to synthesize cDNA template using the Invitrogen SuperScript III/IV kit (with random primers). Gene-specific primer pairs are listed in Supplemental Table 2. Amplification to measure abundance of specific transcripts was performed on an Applied Biosystems StepOne Real-Time PCR system, an Applied Biosystems QuantStudio3, or 7900HT Fast Real-Time PCR System (ABI) using SYBR-Green PCR Master Mix or PowerTRACK SYBR-Green PCR Master Mix (Applied Biosystems). (Statistics were only performed on samples analyzed on the same machine and prepped with the same qPCR master mix). Relative quantitation of gene expression using the ddCT method (Applied Biosystems-Guide to Performing Relative Quantitation of Gene Expression Using Real-Time Quantitative PCR) between control and experimental treatments was determined using the *Hypoxanthine-guanine phosphoribosyltransferase* (*HPRT*) and *Glyceraldehyde 3-phosphate dehydrogenase* (*GAPDH*) transcripts as the endogenous references. Primer sequences are provided within Table 1. Graphing and statistics were performed using Excel. p-values were calculated using either Student's T-test (when data were normally distributed), or Mann-Whitney U test (when data were not normally distributed).

Hybridization chain reaction in situ on 3D retinal organoids and adult human retina.

HCR procedures were carried out according to the manufacturer's instructions (Molecular Instruments) [26], with the exceptions that we did not incorporate a proteinase K treatment prior to the post-fixation steps, and the concentration of hairpins used was doubled for *LWS* and *MWS*. In brief, retinal tissues were fixed overnight in phosphate-buffered 4% paraformaldehyde at 4°C. Tissues were then washed in phosphate-buffered saline (PBS), dehydrated in MeOH, and stored in MeOH at -20°C at least overnight. Tissues were rehydrated in a graded MeOH/PBS/0.1% Tween 20 series, and post-fixed with 4% paraformaldehyde in PBS prior to hybridization. Hybridization was done overnight at 37°C. Tissues were washed with the manufacturer's wash buffer, and then 5XSSCT (standard sodium citrate with 0.1% Tween-20), and the amplification/chain reaction steps were performed following the manufacturer's protocol. Probe sets were designed and generated by Molecular Instruments and can be ordered directly from their website.

HCR was performed on de-identified adult human retina (Rocky Mountain Lions Eye Institute) using the same procedure; however, hairpin concentrations were not doubled.

Confocal Microscopy.

Whole, HCR-processed 3D retinal organoids and human retinas were mounted in glycerol and imaged with a 20X dry lens and a 40X water immersion lens using a Nikon-Andor spinning disk confocal microscope and a Zyla sCMOS camera using Nikon Elements software. Images were brightness/contrast adjusted in FIJI (ImageJ).

Droplet digital PCR (ddPCR).

Droplet digital PCR was performed according to the manufacturer's instructions (Bio-Rad). In brief, In brief, gene blocks containing *LWS* or *MWS* mRNA sequences were synthesized. The *LWS* and *MWS* gene blocks were diluted separately in TE buffer (Tris and EDTA). *LWS* and *MWS* primer/probe master mixes (Bio-Rad) and water were added to ddPCR SuperMix for Probes (Bio-Rad) to create separate *LWS* and *MWS* SuperMix master mixes. The *LWS* and *MWS* SuperMix master mixes were added to separate wells on a ddPCR plate; then, diluted *LWS* and *MWS* g-blocks were added to wells. Droplets were generated

using a Bio-Rad QX200 droplet generator. PCR was performed on a C1000 Touch thermal cycler (Bio-Rad), and droplets were analyzed using the Bio-Rad QX200 droplet reader.

Results

Opsin Expression in 180d Retinal Organoids: Additional Data and Combined T3/RA Treatment.

Previous work in our lab has shown that treatment with either T3 or RA alters transcript abundance of opsins in 3D retinal organoids up to 180 days. Here, we wanted to build on those results by collecting additional samples at 180d, using the treatment strategy in method 1. Previously, we found that T3 upregulates L opsin transcript at 180d while downregulating M, S, and rhodopsin transcript abundance. RA downregulated L and M while upregulating S and rhodopsin. Additional results at 180 days largely corroborate these data (Fig. 1). T3 treatment upregulated L opsin and downregulated M and S, with a downward trend in rhodopsin transcript abundance. Our results showed that RA downregulated M opsin transcript abundance and did not alter the abundance of other transcripts. Though analyzing the data together would be ideal, a different qPCR machine and qPCR mastermix was used to obtain new 180d data, introducing a potentially confounding variable in combining the two datasets. Overall, our results indicate that T3 and RA do alter opsin transcript abundance in 180d retinal organoids compared to control.

At 180d, using method 1, a combined T3 and RA treatment condition resulted in the downregulation of M and S opsin, and no change in L or rhodopsin transcript abundance. At 180 days, previous results showed T3 upregulating L opsin transcript abundance while RA downregulated it. The combined T3/RA treatment showed no change in L opsin transcript levels. Both T3 and RA downregulated M opsin transcript abundance, and as such the combined treatment did as well. For rhodopsin, T3 downregulated it in previous results while RA upregulated it, and so the combined T3/RA treatment showed no change in rhodopsin transcript abundance compared to control. Interestingly, however, while T3 downregulated S opsin transcript abundance and RA upregulated it previously, the combined T3/RA treatment downregulated S opsin transcript abundance rather than showing no change. This result is more similar to the T3 result, though RA concentration was higher than that of T3 (1 μM vs

500 nM). This may have had something to do with the treatment timing, or it could indicate that at 180d T3 has more of an impact on S opsin expression than RA does. Together, these results reveal an interesting ability for RA and T3 to tune opsin expression in different ways. By establishing specific ratios of T3 and RA, we may be able to tightly control the numbers of L cones in an organoid. However, more experimentation needs to be done to determine whether this is possible.

Effect of Late/Lower Concentration Treatment on 180d Retinal Organoids.

Our results from the treatment experiments using method 2 indicate that this new method does result in changes in opsin expression, though treatment timing and concentration may alter the effects of TH and RA on opsin expression. Due to the alteration of both treatment time and concentration, we cannot determine whether these changes are due to time of treatment or concentration of treatment, but overall we can conclude that method 2 produces different results at 180 days than the original treatment conditions. Method 2 T3 treatment resulted in downregulation of S opsin (similar to method 1); however, the transcript abundance of the other opsins did not change (Fig. 2). This could indicate that method 2 resulted in less of an effect on opsin expression in the organoids; however, more data need to be collected to fully conclude this.

According to our unpublished data, at 90 days (when T3 was added in method 2) opsin mRNA can be detected by qPCR, and immature photoreceptors can be identified (Zhong 2014). The difference in *SWS* transcript abundance compared to control could be due to the development of more cones, or it could be possible that at some level, opsin expression in organoids is plastic to TH treatment after cones have developed and begun expressing opsins. Additionally, the treatment with 100nM T3 lasted for 90 days; however, the effects on opsin expression differed compared to the 120 day results for the normal treatment (in which organoids would have been treated with T3 for 90 days). S opsin expression was still downregulated with method 2 (T3 treatment), as it was in the method 1 120 day treatment, but in the T3 condition, L, M, and rhodopsin transcript abundance did not change compared to control, though they did in the 120 day method 1 treatment. This indicates that the effects of a 90 day treatment depend on treatment timing or treatment concentration.

In the method 2 combined T3/RA treatment, M opsin transcript abundance decreased while rhodopsin transcript abundance increased. These results most closely match the RA 180 day results, but are not exactly the same.

Effect of Late/Lower Concentration Treatment on 120d retinal organoids.

Previous work showed that at 120 days, T3 upregulated *LWS* transcript abundance and downregulated *MWS, SWS,* and *RHO* transcript abundance. RA downregulated *MWS* and *ROD*.

With method 2, T3 did not change *RHO* or *MWS* transcript abundance, but resulted in a downward trend in *SWS* transcript abundance (Fig. 3). While previous 120d experiments did not include a combined RA/T3 treatment, method 2 RA/T3 treatment resulted in a downward trend in *SWS* transcript abundance and did not alter transcript abundance of *LWS, RHO,* or *MWS.* These results indicate that method 2 does result in altered opsin transcript abundance in 120d retinal organoids, providing more support to the feasibility of this new treatment protocol.

The method 2 treatment for 120d retinal organoids did not match the results for 120d organoids after the normal treatment strategies, indicating treatment time and/or concentration impacts the effects of T3 and RA treatment.

HCR of 3D retinal organoids and human retinas.

Due to the similarity of the L and M opsin transcripts (and proteins), selective labeling cells of each type by *in situ* or by using antibodies has previously been impossible. Our HCR results show that we can detect cones in our retinal organoids using the expression of cone arrestin (*cARR*) (data not shown). Further, we were able to detect *LWS* and *MWS* RNA in the arrestin+ organoid cones. Interestingly, we found that many arrestin+ cones appeared to coexpress *LWS* and *MWS* (data not shown). This could be due to the fact that the cells are in the process of switching opsins, which is a phenomenon that is known to happen with zebrafish LWS and LWS2 cones when fish are treated with exogenous TH. Alternatively, because the cell lines used to generate the organoids were female, each opsin could be undergoing transcription on different X chromosomes. X-inactivation has not yet

been studied in human retinal organoids, so it is unknown whether both chromosomes are active in the organoids, or if one chromosome is inactivated as is the case in retinal tissues from human patients.

We also performed HCR *in situ* on adult human retina (Fig. 4). We were able to clearly detect *carr* in the human retina, indicating that arrestin+ cells in the organoids are, in fact, cones. Our *LWS* and *MWS* showed potential colocalization of *LWS* and *MWS* mRNA, perhaps due to the lower concentration of hairpins. More experiments need to be done for us to feel confident that we can detect *LWS* and *MWS* in human retina, using fluorescence channels that minimize background, such as far-red, and using higher hairpin concentrations.

Droplet Digital PCR Method for Analyzing Opsin Expression.

Droplet digital PCR provides an additional highly sensitive method of quantifying transcript abundance, and provides an opportunity to evaluate *LWS* and *MWS* transcript abundance at once in a single sample. We found that our *LWS* assay detected *LWS* g-block accurately and did not detect *MWS* g-block. Our *MWS* assay detected *MWS* g-block, but not *LWS* g-block. Our results from the ddPCR experiments show that we can differentiate between *LWS* and *MWS* cDNA, suggesting that ddPCR is a viable option for evaluating opsin transcript expression in human retinal organoids (Fig 5A).

We also found that our ddPCR assays are quantitative. Samples spiked with increasing predicted copies of *LWS* or *MWS* g-block resulting in a corresponding increase in the number of positive droplets (Fig 5. B,C). Overall, these results indicate that ddPCR can be used to corroborate qPCR results in determining the effects of RA and T3 treatment on 3D retinal organoids.

Discussion and Future Studies

Overall, the results presented here represent a work in progress and an update on ongoing experiments in determining the effect of T3 and RA on opsin expression in retinal organoids. We found that a new treatment strategy (method 2) does result in changes in opsin expression compared to control, supporting the feasibility of this method. Method 2 also produces different treatment effects on opsin expression in retinal organoids, indicating that

treatment timing and concentration are important in determining optimal conditions for organoid growth. Additional work needs to be done in determining whether method 2 results in better lamination and surface topography of late-stage organoids. Future studies altering only timing or only treatment concentration could be interesting as well, allowing us to determine the specific roles of timing and concentration in altering the effects of T3 and RA on *LWS* and *MWS* expression in 3D retinal organoids.

The results from the method 2 180d T3 treatment and the method 2 120d T3 treatment could indicate that cone opsin expression in organoids may be plastic to thyroid hormone treatment after the onset of opsin expression (~90 days according to our unpublished qPCR results, Fig. 1). Interestingly, a color contrast study in adult hypothyroid patients showed that patients experienced changes in their color-contrast sensitivity after becoming euthyroid due to treatment [27]. Alternatively, these results could be due to the development of new cones or the degradation of S cones after 90 days. More experiments need to be done to determine which of these mechanisms mediate this result. For example, using HCR to count numbers of cones in 3D retinal organoids at 90 and 120 days. Or using organoids that report opsin expression with fluorescent proteins to track opsin expression over time in single cones.

While HCR results for 3D retinal organoids were promising, showing arrestin+ cells expressing *LWS* and *MWS*, additional experiments should be performed to ensure that apparent coexpression of *LWS* and *MWS* is not due to cross reactivity. We will perform further experiments on additional samples of adult human retina, with higher hairpin concentration and using channels that minimize autofluorescence, to confirm that we can detect *LWS* and *MWS* transcript.

Our ddPCR results indicate that our *LWS* and *MWS* assays work on g-blocks, and most importantly, specifically detect *LWS* or *MWS* transcripts. Future directions for ddPCR experiments would be to confirm the ability of our *LWS* and *MWS* assays to function with human cDNA and cDNA from retinal organoids.

Retinal organoids represent a promising avenue for future cell replacement strategies. Previous results from our lab showed that T3 and RA can alter *LWS* and *MWS* opsin

expression in human iPSC-derived 3D retinal organoids. New results indicate that altering treatment timing and concentration may be important in creating retinal organoids with optimal numbers of L, M, and S cones.

References

1. Saaddine, V. Narayan, and Vinicor. *Vision Loss: A Public Health Problem*. Vision Health Initiative 2019 December 19, 2022 [cited 2023 6/29/23].
2. Hartong, D.T., E.L. Berson, and T.P. Dryja, *Retinitis pigmentosa.* Lancet, 2006. **368**(9549): p. 1795-809.
3. Fleckenstein, M., T.D.L. Keenan, R.H. Guymer, U. Chakravarthy, S. Schmitz-Valckenberg, C.C. Klaver, W.T. Wong, and E.Y. Chew, *Age-related macular degeneration.* Nat Rev Dis Primers, 2021. **7**(1): p. 31.
4. Varadarajan, S.G., J.L. Hunyara, N.R. Hamilton, A.L. Kolodkin, and A.D. Huberman, *Central nervous system regeneration.* Cell, 2022. **185**(1): p. 77-94.
5. Gasparini, S.J., K. Tessmer, M. Reh, S. Wieneke, M. Carido, M. Volkner, O. Borsch, A. Swiersy, M. Zuzic, O. Goureau, T. Kurth, V. Busskamp, G. Zeck, M.O. Karl, and M. Ader, *Transplanted human cones incorporate into the retina and function in a murine cone degeneration model.* J Clin Invest, 2022. **132**(12).
6. Garita-Hernandez, M., M. Lampic, A. Chaffiol, L. Guibbal, F. Routet, T. Santos-Ferreira, S. Gasparini, O. Borsch, G. Gagliardi, S. Reichman, S. Picaud, J.A. Sahel, O. Goureau, M. Ader, D. Dalkara, and J. Duebel, *Restoration of visual function by transplantation of optogenetically engineered photoreceptors.* Nat Commun, 2019. **10**(1): p. 4524.
7. Zhong, X., C. Gutierrez, T. Xue, C. Hampton, M.N. Vergara, L.H. Cao, A. Peters, T.S. Park, E.T. Zambidis, J.S. Meyer, D.M. Gamm, K.W. Yau, and M.V. Canto-Soler, *Generation of three-dimensional retinal tissue with functional photoreceptors from human iPSCs.* Nat Commun, 2014. **5**: p. 4047.
8. Bell, C.M., D.J. Zack, and C.A. Berlinicke, *Human Organoids for the Study of Retinal Development and Disease.* Annu Rev Vis Sci, 2020. **6**: p. 91-114.
9. Collin, J., R. Queen, D. Zerti, B. Dorgau, R. Hussain, J. Coxhead, S. Cockell, and M. Lako, *Deconstructing Retinal Organoids: Single Cell RNA-Seq Reveals the Cellular Components of Human Pluripotent Stem Cell-Derived Retina.* Stem Cells, 2019. **37**(5): p. 593-598.
10. O'Hara-Wright, M. and A. Gonzalez-Cordero, *Retinal organoids: a window into human retinal development.* Development, 2020. **147**(24).
11. Fligor, C.M., K.B. Langer, A. Sridhar, Y. Ren, P.K. Shields, M.C. Edler, S.K. Ohlemacher, V.M. Sluch, D.J. Zack, C. Zhang, D.M. Suter, and J.S. Meyer, *Three-Dimensional Retinal Organoids Facilitate the Investigation of Retinal Ganglion Cell Development, Organization and Neurite Outgrowth from Human Pluripotent Stem Cells.* Sci Rep, 2018. **8**(1): p. 14520.
12. Sanjurjo-Soriano, C., N. Erkilic, K. Damodar, H. Boukhaddaoui, M. Diakatou, M. Garita-Hernandez, D. Mamaeva, G. Dubois, Z. Jazouli, C. Jimenez-Medina, O. Goureau, I. Meunier, and V. Kalatzis, *Retinoic acid delays initial photoreceptor differentiation and results in a highly structured mature retinal organoid.* Stem Cell Res Ther, 2022. **13**(1): p. 478.
13. Wahle, P., G. Brancati, C. Harmel, Z. He, G. Gut, J.S. Del Castillo, A. Xavier da Silveira Dos Santos, Q. Yu, P. Noser, J.S. Fleck, B. Gjeta, D. Pavlinic, S. Picelli, M. Hess, G.W. Schmidt, T.T.A. Lummen, Y. Hou, P. Galliker, D. Goldblum, M. Balogh, C.S. Cowan, H.P.N. Scholl, B. Roska, M. Renner, L. Pelkmans, B. Treutlein, and J.G. Camp, *Multimodal spatiotemporal phenotyping of human retinal organoid development.* Nat Biotechnol, 2023.
14. Li, X., L. Zhang, F. Tang, and X. Wei, *Retinal Organoids: Cultivation, Differentiation, and Transplantation.* Front Cell Neurosci, 2021. **15**: p. 638439.
15. Fligor, C.M., K.C. Huang, S.S. Lavekar, K.B. VanderWall, and J.S. Meyer, *Differentiation of retinal organoids from human pluripotent stem cells.* Methods Cell Biol, 2020. **159**: p. 279-302.

16. Eldred, K.C., S.E. Hadyniak, K.A. Hussey, B. Brenerman, P.W. Zhang, X. Chamling, V.M. Sluch, D.S. Welsbie, S. Hattar, J. Taylor, K. Wahlin, D.J. Zack, and R.J. Johnston, Jr., *Thyroid hormone signaling specifies cone subtypes in human retinal organoids.* Science, 2018. **362**(6411).
17. Jeremy Nathans, D.T., David S. Hogness, *Molecular Genetics of Human Color Vision: The Genes Encoding Blue, Green, and Red Pigments.* Science, 1986. **232**.
18. Vollrath, D., J. Nathans, and R.W. Davis, *Tandem Array of Human Visual Pigment Genes at Xq28.* Science, 1988. **240**: p. 1669-1672.
19. Peng, G.H. and S. Chen, *Active opsin loci adopt intrachromosomal loops that depend on the photoreceptor transcription factor network.* Proc Natl Acad Sci U S A, 2011. **108**(43): p. 17821-6.
20. Chinen, A., T. Hamaoka, Y. Yamada, and S. Kawamura, *Gene Duplication and Spectral Diversification of Cone Visual Pigments of Zebrafish.* Genetics, 2003. **163**: p. 663–675.
21. Hofmann, C.M. and K.L. Carleton, *Gene duplication and differential gene expression play an important role in the diversification of visual pigments in fish.* Integr Comp Biol, 2009. **49**(6): p. 630-43.
22. Mackin, R.D., R.A. Frey, C. Gutierrez, A.A. Farre, S. Kawamura, D.M. Mitchell, and D.L. Stenkamp, *Endocrine regulation of multichromatic color vision.* Proc Natl Acad Sci U S A, 2019. **116**(34): p. 16882-16891.
23. Roberts, M.R., M. Srinivas, D. Forrest, G.M.d. Escoba, and T.A. Reh, *Making the gradient: Thyroid hormone regulates cone opsin expression in the developing mouse retina.* Proc Natl Acad Sci U S A, 2006. **103**(16): p. 6218–6223.
24. Hadyniak, S.E., K.C. Eldred, B. Brenerman, K.A. Hussey, J.F.D. Hagen, R.C. McCoy, M.E.G. Sauria, J.A. Kuchenbecker, T. Reh, I. Glass, M. Neitz, J. Neitz, J. Taylor, and R.J. Johnston, *Temporal regulation of green and red cone specification in human retinas and retinal organoids.* (pre-print) bioRxiv, 2022.
25. Patel, J., K. Landers, H. Li, R.H. Mortimer, and K. Richard, *Thyroid hormones and fetal neurological development.* J Endocrinol, 2011. **209**(1): p. 1-8.
26. Choi, H.M.T., M. Schwarzkopf, M.E. Fornace, A. Acharya, G. Artavanis, J. Stegmaier, A. Cunha, and N.A. Pierce, *Third-generation in situ hybridization chain reaction: multiplexed, quantitative, sensitive, versatile, robust.* Development, 2018. **145**(12).
27. Cakir, M., B. Turgut Ozturk, E. Turan, G. Gonulalan, I. Polat, and K. Gunduz, *The effect of hypothyroidism on color contrast sensitivity: a prospective study.* Eur Thyroid J, 2015. **4**(1): p. 43-7.

Tables

Table 4.1: Summary of Results

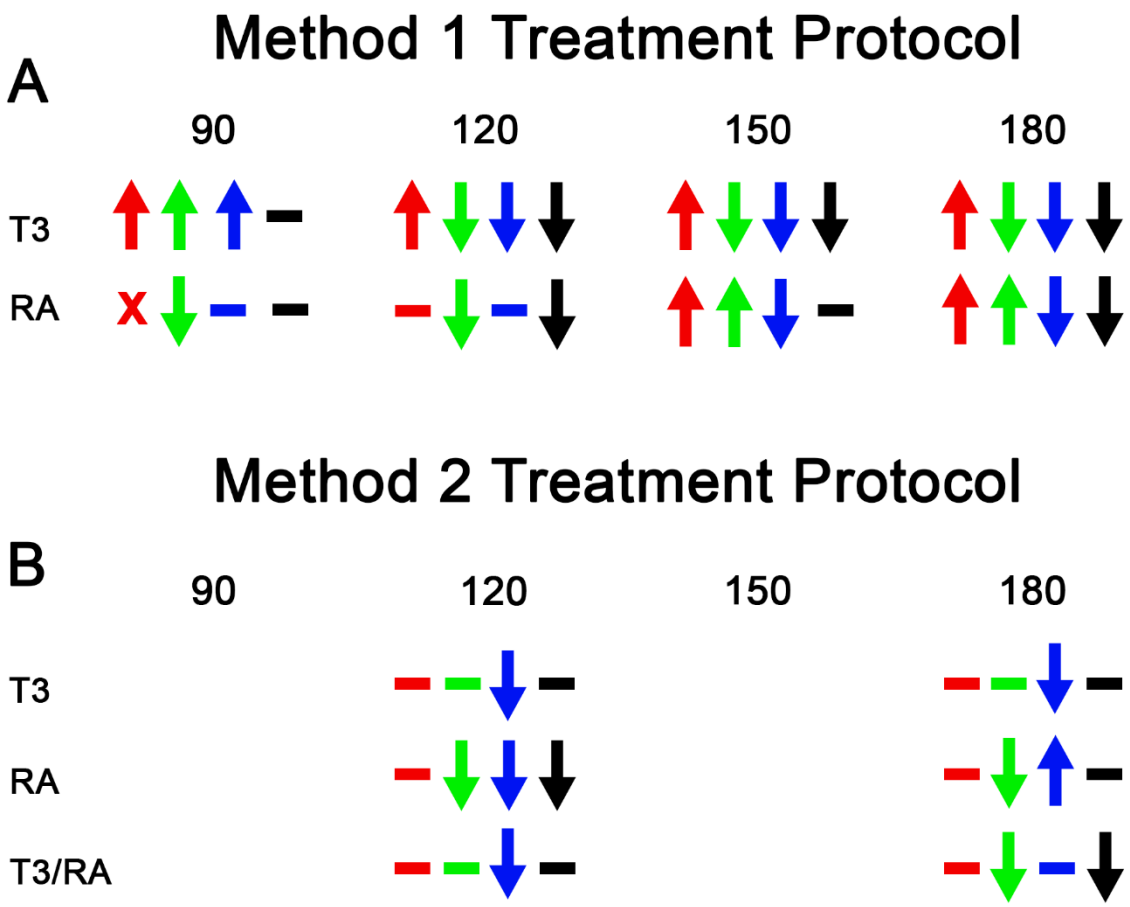

Note: up arrows indicate increased transcript abundance, down arrows indicate decrease in transcript abundance, - indicates no change in transcript abundance. Red symbols show results for *LWS* transcript, green symbols show results for *MWS* transcript, blue symbols show results for *SWS* transcript, and black symbols show results for *ROD* transcripts.

Figures

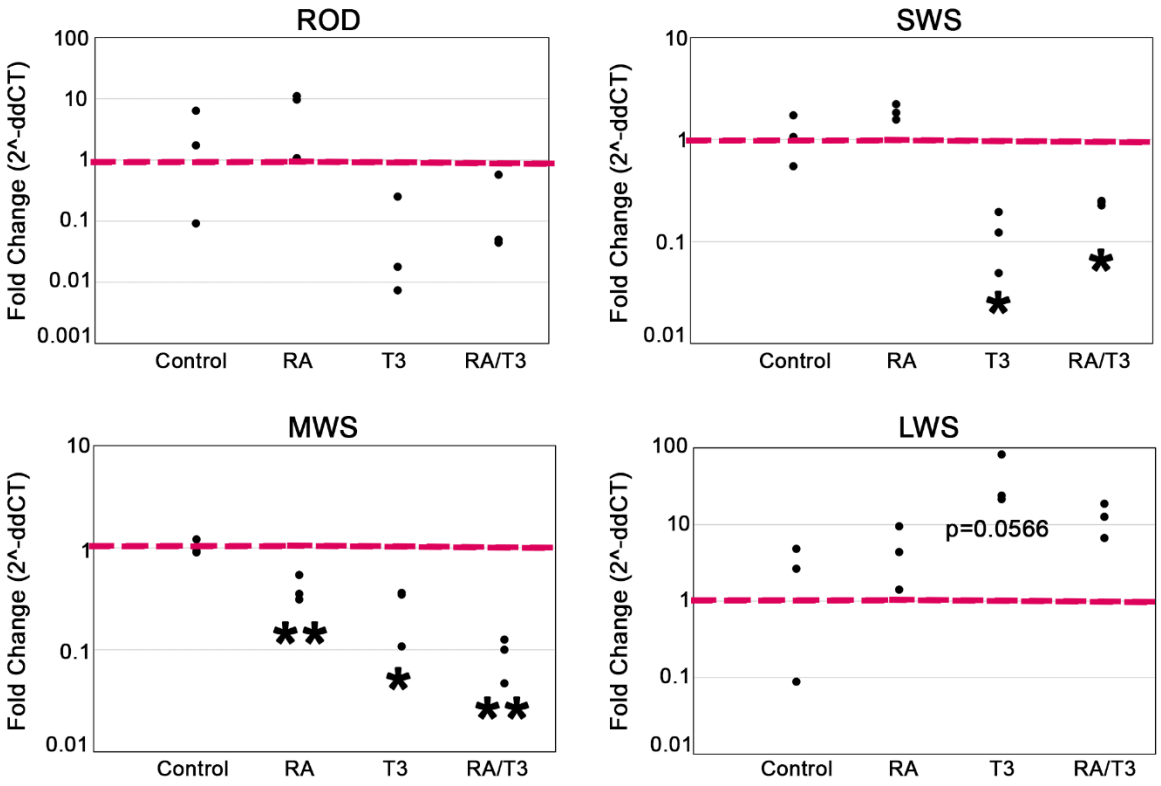

Figure 4.1: qPCR of 180d retinal organoids. A-D) Scatter plots showing fold change (2^-ddCT) in transcript abundance compared to control. Each dot represents one biological sample; n=3 for all. *ROD* showed no change in transcript abundance. *SWS* was downregulated by T3 (p=0.0122, t-test) and combined RA/T3 treatment (p=0.0130, t-test). *MWS* was downregulated by RA (p=0.0078, t-test), T3 (p=0.0244, t-test), and RA/T3 (p=0.00136, t-test) treatments. *LWS* showed an upward trend in transcript abundance for the T3 treatment (p=0.0566).

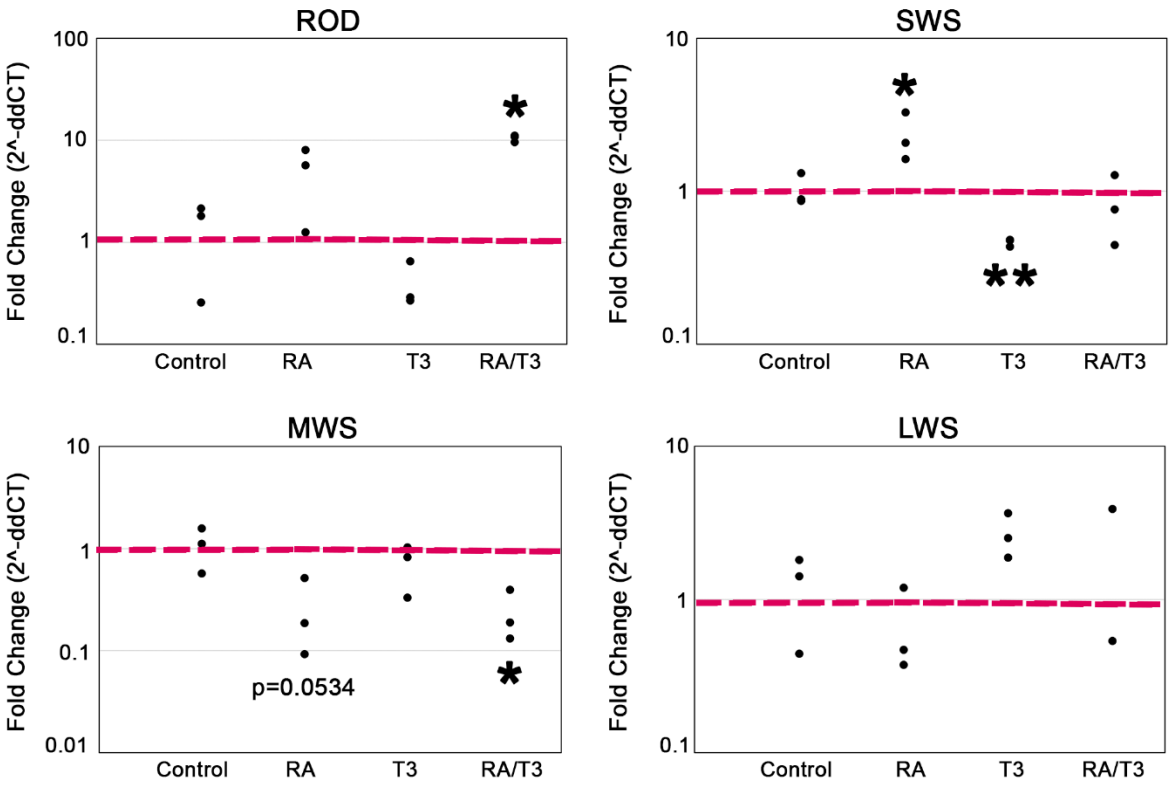

Figure 4.2: qPCR of 180d retinal organoids after method 2 treatments. A-D) Scatter plots showing fold change (2^-ddCT) in transcript abundance compared to control. Each dot represents one biological sample; n=3 for all. *ROD* was upregulated by combined RA/T3 treatment (p=0.0262, t-test). *SWS* was upregulated by RA (p= 0.0312, t-test) and downregulated by T3 (p=0.0053, t-test). *MWS* showed a trend of downregulation by RA (p=0.0534, t-test), and was downregulated significantly by combined RA/T3 (p=0.0248, t-test). *LWS* did not show significant changes in transcript abundance in any treatment condition.

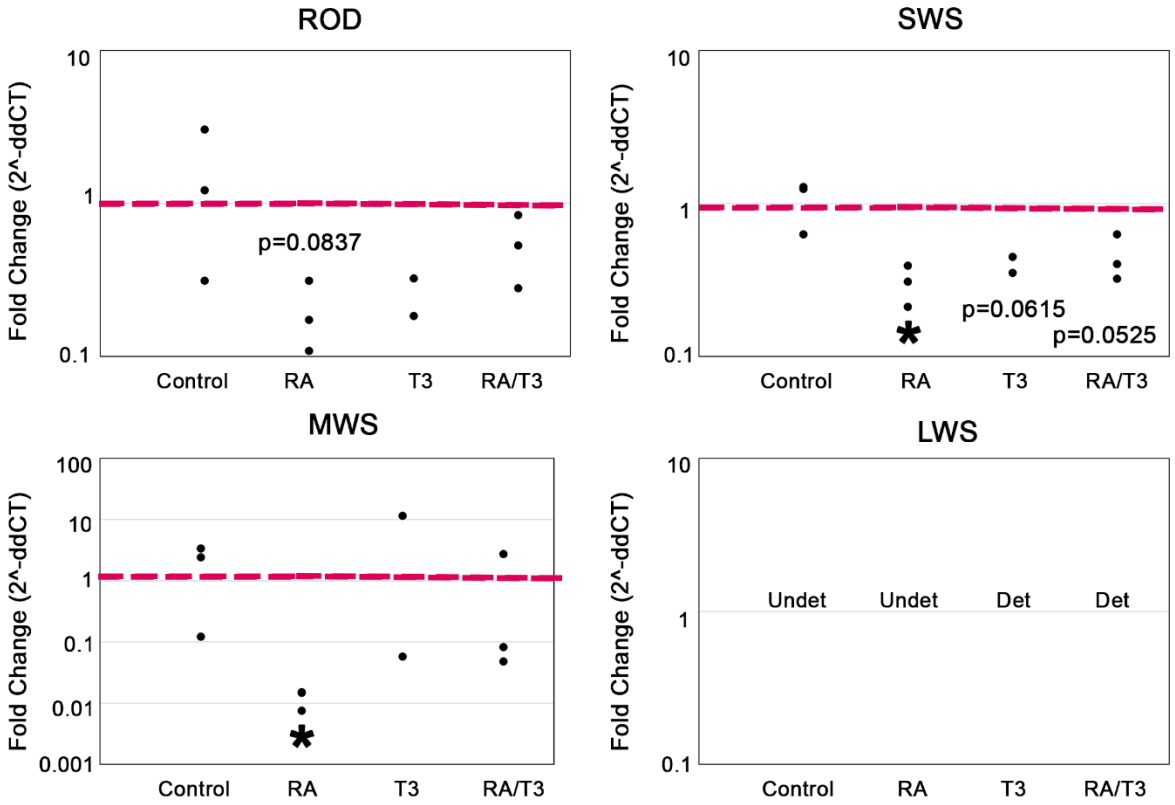

Figure 4.3: qPCR of 120d retinal organoids after method 2 treatments. A-D) Scatter plots showing fold change (2^-ddCT) in transcript abundance compared to control. Each dot represents one biological sample; n=3 for control, RA, and RA/T3; n=2 for T3. *ROD* showed a potential downward trend in transcript abundance with RA treatment (p=0.0837, t-test). *SWS* was downregulated by RA (p= 0.0145, t-test) and showed a trend of downregulation for T3 (p=0.0615, t-test) and RA/T3 (p=0.0525, t-test) treatments. *MWS* was downregulated by RA (p=0.0146, t-test. *LWS* was undetectable in controls, making the ddCT method unusable. We did find that *LWS* was undetectable by qPCR in the control and RA conditions, but was detectable in some T3 and RA/T3-treated samples. This could indicate that *LWS* was upregulated by T3 and RA/T3, but more qPCR needs to be done in order to determine this.

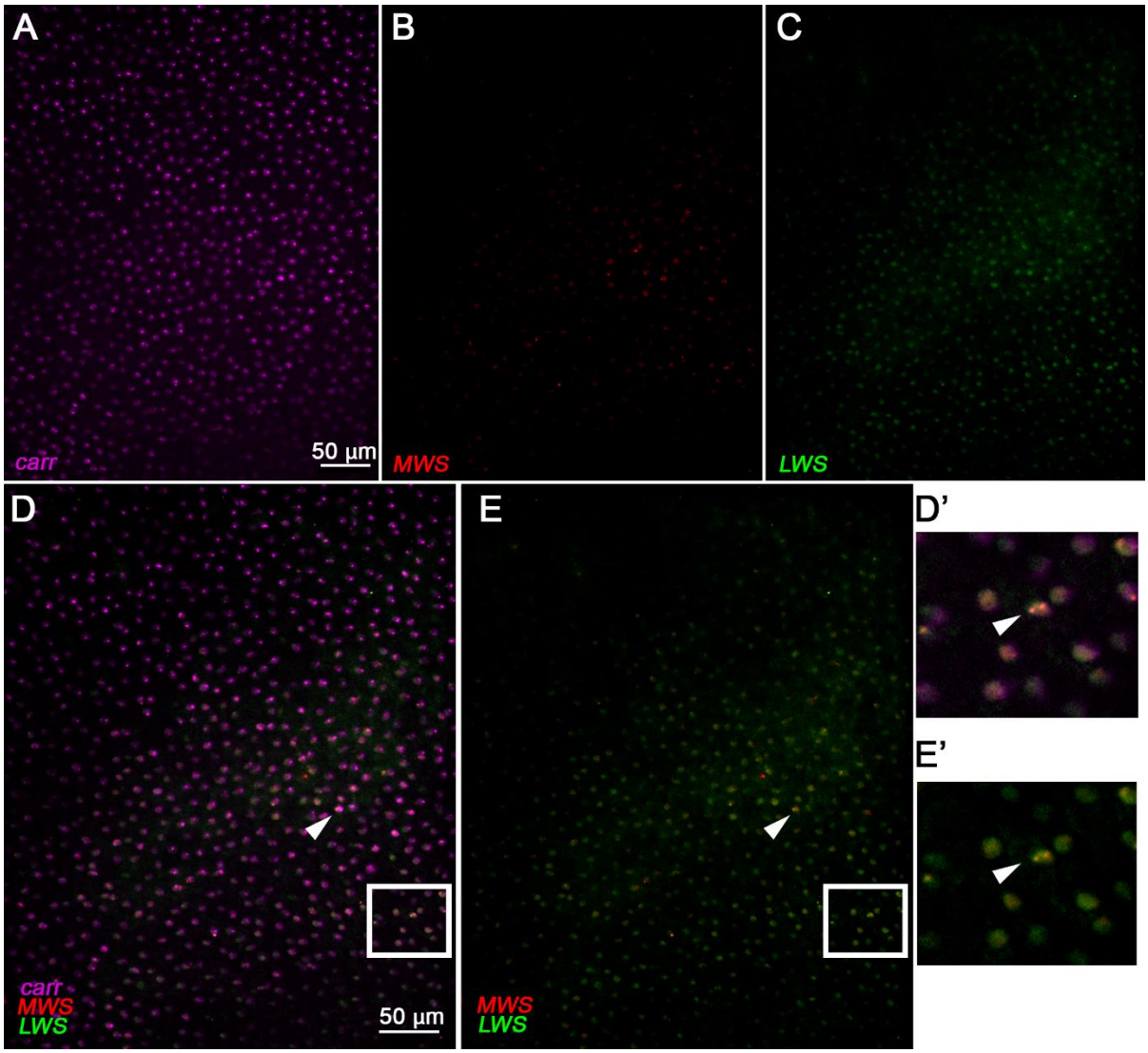

Figure 4.4: HCR *in situ* of adult human retina. A-E) 40x images of human retina. D', E') Enlarged view of insets in D, E. A) Arrestin transcript was detected in human cones, validating our ability to identify cones in organoids. B) *MWS* mRNA localization; signal was very low, potentially autofluorescence. C) *LWS* mRNA localization; signal was also very low, potentially autofluorescence. D) Merged view of all channels. Arrow denotes a cell potentially coexpressing *carr*, *MWS*, and *LWS*. E) *MWS* and *LWS* channels merged. Arrow denotes same cell in D, potentially coexpressing *MWS* and *LWS*. D') Enlarged view of inset in D, arrow denotes another cell potentially coexpressing *carr*, *MWS*, and *LWS*. Cell is different from that noted in D,E. E') Enlarged view of inset in E, arrow denotes another cell potentially coexpressing *MWS*, and *LWS*. Cell is different from that noted in D,E.

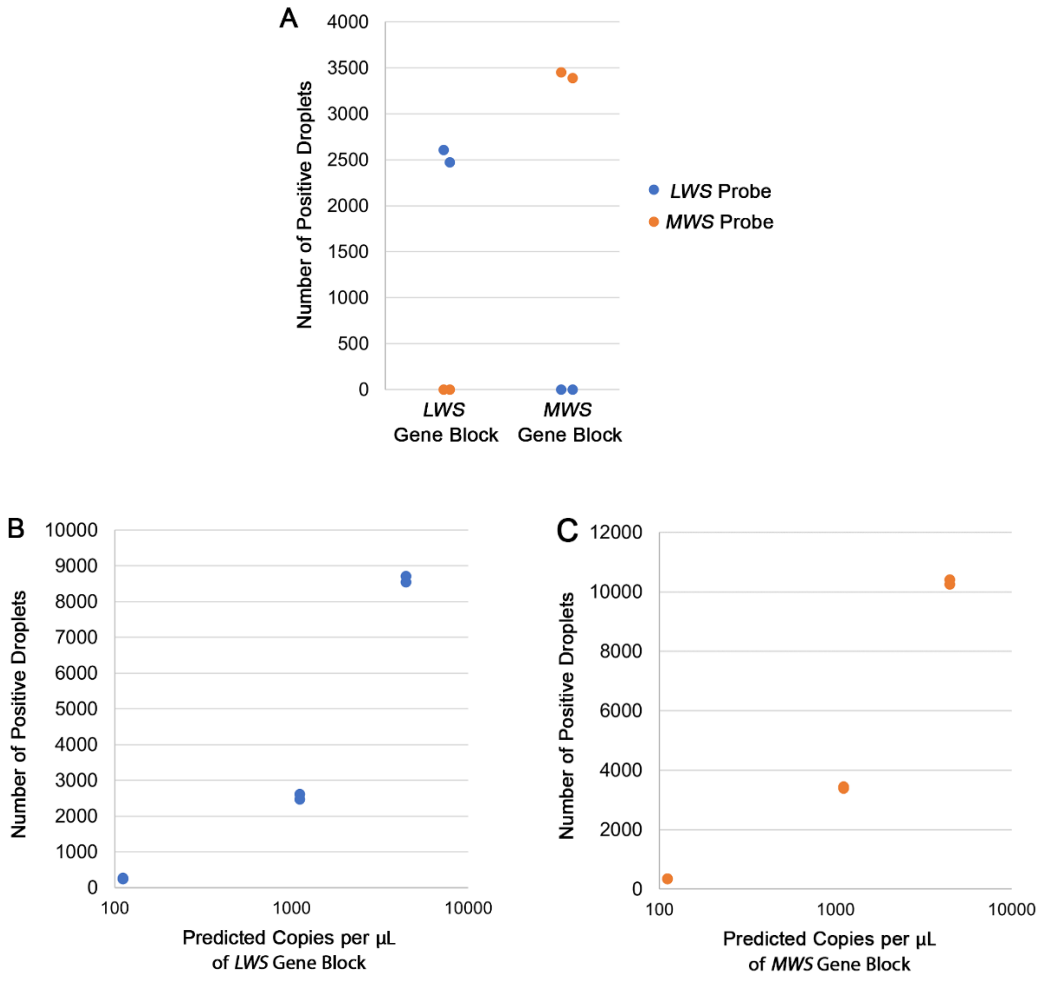

Figure 4.5: ddPCR Proof of Concept. A) Positive droplets detected by *LWS* and *MWS* assays. *LWS* assay detected approximately 2500 positive droplets when wells had *LWS* gene block, and zero positive droplets when wells had *MWS* gene block. *MWS* assay detected approximately 3500 positive droplets when wells had *MWS* gene block, and zero positive droplets when wells had *LWS* gene block. Results in A indicate specificity of ddPCR assays. B) *LWS* assay is quantitative, resulting in more positive droplets with increasing copies/µL of gene block. C) *MWS* assay is quantitative, resulting in more positive droplets with increasing copies/µL of gene block.

Supplemental Information

Supplementary Table S4.1 Primer sequences used in qPCR

Gene	Forward Primer	Reverse Primer
OPN1LW	CCGAGCGGTGGCAAAG	AGCAGACGCAGTACGCAAA
OPN1MW	ACCCCACTCAGCATCATCGT	CCAGCAGAAGCAGAATGCCAGGAC
OPN1SW	CGCCAGCTGTAACGGATACT	TACCAATGGTCCAGGTAGCC
OPN2RHO	TTTTCTGCTATGGGCAGCTC	CATGAAGATGGGACCGAAGT
HPRT	TGCTGACCTGCTGGATTACAT	TTGCGACCTTGACCATCTTT
GAPDH	CCCCACCACACTGAATCTCC	GGTACTTTATTGATGGTACATGACAAG